AD_____

Award Number: W81XWH-12-1-0259

TITLE: Genomic Basis of Prostate Cancer Health Disparity Among African-American Men

PRINCIPAL INVESTIGATOR: Harry Ostrer, M.D.

CONTRACTING ORGANIZATION: Albert Einstein College of Medicine of Yeshiva University
Bronx, NY 10461

REPORT DATE: July 2013

TYPE OF REPORT: Annual

PREPARED FOR: U.S. Army Medical Research and Materiel Command
Fort Detrick, Maryland 21702-5012

REPORT DOCUMENTATION PAGE

Form Approved
OMB No. 0704-0188

1. REPORT DATE	2. REPORT TYPE	3. DATES COVERED
July 2013	Annual	1 July 2012 – 30 June 2013

4. TITLE AND SUBTITLE

Genomic Basis of Prostate Cancer Health Disparity Among African-American Men

5a. CONTRACT NUMBER

5b. GRANT NUMBER
W81XWH-12-1-0259

5c. PROGRAM ELEMENT NUMBER

6. AUTHOR(S)

Harry Ostrer, M.D.

E-Mail: harry.ostrer@einstein.yu.edu

5d. PROJECT NUMBER

5e. TASK NUMBER

5f. WORK UNIT NUMBER

7. PERFORMING ORGANIZATION NAME(S) AND ADDRESS(ES)

Albert Einstein College of Medicine of Yeshiva University
Bronx, NY 10461

8. PERFORMING ORGANIZATION REPORT NUMBER

9. SPONSORING / MONITORING AGENCY NAME(S) AND ADDRESS(ES)
U.S. Army Medical Research and Materiel Command
Fort Detrick, Maryland 21702-5012

10. SPONSOR/MONITOR'S ACRONYM(S)

11. SPONSOR/MONITOR'S REPORT NUMBER(S)

12. DISTRIBUTION / AVAILABILITY STATEMENT
Approved for Public Release; Distribution Unlimited

13. SUPPLEMENTARY NOTES

14. ABSTRACT

The hypothesis for this study is that copy number alteration (amplification and deletion) in a limited repertoire of genes Is highly predictive of prostate cancer metastasis. This signature is present in primary prostate cancers at the time of diagnosis and is enriched in the primary prostate cancers of African-American men, thus accounting for the health disparity of prostate cancer metastasis among them. The biological effect of these copy number events is to convey an escape from anoikis, as well as the other features that occur with metastasis. The current study will confirm this signature in prostate cancers that have been shown to metastasize , compared to those that have not and to determine the prevalence of this high-risk signature in the prostate cancers of African-American men matched for stage compared to those of European-American men. This study will also demonstrate that the signature can be detected in prostate cancer biopsies and correlated between the biopsy and associated tumor specimens. This study will answer an important question about the apparent health disparity of prostate cancer metastasis as well as develop a clinically useful tool that could be used to select treatment for men diagnosed with prostate cancer.

15. SUBJECT TERMS
Prostate cancer, health disparity, metastasis, African-American men, genomics, copy number alteration

16. SECURITY CLASSIFICATION OF:			17. LIMITATION OF ABSTRACT	18. NUMBER OF PAGES	19a. NAME OF RESPONSIBLE PERSON
a. REPORT	b. ABSTRACT	c. THIS PAGE			USAMRMC
U	U	U	UU	88	19b. TELEPHONE NUMBER *(include area code)*

Table of Contents

INTRODUCTION

Compared to European-American (EA) men, African-American (AA) men have a 2-fold greater risk of dying from metastatic prostate cancer (1-2). For both groups, proper categorization of prostate cancer biopsies as high or low-risk for metastasis at the time of diagnosis would optimize treatment, improving outcomes and minimizing toxicity. The Ostrer laboratory has demonstrated that the specific genes within metastatic prostate cancers have been altered by amplification (increase in the copy number) or deletion (decrease in the copy number) (3). These genes appeared to have been selected by the advantages that they conveyed to tumors, such as escape from cell death ('anoikis'). These amplified or deleted metastasis genes are enriched 2.5-fold in the primary prostate cancers of AA men – a degree of enrichment that is similar to the enhanced likelihood of metastasis. The current study is designed to confirm these observations about gene patterns predictive of metastatic potential in new cohorts of men for whom outcome data are available The current study will also provide DNA sequence of the exomes (expressed part of the genomes) in a subset of these tumors and a risk model that can be used for categorizing newly diagnosed prostate cancers as high or low-risk for metastasis. These methods will be applied to prostate cancer biopsy specimens to demonstrate that they could be used at the time of diagnosis for prediction of outcome. This study will be beneficial to all men with prostate cancer, because it will provide a diagnostic tool that could be used for selection of therapy. It is especially beneficial for African-American men who have a greater likelihood of disease and metastasis and could provide a precise answer for the challenging problem of this health disparity.

KEYWORDS

Prostate cancer, metastasis, African-American men, health disparity, genomics, copy number alteration, predictive signature.

OVERALL PROJECT SUMMARY

Year 1: The main efforts during the first year of the project were review of the clinical data for the subjects in the study to verify their inclusion, selection of formalin-fixed paraffin-embedded (FFPE) tissue blocks, and macrodissection of tumor or normal tissue for genetic analysis. Notably, IRB approval was secured from Duke and authorized by the U.S. Army Medical Research and Materiel Command Human Research Protection Office. Cases were identified among men who received radical prostatectomy for prostate cancer and who had accurate long-term follow-up information. These that had distant metastases have been frequency matched to men cured by radical prostatectomy by age (within 5-years), race (EA vs. AA men), pathological stage (exact match), margin status (exact match), grade (Gleason score, exact match), surgery year (within 3 years), PSA (<10, 10-20, and >20) and location (North Carolina versus New York). There is currently no accepted definition of "cured" after surgery, since late recurrences occur and the cure by surgery subgroup will undoubtedly be confounded by high-risk primary tumors. For this study, we have used PSA <0.2 ng/ml five years after surgery as a surrogate marker for "cured" because: (a) PSA recurrences (PSA >0.2 ng/ml) are uncommon after 5 years and (b) Even when PSA recurrences do occur after 5 years, they are rarely fatal (4).

Among the identified cases, the Pathology Departments at Duke and Einstein reviewed the pre-existing H&E slides for evidence of cancer. The pathologists selected the two blocks with the highest tumor content and one that was tumor free. We retrieved the corresponding FFPE tissue blocks and cut 12 slices each of 5 micron thickness. These sections were placed in 2 ml Eppendorf tube, bar-coded with a unique de-identified code for each patient and assembled for genomic analysis.

The biomarkers are copy number alterations (CNAs) detected by molecular inversion probe (MiPS) technology using the Affymetrix Oncoscan v2 SNP array developed specifically for genomic DNA samples extracted from FFPE tissues. This array has been applied to more than 5000 samples with an average pass rate of 92%. Among the features of the method are a wide dynamic range (0-60 copies) and interrogation of the entire genome by analysis of more than 335,000 markers. To assess the validity of our metastasis signature and MPS prediction model, we tested a Duke cohort that was made up of a group of primary tumors that metastasized following radical prostatectomy (mPT, n=12), a group of high-risk tumors that did not develop distant metastases (hiPTs, n=8), and, a group of low-risk tumors that did not develop distant metastases (iPTs, n=7). The high-risk designation of the hiPT groups was assigned based on whether the patient experienced biochemical recurrence and received adjuvant radiation and/or hormone therapy after surgery whereas the iPTs represent tumors of men that were considered low-risk and did not receive adjuvant therapy.

The MPS score was calculated for the Duke cohort (Figure) and shown to distribute as expected for mPTs, iPTs and hiPTs. The receiver operating characteristics-area under the curve analysis (ROC-AUC) applied only to the Duke cohort mPTs and iPTs resulted in an accuracy of 0.91. The Duke cohort mPTs and hiPTs/iPTs pooled with the surgical

validation set previously described resulted in a 0.77 accuracy as measured by the ROC-AUC.

Figure. Boxplots of MPS score (Y-axis) of primary tumor samples from the Duke cohort validation study (right panel) shown relative to previously studied cohorts (left and middle panels) (3). METS are metastases. mPTs are primary tumors that went on to metastasize. Ln+PTs are tumors that spread to regional lymph nodes. Control PTs are primary tumors whose natural history is unknown. Cell lines are derived from tumors of various origins.

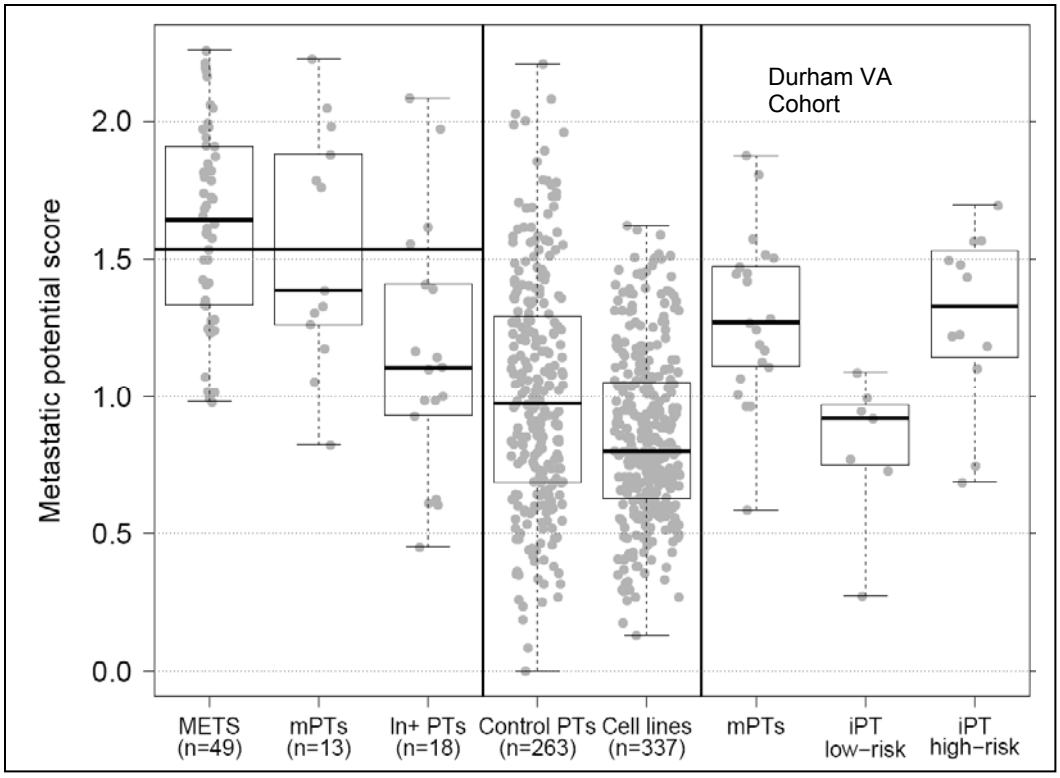

Thus, the every step in the subject identification, tumor assessment, block retrieval, dissection, DNA extraction, Oncoscan v2 array and data analysis met our expectation and suggested that we could meet the goals of Specific Aim 1 of our study.

To identify samples that were suitable for whole exome sequencing (Aim 3), we selected 6 matched pairs of tumor-normal that were frozen immediately following resection. As outcome information is not available for these, we chose to identify those with high and low metastatic potential scores, based on CNA profiles. To do so, the samples were dissected, DNA was extracted and Affymetrix v6 arrays were run, then MPS scores were calculated. Among these 1 was identified to have high MPS scores and 5 were identified to have low MPS scores. From these, 1mPT sample and 1iPT sample were selected for whole exome sequencing.

KEY RESEARCH ACCOMPLISHMENTS

In a replication study, MPS score was shown to be an accurate predictor of metastatic risk (0.91 ROC-AUC) using Oncoscan v2 arrays.

CONCLUSION

The salient feature of this study involves translation of the basic research of tumor biology into a risk model that can provide informed clinical decisions for men with prostate cancer and their physicians. This will determine whether prostate cancers are treated aggressively, because they are deemed to have high metastatic potential, or whether they are treated with active surveillance, because they are deemed indolent. These findings are now being applied to studying the health disparity of prostate cancer metastasis.

PUBLICATIONS, ABSTRACTS, AND PRESENTATIONS

Publication

Pearlman A, Campbell C, Brooks E, Genshaft A, Shahjahan S, Ittman M, Bova GS, Melamed J, Holcomb I, Schneider RJ, Ostrer H. Clustering based method for developing a genomic copy number alteration signature for predicting the metastatic progression of prostate cancer. J Prob Stat 2012; Article ID 873570.

Presentation

November 8, 2012, American Society of Human Genetics**, "**Prostate cancer metastasis prognostic bio-marker development," by Alexander Pearlman, Ph.D.

INVENTIONS, PATENTS AND LICENSES

Patent application

"Genomic Signatures of Metastasis in Prostate Cancer" Date of application to U.S. Patent and Trademark Office May 5, 2012

REPORTABLE OUTCOMES

Development of an accurate predictive score for risk of metastasis in prostate cancer surgical specimens.

REFERENCES

1. American Cancer Society AC. Learn About Cancer. 2013; Available from: http://www.cancer.org/Cancer/ProstateCancer/index.
2. Dash A, Lee P, Zhou Q, Jean-Gilles J, Taneja S, Satagopan J, et al. Impact of socioeconomic factors on prostate cancer outcomes in black patients treated with surgery. Urology. 2008;72:641-6.
3. Pearlman A, Campbell C, Brooks E, Genshaft A, Shajahan S, Ittman M, et al. Clustering based method for developing a genomic copy number alteration signature for predicting the metastatic progression of prostate cancer. J Prob Stat. 2012; Article ID 873570.
4. Freedland SJ, Humphreys EB, Mangold LA, Eisenberger M, Partin AW. Time to prostate specific antigen recurrence after radical prostatectomy and risk of prostate cancer specific mortality. J Urol. 2006;176:1404-8.

Hindawi Publishing Corporation
Journal of Probability and Statistics
Volume 2012, Article ID 873570, 19 pages
doi:10.1155/2012/873570

Research Article

Clustering-Based Method for Developing a Genomic Copy Number Alteration Signature for Predicting the Metastatic Potential of Prostate Cancer

Alexander Pearlman,[1] Christopher Campbell,[1] Eric Brooks,[2] Alex Genshaft,[2] Shahin Shajahan,[2] Michael Ittman,[3] G. Steven Bova,[4] Jonathan Melamed,[5] Ilona Holcomb,[6] Robert J. Schneider,[7] and Harry Ostrer[1]

[1] *Department of Pathology, Albert Einstein College of Medicine, Bronx, NY 10461, USA*
[2] *Human Genetics Program, Department of Pediatrics, NYU Langone Medical Center, New York, NY 10016, USA*
[3] *Department of Pathology, Baylor College of Medicine, Houston, TX 77030, USA*
[4] *Department of Pathology, Johns Hopkins University School of Medicine, Baltimore, MD 21205, USA*
[5] *Department of Pathology, NYU Langone Medical Center, New York, NY 10016, USA*
[6] *Department of Pathology, Stanford University School of Medicine, Stanford, CA 94305, USA*
[7] *NYU Cancer Institute and Department of Microbiology, NYU Langone Medical Center, New York, NY 10016, USA*

Correspondence should be addressed to Alexander Pearlman, apearlman@gmail.com

Received 1 March 2012; Revised 17 May 2012; Accepted 31 May 2012

Academic Editor: Xiaohua Douglas Zhang

The transition of cancer from a localized tumor to a distant metastasis is not well understood for prostate and many other cancers, partly, because of the scarcity of tumor samples, especially metastases, from cancer patients with long-term clinical follow-up. To overcome this limitation, we developed a semi-supervised clustering method using the tumor genomic DNA copy number alterations to classify each patient into inferred clinical outcome groups of metastatic potential. Our data set was comprised of 294 primary tumors and 49 metastases from 5 independent cohorts of prostate cancer patients. The alterations were modeled based on Darwin's evolutionary selection theory and the genes overlapping these altered genomic regions were used to develop a metastatic potential score for a prostate cancer primary tumor. The function of the proteins encoded by some of the predictor genes promote escape from anoikis, a pathway of apoptosis, deregulated in metastases. We evaluated the metastatic potential score with other clinical predictors available at diagnosis using a Cox proportional hazards model and show our proposed score was the only significant predictor of metastasis free survival. The metastasis gene signature and associated score could be applied directly to copy number alteration profiles from patient biopsies positive for prostate cancer.

1. Introduction

Prostate cancer is a common public health problem. In 2012, this disease was expected to be diagnosed in an estimated 241,740 men (29% of all male cancers) and to result in 28,170 deaths (9% of male cancer deaths) [1]. If left untreated, around 70% of prostate cancers remain asymptomatic and indolent for decades [2]. If treated with radical prostatectomy or radiation therapy, the risk of metastasis is reduced, but erectile dysfunction, urinary incontinence, and rectal bleeding may occur, affecting the patient's quality of life. Because it is currently difficult to determine accurately which patients will develop metastatic disease, physicians treat patients with mid-to-late stage local disease aggressively, even when such treatment may not be required. Clinical parameters, such as, serum concentration of prostate-specific antigen (PSA), extension beyond surgical margins, invasion of seminal vesicles, extension beyond the capsule, surgical Gleason score, prostate weight, race, and year of surgery, are employed in existing nomograms for prediction of local recurrences after surgery [3], but, many of these parameters are not available at diagnosis and cannot be used for guiding therapeutic decisions. Development of a robust risk model from a biopsy that accurately predicts the potential of a local prostate cancer to metastasize would justify aggressive treatment in high-risk cases and improve the quality of life for men with indolent disease by allowing them to avoid treatment-related side effects. Thus, the goal of this study was to develop a method to identify tumor genomic biomarkers that could be applied to prediction models that help guide clinical treatment decisions.

The method chosen for developing the predictive model was the analysis of genomic DNA copy number alterations (CNAs) in prostate cancers, because these cancers have long been known to harbor multiple genomic imbalances that result from CNAs [4, 5]. High-resolution measurements of CNAs have functional value, in some cases providing evidence for alterations in the quantity of normal, mutant, or hybrid-fusion transcripts and proteins in the cancer cells. The resulting changes in abundance or altered structure of RNA transcripts and proteins (e.g., truncating dominant negative mutations) may impact the fitness of the cell and provide some of the mechanisms necessary for distant site migration, invasion, and growth. From the multiple CNAs identified in tumors, CNA-based gene signatures were developed into a score that suggested the ability to predict metastasis free survival.

2. Methods

2.1. Cohorts and Samples

We studied four publically available prostate cancer cohorts and a fifth cohort reported here: (1) 294 primary tumors and matched normal tissue samples from NYU School of Medicine (NYU $n = 29$), Baylor College of Medicine (Baylor $n = 20$) [6], Memorial Sloan-Kettering Cancer Center (MSK $n = 181$) [7], and Stanford University (SU $n = 64$ (single reference used for each tumor)) [8]. (2) 49 metastatic tumors and matched normal samples from Johns Hopkins School of Medicine (Hopkins $n = 13$) [9] and MSK ($n = 36$) [7]. The 13 patients in the Hopkins cohort had multiple metastases dissected at autopsy, totaling 55 samples for the study. We also studied a sixth, publically available cohort of 337 cell lines originating from varying tumor cell types (ArrayExpress ID: E-MTAB-38).

2.2. Sample Processing

Genomic DNA (gDNA) from the NYU cohort was extracted from fresh-frozen prostate tumors using a Gentra DNA extraction kit (Qiagen). Purified gDNA was hydrated in reduced TE buffer (10 mM Tris, 0.1 mM EDTA, pH 8.0). The gDNA concentration was measured using the NanoDrop 2000 spectrophotometer at optical density (OD) wavelength of 260 nm. Protein and organic contaminations were measured at OD 280 nm and 230 nm, respectively. Samples that passed OD quality control thresholds were then run on a 1% agarose gel to assess the integrity of the gDNA. 500 ng of gDNA samples was run on the Affymetrix Human SNP Array 6.0 at the Rockefeller University Genomics Resource Center using standard operating procedures. Samples that were obtained from public sources were processed according to the methods outlined in their respective publications. Affymetrix .cel files were processed using the Birdseed v2 algorithm [10].

2.3. Study Design

The case samples in this study were either metastatic tumors (METS) or primary tumors from men treated with radical prostatectomy that were clinically followed up and reported to develop distant metastases (mPTs). METS and mPTs are clearly discernible phenotypes that can be classified unequivocally as cases. The control samples were defined as primary tumors that had not progressed to form distant metastases following radical prostatectomy either because clinical followup was not available or because the treatment rendered the patient not informative for this outcome. Radical prostatectomy treats both indolent primary tumors (iPTs) that would not metastasize and primary tumors that would otherwise progress to form metastases, if left untreated. Thus, the control primary tumors actually represent a mixture of iPTs and unrealized mPTs. Assuming a randomly sampled cohort, it is expected that about 30% of the control group of primary tumors would be unrealized mPTs [2]. Considering the scarcity of clinically informative mPTs and iPTs for study, our strategy for identifying CNA biomarkers from tumors with inferred metastatic outcomes allowed a greater number of individual genomes to be used. Accordingly, all of the clinically informative mPTs available to us were not used to identify the biomarkers and only tested in a Cox proportional hazard model to assess the clinical usefulness of these predictors. Future tumor cohort study design using the method presented in this paper should consider the prevalence of metastatic progression to assure a large enough representation of both mPTs and iPTs. The natural history of prostate cancer, without medical intervention, (e.g., watchful waiting or active surveillance) is well documented [2]. Assuming a randomly sampled cohort, this information allowed us to estimate the prevalence of mPTs to be 30%.

2.4. Cancer Genomics Copy Number Algorithm

A genomic DNA copy number analysis pipeline (Figure 1) was designed using the R-statistical software [11] (R) to process the raw intensity data through a series of computational steps resulting in ranked lists of genes and associated significance that could be used for functional mining and prediction model development. The R-package will be provided upon request and raw and processed data can be obtained from Gene Expression Omnibus accession# GSE27105.

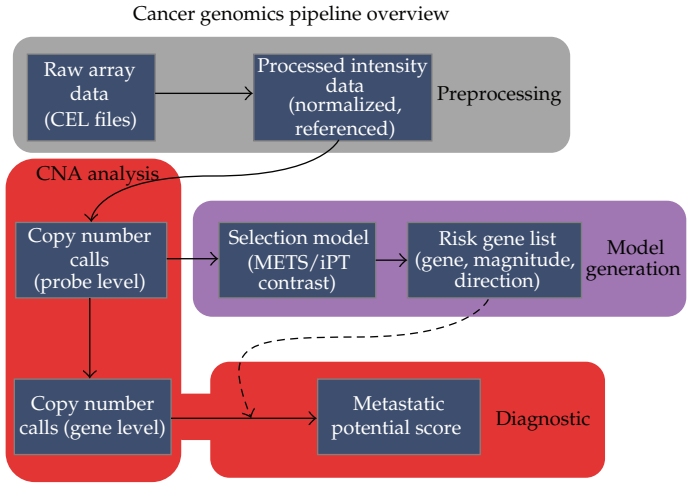

Figure 1: Array CGH analysis pipeline for processing pixel image data from Affymetrix SNP arrays to produce genotype and signal intensity measures for copy number analysis used for developing bioclinical models and diagnostics.

2.5. *Raw Data Processing*

Signal intensity files (.cel) for the Affymetrix SNP Array 6.0 or 500 k mapping arrays were processed using the Affymetrix Power Tools, Birdseed V2 [10], and BRLMM [12] algorithms, respectively, resulting in genotype allele calls and signal intensity measures for each SNP and copy number probe. After the first stage, the genotype calls were prepared for downstream principal component analysis for ethnic identification and quality control testing, especially important when investigating racially driven health disparities (Figure 2). Men of African descent have an increased incidence, earlier onset, and more aggressive form of the disease than those of European origin. Even when adjusted for the increased level of incidence in African Americans, the mortality rate of African American men is more than twice that of Caucasian men [1]. Although not presented in the current work, sophisticated CNA models of metastatic disease may provide a biological explanation for the epidemiological observations of racial health disparity of metastasis.

The probe-summarized intensity signals were log transformed and standardized (mean centered, standard deviation scaled) on an individual array basis and the relative copy number was calculated by subtracting the normal from the tumor intensity for each patient on a probe basis. The resulting copy number profile (CN) represented the amplification and deletion events that accumulated in each cancer sample tested.

Next, the probes were ordered as they appear in the genome and the copy number signal data (CN) was smoothed. The smoothing was conducted using a running median function (runmed in *R*, with endrule parameter equal to "median"). The smoothing function was termed $S(\mathrm{CN})_k$, where k represents the probe width of the smoothing window. The values of k usually range from 5 to 151, depending on the array's probe density and were chosen not to exceed a biologically meaningful span of total genetic distance. Considerations for k should include the average alteration size (estimated empirically from each data set) and distance between probes as determined by the array probe density. As an extreme example, smoothing the entire arm of a chromosome will remove all local variation that

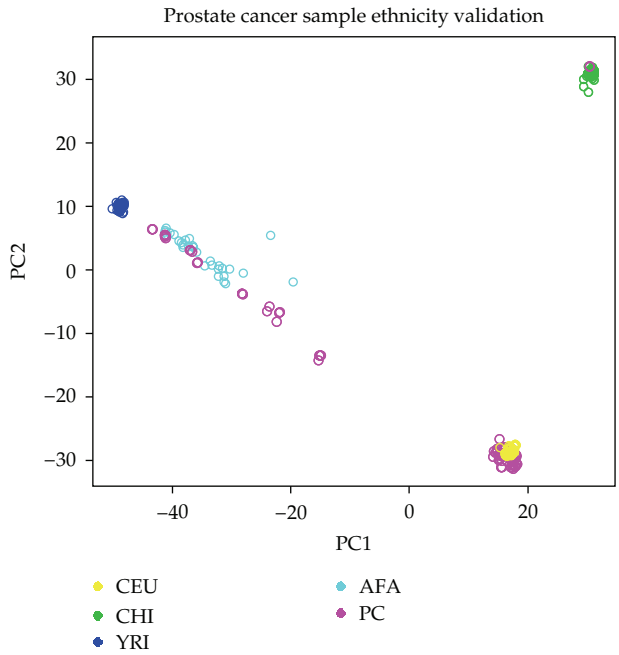

Figure 2: Principal component analysis identity testing of a variety of normal SNP profiles from the germline DNA of prostate cancer patients (PC) used in the study compared to a set of HapMap normal reference populations from Nigeria (YRI), Europe (CEU), China (CHB), or, of African American (AFA) decent. The x and y axes represent the 1st and 2nd eigenvectors.

exists on that arm. The function $S(\mathrm{CN})_k$ thus yielded n smoothing profiles per sample, with n representing the number of different values used for k. An example of the multiple n values used for chromosome 1 of a particular sample is shown in Figure 3.

2.6. Copy Number Alteration Calling Algorithm

The next part of this stage involved assigning copy number events to each probe. The reason we developed a CNA caller from scratch was because the standard calling algorithms required parameter inputs that were dependent on the signal-to-noise distribution of the copy number measures. Because cancer samples' signal-to-noise are notoriously variable, both on a chromosome basis (within a sample profile) and across samples, this made the standard CNA calling approaches inefficient without significant reconfiguration. Therefore, we developed a method that was dynamic to the signal-to-noise variation observed in cancer genomes. We validate the effectiveness our approach (Figure 4) using a benchmark simulation data set used to test a variety of algorithms [13]. Given that SNP arrays are not designed to provide quantitative measures of copy number (but do respond linearly to CNAs), we restrict our calls to three categories: amplifications (1), deletions (−1), and neutral events (0). To determine the "center" of the genome so that thresholds can be drawn, we assume that a majority of the intensity values reflect a 2-copy state for the referenced sample, that is, the majority of the referenced tumor sample exists in a 2-copy state (manual calling is used for those samples in which this assumption is not valid). To accomplish this, we sample

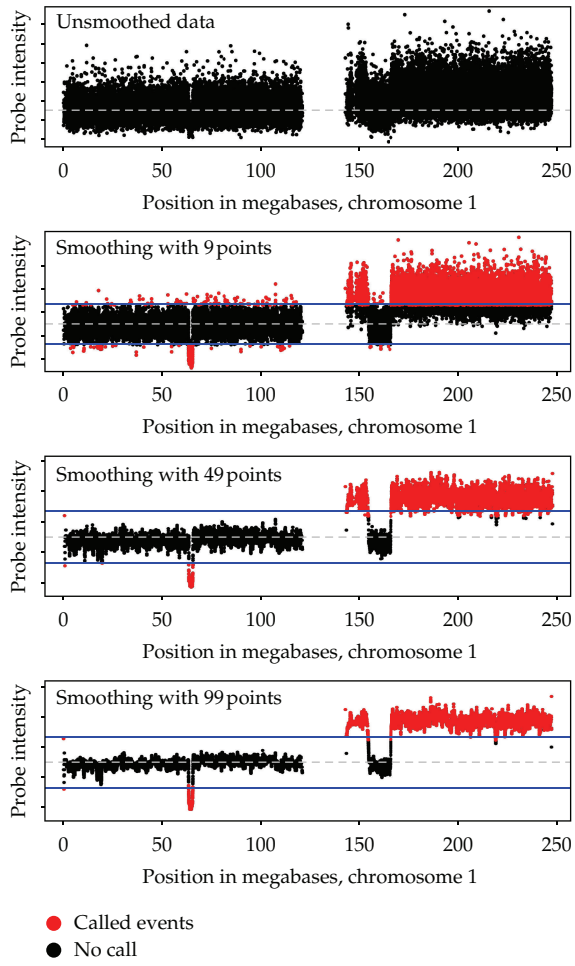

Figure 3: A representative primary tumor chromosome 1 copy number profile (top panel) and corresponding $S(\mathrm{CN})n$ $[k = \{9, 49, 99\}]$ in the bottom panels. Therefore, $n = 3$ because three different smoothing lengths are used. Black probes represent probes that are not called while red probes are the called events that exceed the amplification and deletion thresholds.

10,000 random stretches of probes covering approximately 500 kilobases from the autosomes, calculate the median of each, and use the most frequently occurring value to scale the sample appropriately. Following scaling of the genome, thresholds were drawn based on quantile values and copy number states were assigned to each probe. Since this thresholding scheme was applied to every smoothing, there were n event calls per probe. These calls result in a "ρ" profile, where $T()$ represents the function of trinary binning:

$$\rho_k = T(S(\mathrm{CN})_k). \tag{2.1}$$

The $n\rho$ calls for each probe were then combined by summation, resulting in a composite profile (ρ') that ranged from $-n$ (signifying that a deletion was called at every smoothing

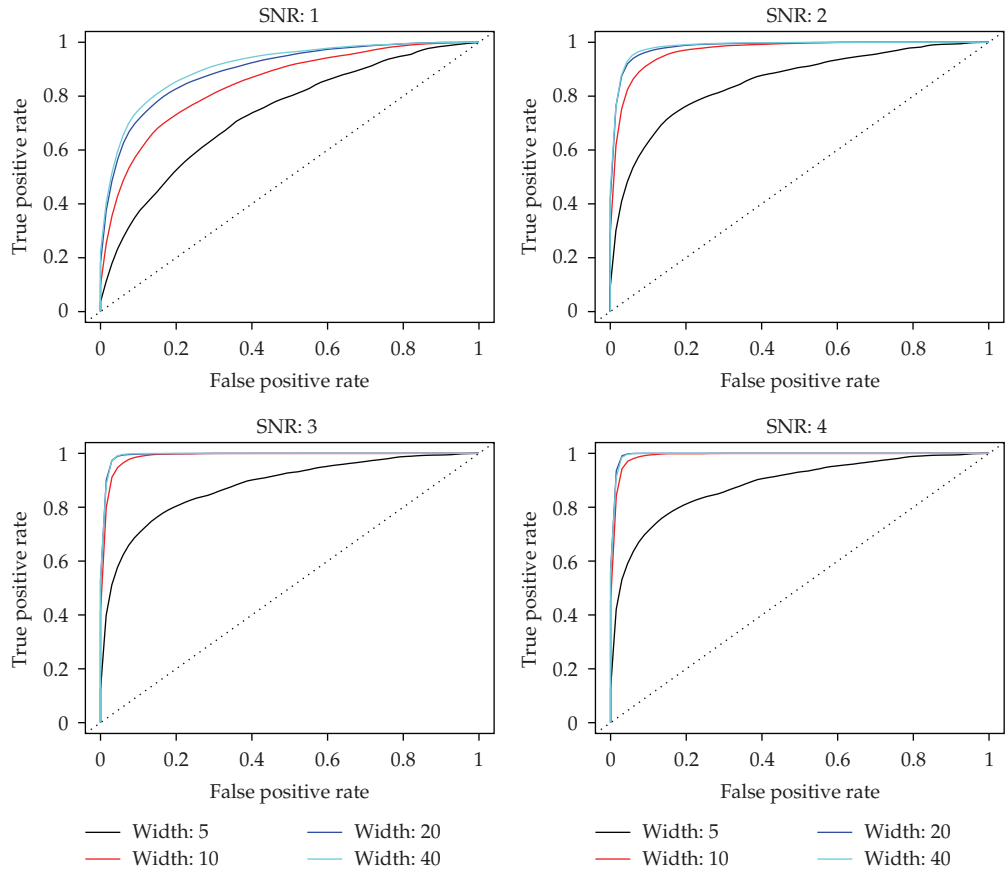

Figure 4: Receiver-operating characteristic curves showing the performance of our CNA-calling algorithm on the simulated data [13]. Each panel represents a different signal-to-noise ratio and the curves represent varying event widths of the simulated data. The x-axis represents the false positive rate, and the y-axis represents the true positive rate. Each curve is generated by testing varying thresholds on 100 simulated chromosomes for the condition specified. The curves are combined using vertical averaging. The dashed line represents the random model.

for that probe) to $+n$ (signifying that an amplification was called at every smoothing for that probe):

$$\rho' = \sum_{i=1}^{n} \rho_i. \tag{2.2}$$

One ρ' profile was thus generated per sample, representing a composite of n smoothings, and this metric was used for the rest of the primary analysis. We benchmarked our copy number calling method using a published simulation data set [13] comprised of randomly generated artificial chromosomes. Each chromosome was generated with an aberration flanking the center probe with Gaussian noise $N(0, 0.25^2)$ superimposed. All combinations of signal to noise (SN = $4, 3, 2,$ and 1) and aberration widths ($W = 40, 20, 10,$ and 5) were produced for a total of 160,000 analysis runs. Receiver-operating characteristics (ROC) were computed from the benchmark simulation dataset [13];

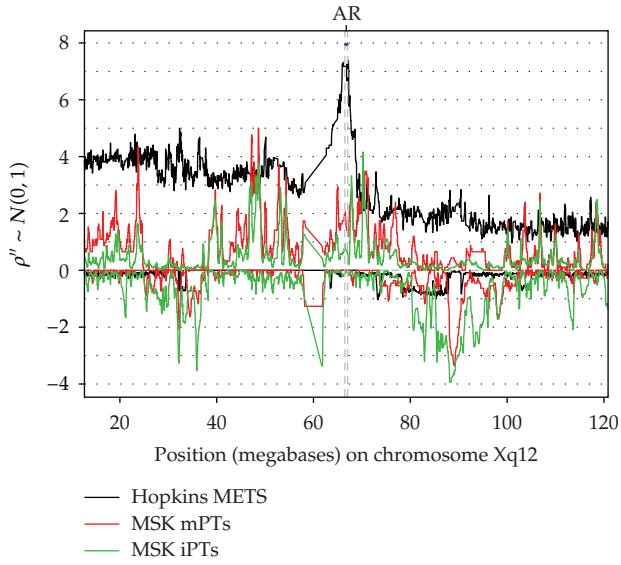

Figure 5: Copy number profile, ρ'' shows an amplification of a region on chromosome X harboring the androgen receptor (AR) locus. The x-axis represents the ordered chromosome position and the y-axis represents standardized population frequencies exhibiting amplifications (above 0) and deletions (below 0). The three populations of tumors are represented as red, black, or green lines for mPTs, androgen ablation treated metastases (METS), and iPTs, respectively.

where ROC is defined as a pair, ROC = (TPR, FPR), TPR = (the number of probes within the aberration width that is above a threshold)/(the total number of probes within the aberration width). FPR = (the number of probes outside the aberration width that is above a threshold)/(the total number of probes outside the aberration width). The threshold values are selected to continuously range over the values of the data points, and since ROC is piecewise constant, only changing when a threshold is equal to the value of a data point, we only need to consider values of the data points in their sorted order. The area under the curve (AUC) of each ROC curve was used to gauge performances.

To examine the frequency of amplification and deletions for subgroups of samples or populations and evaluate the sensitivity of our CNA-calling method, we further combined the ρ' data to create ρ'' by summing across the ρ' profiles on a probe basis across multiple samples. Two values of ρ'' were calculated for population or subpopulation. The first value represented the sum of all positive ρ' values in the population at any probe and was thus called ρ''_{amp}. Likewise, the second value representing the sum of all negative ρ' values in the population at any probe was called ρ''_{del}:

$$\rho''_{\text{amp|del}} = \sum_{i=1}^{n \text{ samples}} \rho'_{[\text{amp|del}]}. \tag{2.3}$$

An example of copy number ρ'' plot (Figure 5) is observed in a select region on chromosome X from metastases of men treated with androgen ablation therapy and primary tumors of iPTs and mPTs from other men not treated. Furthermore, differential analysis of the ρ'' values can be used to identify probes or regions of probes that comprise genes that may contribute to

the phenotype being tested (e.g., iPT versus mPT or response to therapy versus no response to therapy).

2.7. Semisupervised Clustering Algorithm

Since sufficient labels were not available to train a model from primary tumors alone, we first created from a cohort of men that developed distant metastases a simplified summary metastasis profile to capture the high-frequency events, that are in part, assumed to correlate to the outcome. This clustering approach is not unsupervised, class-less clustering because we know some information about one of the components which is the summary profile from known metastasis samples. To reflect the frequency of events observed for individual metastasis CNA profiles in the summary metastasis profile, the average number of ρ' events calculated for the group of metastases was used to set a threshold for the number of total ρ' events used to build the summary metastasis profile. The actual probes chosen for the metastasis summary profile were based on their ranked frequency which resulted in a threshold of at least 25% of the samples exhibiting the event. Although not tested here, the theoretical specificity of the summary profile is expected to decrease as the threshold for minimum number of events called decreases, while the sensitivity of the profile decreases as the threshold of minimum number of events called increases. In the case of the MSK cohort, clustering of the 36 metastases ρ' profiles independently yielded two well-separated clusters from which we built two metastasis summary profiles to perform semisupervised clustering with the primary tumors. Alternatively, the 13-patient Hopkins cohort made up of 55 metastases yielded only one homogeneous cluster and associated summary metastasis profile. To overcome the inherent variability with clustering algorithms, we employed a resampling hierarchical clustering method to infer an initial grouping for the unclassified primary tumors. For each iteration, a subset of the individual ρ' profiles from the unknown primary tumors were randomly chosen with replacement and clustered with the summary copy number profile derived from the metastasis samples (one metastasis summary profile from the Hopkins cohort and two from MSK cohort). Therefore, the semisupervised clustering analysis presented here was developed to classify prostate primary tumors into subgroups with different metastatic potential (mPT and iPT) based on their CNA profiles. Distance was calculated using a binary metric, and the samples were joined using hierarchical clustering (complete-linkage method). The cluster tree was divided into two groups at the final join, and the primary tumor samples were scored 1 if they fell in the same cluster as the metastasis profile, and 0 if they were in the other cluster. Using the results from 20,000 resampling iterations of the clustering, a proximity score was generated for each sample, representing the number of times it fell in a cluster with the metastasis profile. A sample with a high score was considered to be more metastatic (mPT), while lower scoring tumors were more indolent (iPT). The similarity scores distributed throughout the possible range of values (0 to 1), allowing us to form distinct groups of tumors with significant contrast between high- and low-metastatic distance to MSK metastasis signature 1 (Figure 6). The group of samples with scores closer to the center of the distribution were omitted to further define the contrast between high- and low-scoring samples.

2.8. Metastasis Genes Inferred through Evolutionary Selection Modelling

Genomic DNA copy number alterations in local and metastatic prostate tumors are typically numerous, systematic in their genomic placement and varied in size from point mutations

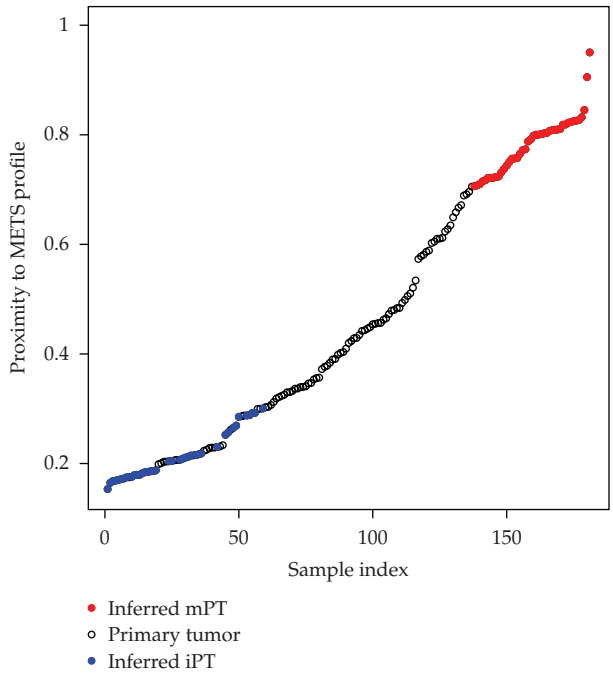

Figure 6: Plot of ranked proximity score for MSK signature 2. Proximity represents the number of times a particular sample clustered with the MSK metastasis profile 2. The samples with higher scores (red points) are classified as inferred mPTs and the samples with lower scores (blue points) are classified as inferred iPTs. Primary tumors (hollow points) interspersed with the blue iPT tumors were excluded as iPTs for MSK signature 2 because they did not consistently classify as iPTs in the proximity analysis using MSK signature 1.

to duplications or deletions of entire chromosomes. Given these observations, geneticists have postulated that Darwinian selection may operate on the genomic instability in tumors [14]. High-resolution measurements of CNAs in somatic tumors have informative value, in some cases reflecting the direction in which the biochemistry of the cell controls the quantity of normal, mutant, or hybrid-fusion transcripts and proteins. During this genomic transformation, the resulting modified transcripts and proteins may impact the fitness of the cell. Guided by these principles of evolutionary selection, our analyses sought to identify the CNA landscape that reflects selection mechanisms of metastasis. Genomic selection towards a metastatic cancer phenotype can be both positive and negative and be observed in CNAs exhibiting both amplifications and deletions. For example, genes that promote metastasis and amplified in metastatic tumors would reflect positive selection, while metastasis suppressor genes that are deleted in metastases reflect negative selection. The genes associated with these regions, altered at high frequency in metastatic tumors and enriched in mPTs more so than iPTs, lead to enhanced metastatic potential. We identified specific CNAs that selected positively for metastatic potential, exhibiting amplifications in metastases and mPTs and deletions in iPTs. CNAs identified to exhibit negative selection for metastatic potential were observed to be deleted in metastases and mPTs and amplified in the iPTs. Therefore, we designed models based on Darwin's evolutionary selection theory to score positive and negative selection based on the mPT and iPT classifications derived through semisupervised clustering using the ρ' data. For each probe on the array, we calculated an enrichment score,

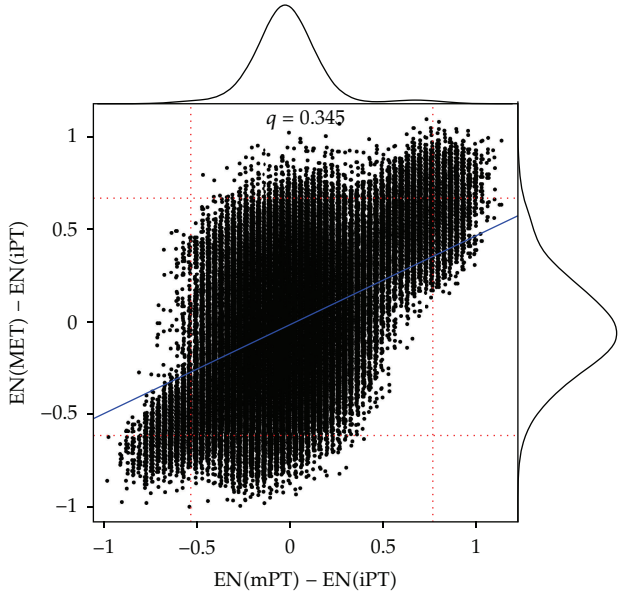

Figure 7: Scatterplot of the enrichment scores of the METS versus those of mPTs, normalized by the enrichment scores of iPTs. Kernel density estimation curves are shown protruding from the x and y axes. The horizontal and vertical dashed red lines denote the trim points (quantiles 0.99 and 0.01). A linear regression line, based on the trimmed values, is shown in blue. The value of q is the Pearson correlation coefficient for the trimmed x and y values.

EN(x), which represented the relative number of amplifications versus deletions, observed in each subgroup (metastasis, mPT and iPT):

$$\mathrm{EN}(x) = \frac{(\#\mathrm{Amp} - \#\mathrm{Del})}{\#\mathrm{Samples}}. \tag{2.4}$$

Next, we modeled the relative enrichment by contrasting the metastasis and mPT copy number alterations with those observed in the iPT group:

$$\mathrm{SM} = e^{[\mathrm{EN(METS)}+q^{*}\mathrm{EN(mPT)}-\mathrm{EN(iPT)}]}. \tag{2.5}$$

The first two enrichment terms (for metastatic and metastatic-like samples) being summed were designed to assign a higher score when the METS and mPT samples had more amplifications than deletions. Greater amplification enrichment in the METS and mPTs resulted in higher scores. The third term, EN(iPT), was higher when the iPT samples exhibit the opposite effect (enrichment for deletions over amplifications). The middle term, EN(mPT), was multiplied by a data-driven coefficient, q, representing the average contribution of mPT on a probe basis (Figure 7).

For example, probes that were amplified in all metastases and mPTs but deleted in all iPTs (positive selection driving the metastasis cells) would yield the highest possible score. Likewise, probes that were deleted in all metastases and mPT samples, but amplified in all iPT samples (negatively select or inhibit the promotion of the metastasis cells), would

reach the minimum possible score. Therefore, regions of the genome that enhance and inhibit metastasis formation will be captured by our evolutionary selection model.

Following this probe scoring method we developed a Z-score model in order to extend this analysis to the gene level. We assign each probe to a gene, provided it falls within 10,000 bp up- or downstream of the transcription start or stop site. The SM scores for the probes within a gene are averaged and compared to the mean and standard deviation of a background distribution, which was calculated by sampling the top 5th percentile of amplified or deleted probes from all genes on the array with the same number of probes as the gene in question. The result is a Z-score for each gene in the genome that is represented on the array.

2.9. Metastatic Potential Score and Survival Analysis

We developed an algorithm based on genomic CNAs to calculate a metastatic potential score (MPS), with a higher score indicating a greater likelihood of metastasis. The MPS score for a new individual patient only depends on the CNA profile of this new patient. It can be calculated without requirement for other samples, since it's simply based on the concordance/discordance relationship to the CNA metastasis gene signature previously identified as selecting for the metastatic phenotype through our selection model. The MPS was calculated using a weighted Z score from the top set of CNAs overlapping metastasis genes determined by the significance of their selection model Z scores. We used $Z \geq 1.7$ as a cutoff point because for standard normal distribution, the tail of 1.7 is about 5%. The metastatic potential score was defined as the following:

$$\text{MPS} = \sum_{i=1}^{n} Z_i' * \text{Dir}_{\text{sig}}(i) * \text{Dir}_{\text{samp}}(i). \tag{2.6}$$

For each tumor profile, logistic adjusted Z scores (Z') from genes ($i \ldots n$) that match the direction of the metastasis gene signature (a vector of −1s and +1s representing whether the gene was deleted or amplified in the signature, resp.) were added, whereas Z' from genes that mismatch the direction of the signature were subtracted. As the direction component of the risk model score (Dir) reflects, if the CNAs of the metastasis signature (Dir_{sig}) and the unknown sample profile (Dir_{samp}) are in the same direction, the coefficient will be 1; if they are in opposing directions, the coefficient will be −1; and if $\text{Dir}_{\text{samp}}(i) = 0$, then the entire term will not count towards the score. For example, if a gene i, that is typically amplified in metastases ($\text{Dir}_{\text{sig}}(i)$) and mPTs, is also amplified in the unknown profile ($\text{Dir}_{\text{samp}}(i)$) that Z score is added, whereas if gene i in the profile is deleted, as expected in iPTs, the Z score is subtracted. Neutral genes that are neither amplified nor deleted in the unknown profile are not scored in this model.

Three metastasis signatures, derived from a combination of five cohorts were used to develop the MPS. The first signature was identified using 49 primary tumors of unknown clinical outcome from NYU ($n = 29$) and Baylor ($n = 20$) and a metastasis cohort from Hopkins ($n = 13$). The other two signatures were identified using 75% of the MSK cohort of primary tumors of unknown outcome ($n = 126$) along with a set of metastatic tumors ($n = 36$) from the same MSK cohort. The CNA-based gene signatures from these 2 sets of cohorts were concatenated and derived into the MPS which we assessed in a Cox proportional hazard model with samples set aside for testing purposes only. The test cases were comprised

of bona fide mPTs (primary tumors that later developed into distant metastasis), whereas the test controls were derived from a random sample of tumors with unknown outcome not used to build the MPS. All presurgery predictors (PSA, clinical stage, biopsy Gleason) and other demographic variables (age at diagnosis and race) were tested independently and in combination with the MPS in Cox proportional hazards survival analysis with the time variable represented by progression to metastasis.

3. Results

3.1. Prediction Models

Our selection models resulted in three hundred and sixty-eight genes (from 3 metastasis signatures) with a CNA status that was concordant among METS and mPTs and contrasted with iPTs ($Z \geq 1.7$) (Supplemental Table 1, see Supplementary Materials available online at doi:10.1155/2012/873570). With these genes, we developed the MPS and tested the accuracy as an independent predictor of metastasis, with a subset of primary tumors ($n = 52$) not used to develop the signatures ($n = 13$ mPTs and $n = 39$ control primary tumors, Table 1). As a continuous predictor, applying the MPS to a Cox proportional hazards model resulted in a significant association to the endpoint of metastasis-free survival (2.88; 95% CI = 1.15 – 7.2; $P = 0.02$) (Table 2).

Patients diagnosed with prostate cancer have several pretreatment variables, such as, clinical stage (combination of digital rectum exam, PSA, and ultrasound/MRI), biopsy Gleason score and other demographic measures (e.g., age or race) to guide the decision to undergo surgery. These variables have marginal clinical utility and, in our cohorts, none of these clinical variables were statistically significant in univariate or multivariate logistic regression models. In multivariate Cox regression models (Table 2), only the MPS score reached statistical significance, indicating, that the MPS score was the only reproducible predictor of metastasis-free survival.

Notably, the clinical stage was specific when palpable tumor was detected (T2 or greater); however, it lacked sensitivity, because 47% (9/19) of pathological stage-4 cases that evaluated *ex-vivo* were diagnosed as T1C before surgery [7]. Twenty-seven percent (13 out of 49) of clinical stage T1C tumors that were upstaged following prostatectomy resulted in distant metastasis formation. Therefore, staging at the time of biopsy can seriously underestimate the severity of disease. Similarly, the biopsy Gleason score versus the postsurgery Gleason score was underestimated in 38% of cases and overestimated in 8% [7] (Figure 8).

3.2. Metastatic Potential Score Distributions

Significant differences as measured by Mann-Whitney test of the MPS were observed for the metastasis ($P < 0.001$) and mPT ($P = 0.001$) groups, compared to the control primary tumors (Figure 9). The MPS in the lymph-node-positive primary tumors (derived from the MSK ($n = 9$) and Stanford ($n = 9$) cohorts did not differ significantly from the control tumor group ($P_{\text{MSK}} = 0.34, P_{\text{Stanford}} = 0.13, P_{\text{Combined}} = 0.08$), which reflected the marginal ability of this clinical parameter to predict distant metastasis in previous reports [15].

Consistent with our assumption that the control cohorts contained a fraction of mPTs, their MPS overlapped the MPS range of the cases. Furthermore, control primary tumors

Table 1: Clinical And histological characteristics of samples used to validate the metastatic potential score model.

	Case	Control
n	13	39
Age		
Mean	59.5	59.1
Median	61	58
Standard deviation	7.1	7.3
Range	46–67	46–73
Race		
Asian	0 (0%)	1 (1.9%)
Black	1 (1.9%)	4 (7.7%)
Unknown	0 (0%)	2 (3.8%)
White Non-Hispanic	12 (23.1%)	32 (61.5%)
Clinical stage		
T1C	4 (7.7%)	23 (44.2%)
T2	5 (9.6%)	16 (30.8%)
T3	4 (7.7%)	0 (0%)
T4	0 (0%)	0 (0%)
Biopsy Gleason score		
5	0 (0%)	0 (0%)
6	4 (7.7%)	26 (50%)
7	7 (13.5%)	10 (19.2%)
8	2 (3.8%)	2 (3.8%)
9	0 (0%)	1 (1.9%)
Prediagnosis biopsy PSA (ng/mL)		
Median	6.9	5.6
<4	2 (3.8%)	6 (11.5%)
4–10	6 (11.5%)	24 (46.2%)
>10	4 (7.7%)	7 (13.5%)
Pretreatment PSA (ng/mL)		
Median	12.8	5.6
<4	2 (3.8%)	7 (13.5%)
4–10	4 (7.7%)	26 (50%)
>10	7 (13.5%)	6 (11.5%)

Table 2: Cox proportional hazards model analysis of the metastatic potential score and clinical predictors.

Component	Hazard ratio	*P*	95% CI
Univariate			
MPS	2.87	0.02	1.2–7.2
Pretreatment PSA	1.00	0.04	1.0–1.1
Clinical stage T2-T3	1.27	0.70	0.4–4.2
Multivariate			
MPS	2.61	0.05	1.0–6.8
Clinical stage T2-T3	0.90	0.87	0.3–3.1
Pretreatment PSA	1.00	0.18	1.0-1.0

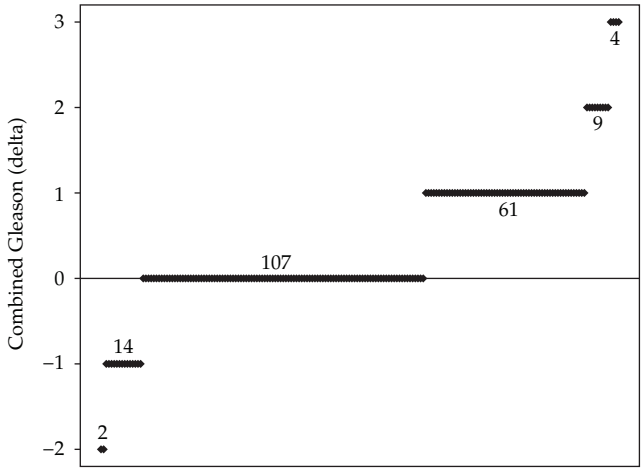

Figure 8: Biopsy versus pathology Gleason score. The difference between the Gleason score as measured from a biopsy of the tumor relative to the pathological assessment of the score using the radical prostatectomy surgical specimen (y-axis). The x-axis represents the sample index.

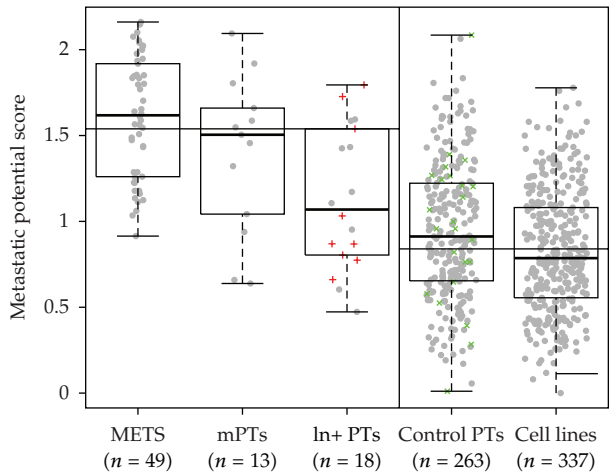

Figure 9: Boxplot showing the metastatic potential scores for all samples involved in the analysis. All high-risk tumors are shown in the left three boxes (metastases, progressors, and lymph-node-positive samples), while unknown control primary tumors and the publically available cell line data are shown in the right boxes. The red "+" symbols in the lymph-node-positive box represent those samples from the MSK dataset, distinguishing them from the SU cohort lymph-node-positive samples. The green "x" symbols in the control primary tumors plot represent selected low-risk primary tumors (individuals with no biochemical recurrence (PSA) for at least 80 months).

(from MSK cohort) that did not recur biochemically (as measured by PSA) after 80 months of followup, (represented by green Xs in Figure 9) were not significantly correlated with the MPS. To determine whether other cancer types exhibited a similar metastatic landscape of CNAs to that observed in prostate cancer, we calculated the metastatic potential score for 337 cancer cell lines. We observed an overall distribution that overlapped with low-risk prostate primary tumors (Figure 9). However, 22 of the 337 cell lines ranked by MPS were above the

75th percentile of the prostate primary tumors and metastases. These cell lines originated from tumors of the lung ($n = 10$), breast ($n = 3$), colon ($n = 2$), and melanoma ($n = 2$). Other singletons in this group of 22 cell lines originated from thyroid, rectum, pharynx, pancreas, and kidney.

3.3. *Biomarker Functional Significance*

Another way to validate our algorithms is by data mining the functional attributes of the metastasis genes identified by the selection model. As expected, many of the top-ranking metastasis genes identified have molecular functions related to alteration of nuclear and extracellular matrix structure and metabolic modification that enhance processes characteristic of escape from anoikis (a key metastasis specific process). A heat map of the CNA events of signature genes for all prostate tumors is suggestive of a path toward the different high frequency amplification versus deletion events that contrast the high-risk and low-risk tumors (Figure 10). The mid-risk region with its relative paucity of signature events may represent the starting point of two alternative pathways of subsequent copy number alteration, one leading to metastasis and the other to an indolent state. The locking in of these "antimetastasis" events in indolent tumors may explain why they failed to metastasize despite extended periods of watchful waiting.

One of the top predictor genes, the solute carrier family SLC7A5 gene, deleted on chromosome 16q24.2, encodes a neutral aminoacid transporter protein (LAT1) that has been implicated in multiple cancers (prostate [16], breast [17], ovarian [18], lung [19], and brain [20]) and has been shown to have utility as a diagnostic [21–23] and drug target in cell line [24–26] and preclinical animal models [27]. The normal function of LAT1 is to regulate cellular aminoacid concentration, L-glutamine (efflux) and L-leucine (influx). Reduced activity of LAT1 results in increased concentrations of L-glutamine which has been shown to constitutively fuel mTOR activity [28]. Seven other solute carrier superfamily members (SLCO5A1, SLC7A2, SLC10A5, SLC26A7, SLC25A37, SLC38A8, and SLC39A14) were predictive of metastatic potential in our models, likely creating a cellular environment conducive to metastasis.

A second subset of signature genes included 6 Cadherin family members encoding calcium dependent cell adhesion glycoproteins (CDH2, CDH8, CDH13, CDH15, CDH17, and PCDH9). Many of the Cadherin family proteins have putative functions associated with metastasis progression [29] and have been included in diagnostic panels [30, 31].

A third subset of 5 genes predicted to contribute to metastatic potential were potassium channels, KCNB2, KCNQ3, KCNAB1, KCTD8, and KCNH4. Notably, 3 other potassium channels reside in the highly amplified region between 8q13 and 8q24 (KCNS2, KCNV1 and KCNK9) that did not rank high in our analysis but may have weak or modifier effects. High levels of cytoplasmic potassium ion concentrations have been shown to inhibit the hallmark mitochondrial apoptotic cascade of membrane disruption and ensuing release of cytochrome C, caspase, and nuclease degradation of cellular components [32]. Furthermore, another study showed that the methylation status of potassium channel, KCNMA1 (10q22.3), was predictive of prostate cancer recurrence [33]. The activity of voltage-gated potassium channels in prostate cancer cell lines, LNCaP (low metastatic potential) and PC3 (high metastatic potential), were observed to be markedly different [34]. The complete set of metastasis signature genes likely represents various subsets of functions. Representation of different gene family members suggests that each tumor may have a unique profile to

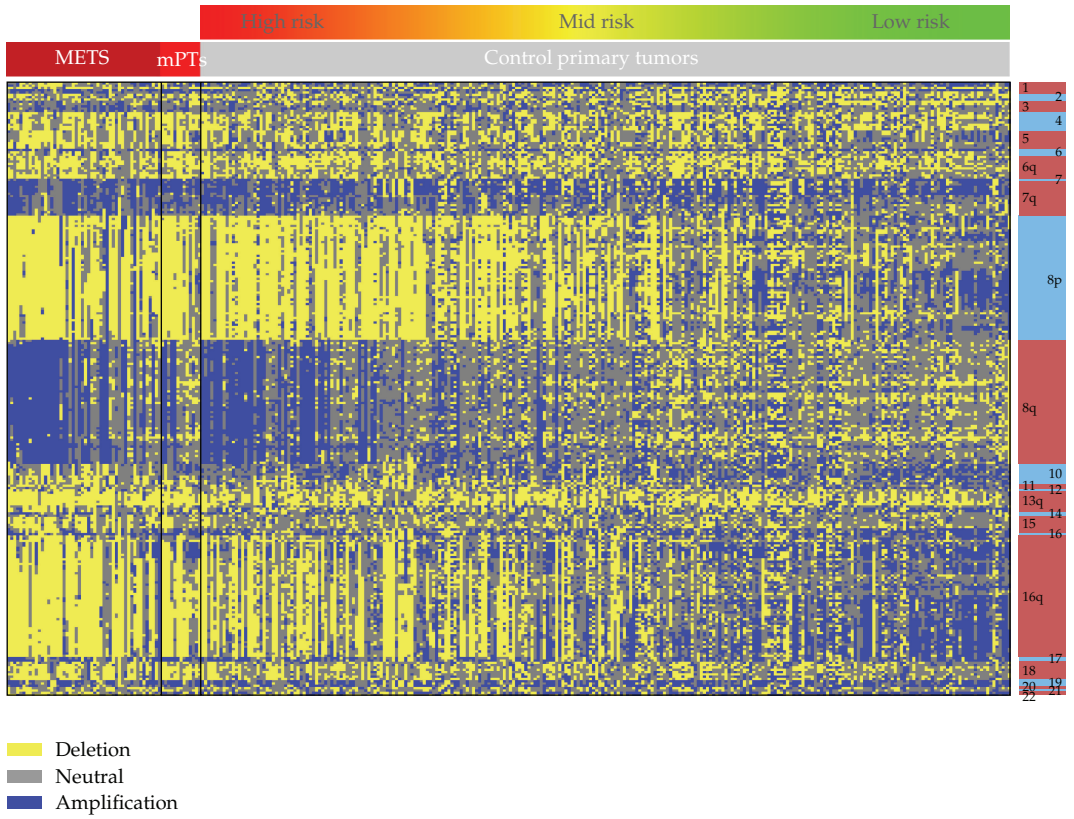

Figure 10: Heatmap showing copy number amplifications and deletions for tumor samples in the gene signature. The genes are arranged in genomic order; position is indicated by the colored bar on the right. The tumor samples (x-axis) are arranged by subtype (metastatic (METS), progressors (mPTs), and control primary tumors) and further sorted by their metastatic potential score. A strong pattern emerges in the metastasis samples on the left and is shared by the progressors and high-risk primary tumors. Further towards the right, the metastatic pattern diminishes and even shows a reversal in copy number pattern in some chromosomal areas.

progress to metastasis, yet different members of a gene family may contribute to a functional redundancy. Notably, the genomic DNA landscape around the androgen receptor locus on chromosome X represents a compelling observation linking CNAs to a functional cause and effect response of androgen ablation therapy (Figure 5).

4. Summary

In this study, we developed a semisupervised clustering algorithm that can infer the classification of a primary tumor based on metastatic risk. This was essential to overcome the limitations inherent to prostate cancer cohorts for collecting long-term clinical outcome data. Our novel approach to modeling the CNA data based on Darwin's evolutionary selection theory allowed us to identify genes associated with the specific metastatic processes of anoikis. Current clinical models for assessing risk are aimed at predicting biochemical recurrence, rather than metastasis, and do not include genomic information. This limitation

was underscored in a study with a large cohort of greater than 10,000 men who had undergone radical prostatectomy [35]. Within that cohort, about 20% of men developed biochemical recurrence within 5 years of the procedure, but subsequently only 10% of the men with biochemical recurrence developed distant metastases after 12 years.

This proposed new classification method and selection model allowed us to develop a metastatic potential score that could be used for predicting an individual's metastasis-free survival at the time of diagnosis. With validation in additional cohorts and statistical models with known metastasis outcome, this approach may lead to a significant advancement in determining whether aggressive treatment of prostate cancer is necessary. This predictor might be important for correctly categorizing men at the time of diagnosis and could predict whether surgery, radiation therapy, or watchful waiting was warranted. Because the proposed tool, tumor genomic analysis, is comprehensive for identifying the genetic changes that are associated with the pathogenesis of metastasis, there is a greater likelihood of selecting a sufficient number of markers that are both sensitive and specific predictors. This method could be applied to other cancers (e.g., breast) that exhibit variation in the metastatic potential of the primary tumor and have similar difficulties in collecting tumor samples with long-term clinical outcome data.

Acknowledgments

The authors would like to thank Dr. Kelly Maxwell for extracting the genomic DNA for the NYU cohort and all of the reviewers for their thoughtful suggestions.

References

[1] A. Jemal, R. Siegel, E. Ward, Y. Hao, J. Xu, and M. J. Thun, "Cancer statistics, 2009," *CA—A Cancer Journal for Clinicians*, vol. 59, no. 4, pp. 225–249.

[2] L. Klotz, L. Zhang, A. Lam, R. Nam, A. Mamedov, and A. Loblaw, "Clinical results of long-term follow-up of a large, active surveillance cohort with localized prostate cancer," *Journal of Clinical Oncology*, vol. 28, no. 1, pp. 126–131, 2010.

[3] M. Ohori, M. Kattan, P. T. Scardino, and T. M. Wheeler, "Radical prostatectomy for carcinoma of the prostate," *Modern Pathology*, vol. 17, no. 3, pp. 349–359, 2004.

[4] R. Beroukhim et al., "The landscape of somatic copy-number alteration across human cancers," *Nature*, vol. 463, pp. 899–905, 2010.

[5] J. Sun, W. Liu, T. S. Adams et al., "DNA copy number alterations in prostate cancers: a combined analysis of published CGH studies," *Prostate*, vol. 67, no. 7, pp. 692–700, 2007.

[6] P. Castro, C. J. Creighton, M. Ozen, D. Bcrel, M. P. Mims, and M. Ittmann, "Genomic profiling of prostate cancers from African American men," *Neoplasia*, vol. 11, no. 3, pp. 305–312, 2009.

[7] B. S. Taylor et al., "Integrative genomic profiling of human prostate cancer," *Cancer Cell*, vol. 18, pp. 11–22, 2010.

[8] J. Lapointe, C. Li, C. P. Giacomini et al., "Genomic profiling reveals alternative genetic pathways of prostate tumorigenesis," *Cancer Research*, vol. 67, no. 18, pp. 8504–8510, 2007.

[9] W. Liu, S. Laitinen, S. Khan et al., "Copy number analysis indicates monoclonal origin of lethal metastatic prostate cancer," *Nature Medicine*, vol. 15, no. 5, pp. 559–565, 2009.

[10] J. M. Korn, F. G. Kuruvilla, S. A. McCarroll et al., "Integrated genotype calling and association analysis of SNPs, common copy number polymorphisms and rare CNVs," *Nature Genetics*, vol. 40, no. 10, pp. 1253–1260, 2008.

[11] R. D. C. Team, *R Foundation for Statistical Computing*, Vienna, Austria, 2009.

[12] N. Rabbee and T. P. Speed, "A genotype calling algorithm for affymetrix SNP arrays," *Bioinformatics*, vol. 22, no. 1, pp. 7–12, 2006.

[13] W. R. Lai, M. D. Johnson, R. Kucherlapati, and P. J. Park, "Comparative analysis of algorithms for identifying amplifications and deletions in array CGH data," *Bioinformatics*, vol. 21, no. 19, pp. 3763–3770, 2005.

[14] D. P. Cahill, K. W. Kinzler, B. Vogelstein, and C. Lengauer, "Genetic instability and darwinian selection in tumours," *Trends in Cell Biology*, vol. 9, no. 12, pp. M57–M60, 1999.
[15] S. A. Boorjian, R. H. Thompson, S. Siddiqui et al., "Long-term outcome after radical prostatectomy for patients with lymph node positive prostate cancer in the prostate specific antigen era," *Journal of Urology*, vol. 178, no. 3, pp. 864–871, 2007.
[16] T. Sakata, G. Ferdous, T. Tsuruta et al., "L-type amino-acid transporter 1 as a novel biomarker for high-grade malignancy in prostate cancer," *Pathology International*, vol. 59, no. 1, pp. 7–18, 2009.
[17] K. Kaira, N. Oriuchi, H. Imai et al., "L-type amino acid transporter 1 and CD98 expression in primary and metastatic sites of human neoplasms," *Cancer Science*, vol. 99, no. 12, pp. 2380–2386, 2008.
[18] M. Kaji, M. Kabir-Salmani, N. Anzai et al., "Properties of L-type amino acid transporter 1 in epidermal ovarian cancer," *International Journal of Gynecological Cancer*, vol. 20, no. 3, pp. 329–336, 2010.
[19] H. Imai, K. Kaira, N. Oriuchi et al., "L-type amino acid transporter 1 expression is a prognostic marker in patients with surgically resected stage I non-small cell lung cancer," *Histopathology*, vol. 54, no. 7, pp. 804–813, 2009.
[20] K. Kobayashi, A. Ohnishi, J. Promsuk et al., "Enhanced tumor growth elicited by L-type amino acid transporter 1 in human malignant glioma cells," *Neurosurgery*, vol. 62, no. 2, pp. 493–503, 2008.
[21] J. M. S. Bartlett, J. Thomas, D. T. Ross et al., "Mammostrat as a tool to stratify breast cancer patients at risk of recurrence during endocrine therapy," *Breast Cancer Research*, vol. 12, no. 4, article no. R47, 2010.
[22] B. Z. Ring, R. S. Seitz, R. A. Beck et al., "A novel five-antibody immunohistochemical test for subclassification of lung carcinoma," *Modern Pathology*, vol. 22, no. 8, pp. 1032–1043, 2009.
[23] B. Z. Ring, R. S. Seitz, R. Beck et al., "Novel prognostic immunohistochemical biomarker panel for estrogen receptor-positive breast cancer," *Journal of Clinical Oncology*, vol. 24, no. 19, pp. 3039–3047, 2006.
[24] X. Fan, D. D. Ross, H. Arakawa, V. Ganapathy, I. Tamai, and T. Nakanishi, "Impact of system L amino acid transporter 1 (LAT1) on proliferation of human ovarian cancer cells: a possible target for combination therapy with anti-proliferative aminopeptidase inhibitors," *Biochemical Pharmacology*, vol. 80, no. 6, pp. 811–818, 2010.
[25] K. Yamauchi, H. Sakurai, T. Kimura et al., "System L amino acid transporter inhibitor enhances anti-tumor activity of cisplatin in a head and neck squamous cell carcinoma cell line," *Cancer Letters*, vol. 276, no. 1, pp. 95–101, 2009.
[26] C. S. Kim, S. H. Cho, H. S. Chun et al., "BCH, an inhibitor of system L amino acid transporters, induces apoptosis in cancer cells," *Biological and Pharmaceutical Bulletin*, vol. 31, no. 6, pp. 1096–1100, 2008.
[27] K. Oda, N. Hosoda, H. Endo et al., "L-Type amino acid transporter 1 inhibitors inhibit tumor cell growth," *Cancer Science*, vol. 101, no. 1, pp. 173–179, 2010.
[28] P. Nicklin, P. Bergman, B. Zhang et al., "Bidirectional transport of amino acids regulates mTOR and autophagy," *Cell*, vol. 136, no. 3, pp. 521–534, 2009.
[29] M. Yilmaz and G. Christofori, "Mechanisms of motility in metastasizing cells," *Molecular Cancer Research*, vol. 8, no. 5, pp. 629–642, 2010.
[30] A. Celebiler Cavusoglu, Y. Kilic, S. Saydam et al., "Predicting invasive phenotype with CDH1, CDH13, CD44, and TIMP3 gene expression in primary breast cancer," *Cancer Science*, vol. 100, no. 12, pp. 2341–2345, 2009.
[31] Y. Lu, W. Lemon, P.-Y. Liu et al., "A gene expression signature predicts survival of patients with stage I non-small cell lung cancer," *PLoS Medicine*, vol. 3, no. 12, article e467, pp. 2229–2243, 2006.
[32] D. Ekhterae, O. Platoshyn, S. Krick, Y. Yu, S. S. McDaniel, and J. X. J. Yuan, "Bcl–2 decreases voltage-gated K^+ channel activity and enhances survival in vascular smooth muscle cells," *American Journal of Physiology, Cell Physiology*, vol. 281, no. 1, pp. C157–C165, 2001.
[33] D. K. Vanaja, M. Ehrich, D. Van Den Boom et al., "Hypermethylation of genes for diagnosis and risk stratification of prostate cancer," *Cancer Investigation*, vol. 27, no. 5, pp. 549–560, 2009.
[34] M. E. Laniado, S. P. Fraser, and M. B. A. Djamgoz, "Voltage-gated K^+ channel activity in human prostate cancer cell lines of markedly different metastatic potential: distinguishing characteristics of PC-3 and LNCaP cells," *Prostate*, vol. 46, no. 4, pp. 262–274, 2001.
[35] T. Nakagawa, T. M. Kollmeyer, B. W. Morlan et al., "A tissue biomarker panel predicting systemic progression after PSA recurrence post-definitive prostate cancer therapy," *PLoS One*, vol. 3, no. 5, Article ID e2318, 2008.

Genomic Signatures of Metastasis in Prostate Cancer

FIELD OF THE DISCLOSURE

[0001] This disclosure relates to metastatic gene signatures. More particularly, this disclosure has identified copy number alterations (CNAs) around genes that are over-represented in metastases, which serve as the basis for predicting whether a primary tumor will metastasize.

BACKGROUND ART

[0002] Prostate cancer is a common public health problem. In 2010, this disease was diagnosed in an estimated 217,730 men (28% of all male cancers) and resulted in 32,050 deaths (11% of male cancer deaths) (Jemal et al., *CA Cancer J Clin* 59(4):225-49 (2009)). If left untreated, the majority of prostate cancers remain asymptomatic and indolent for decades (Klotz et al., *Journal of Clinical Oncology* (2010) 28:126-31). If treated with radical prostatectomy or radiation therapy, the risk of metastasis is reduced, but erectile dysfunction, urinary incontinence and rectal bleeding may occur, affecting the patient's quality of life. Because it is currently difficult to determine accurately which patients will develop metastatic disease, physicians treat patients with mid-to-late stage local disease aggressively, even when such treatment may not be required. Clinical parameters, such as serum concentration of prostate specific antigen (PSA), extension beyond surgical margins, invasion of seminal vesicles, extension beyond the capsule, Gleason score, prostate weight, race and year of surgery, are employed in existing nomograms for prediction of local recurrences (Ohori et al., *Mod Pathol* 17(3): 349-359 (2004)), but local recurrence and, therefore, these parameters have limited utility for predicting progression of the disease to distant sites (Nakagawa et al., *PLoS One* 3(5):e2318 (2008)). Development of a robust risk model that accurately predicts the potential of a local prostate cancer to metastasize would justify

aggressive treatment in high-risk cases and improve the quality of life for men with indolent disease.

SUMMARY OF THE DISCLOSURE

[0003] This disclosure is directed to a method of determining the risk of metastasis of prostate cancer in a human subject who has or had prostate cancer. The method is premised in identification of metastatic signature genes and genomic regions whose copy number alterations are overrepresented in metastases.

[0004] In one embodiment, a metastatic gene signature set includes at least the top 80 genes and genomic regions shown in Table 6. In another embodiment, a metastatic gene signature set includes at least the top 40 genes and genomic regions shown in Table 6. In still another embodiment, a metastatic gene signature set includes at least the top 20 genes and genomic regions shown in Table 6. In yet another embodiment, a metastatic gene signature set includes at least the top 12 genes and genomic regions shown in Table 6.

[0005] In a specific embodiment, the method disclosed herein includes determining in a prostate sample from the subject the number of copies per cell of at least 12 genes and/or genomic regions of a metastatic gene signature set which consists of the top 20 genes and gene regions listed in Table 6; determining alternations in the number of copies per cell for each of the at least 12 genes and/or genomic regions as compared to the number of copies per cell in non-cancer cells; and determining the risk of prostate cancer metastasis based on the copy number alternations (CNAs) determined.

[0006] In one embodiment, the at least 12 genes and/or genomic regions being analyzed are the top 12 genes and genomic regions, namely, the PPP3CC genomic region, the SLCO5A1 genomic region, the SLC7A5 genomic region, the SLC7A2 genomic region, the CRISPLD2 genomic region, the CDH13 gene, the CDH8 gene, the CDH2 gene, the ASAH1 genomic region, the KCNB2 genomic region, the KCNH4 genomic region, and the CTD8 gene.

[0007] In another embodiment, the at least 12 genes and/or genomic regions being analyzed include all of the top 20 genes and genomic regions listed in Table 6, namely, the PPP3CC genomic region, the SLCO5A1 genomic region, the SLC7A5 genomic region, the SLC7A2 genomic region, the CRISPLD2 genomic region, the CDH13 gene, the CDH8 gene, the CDH2 gene, the ASAH1 genomic region, the KCNB2 genomic region, the KCNH4 genomic region, the CTD8 gene, the JPH1 genomic region, the MEST genomic region, the NCALD genomic region, the COL19A1 gene, the MAP3K7 genomic region, the YWHAG gene, the NOL4 genomic region, and the ENOX1 gene.

[0008] According to the method disclosed herein, an increase in the copy number per cell for any of the SLCO5A1 genomic region, the KCNB2 genomic region, the KCNH4 genomic region, the JPH1 genomic region, the NCALD genomic region, or the YWHAG gene, correlates with an increased risk of prostate cancer metastasis; and a decrease in the copy number per cell for any of the PPP3CC genomic region, the SLC7A5 genomic region, the SLC7A2 genomic region, the CRISPLD2 genomic region, the CDH13 gene, the CDH8 gene, the CDH2 gene, the ASAH1 genomic region, the CTD8 gene, the MEST genomic region, the COL19A1 gene, the MAP3K7 genomic region, the NOL4 genomic region, or the ENOX1 gene, correlates with an increased risk of prostate cancer metastasis.

[0009] The copy number of a gene or genomic region can be determined using a nucleic acid probe that hybridizes to the gene or genomic region in the genomic DNA present in the sample. Hybridization can be performed in an array format, for example.

[0010] The risk of metastasis can be determined based on calculating a metastatic potential score:

$$M(SM) = \sum_{i}^{n} Zadjust_i * Dir_{sig}(i) * Dir_{samp}(i)$$

wherein the logistic adjusted Z-scores (*Zadjust*) for each of the genes of the metastatic signature set are set forth in Table 6 and wherein if the CNAs of the signature and the sample are in the same direction, the coefficient (Dir) will be 1; if they are in opposite directions, the

coefficient will be -1; and if no alternation in copy number is detected for a gene, the coefficient for that gene = 0; and comparing the metastatic potential score to a control value, wherein an increase in the score correlates with an increased risk of metastasis.

[0011] Further disclosed herein are diagnostic kits for performing the method of determining the risk of metastasis of prostate cancer. The kits can include nucleic acid probes that bind to one or more metastatic signature genes and genomic regions disclosed herein, and other assay reagents. The nucleic acid probes can be provided on a solid support such as a microarray slide. The kits can also include other materials such as instructions or protocols for performing the method.

BRIEF DESCRIPTION OF THE DRAWINGS

[0012] **Figure 1.** Boxplot showing the metastatic potential scores for all samples involved in the analysis. All high-risk tumors are shown in the left three boxes (metastases, primary tumors that progressed to metastasis, and lymph node positive primary tumors), whereas unknown control primary tumors and the publically available cell line data are shown in the right boxes. The "+" symbols in the lymph node positive box represent those samples from the MSK dataset and indicate that there is no difference between the two lymph node positive cohorts. The "x" symbols in the control primary tumors plot represent selected low-risk primary tumors (individuals with no biochemical recurrence (PSA) for at least 80 months).

[0013] **Figure 2.** *Left graph*, ROC-curve for prediction of primary tumors that progressed to metastasis using the metastatic potential score. The model used to make this prediction was run using a random 75% of samples from the data, whereas the prediction was run using the remaining 25% (13 known mPTs and 39 control primary tumors). The random model is indicated by the diagonal line (AUC = 0.5). The crosshair indicates the cut point used to separate the data for survival analysis (shown in the right graph). *Right graph*, Kaplan-Meier survival curve showing metastasis-free probability. The data were split in half by metastatic potential score and progression status and follow-up time were assessed. Log rank test (p-value) compares the high-risk and low-risk sample groups.

[0014] **Figure 3.** Simulation of a subset of genes were sampled (n=20) and the genes that were over represented in the region where the AUC and r2 were maximized (box) were ranked by their frequency. This simulation was also performed for n= 40, 50, 80, and 100 genes.

[0015] **Figure 4.** Extending window-AUC (red), extending window- r2 (black) based on the sorted hierarchy of genes.

[0016] **Figure 5.** ROC curve (left panel). Kaplan-Meier depiction of Cox proportional hazards model (right panel).

DETAILED DESCRIPTION

[0017] This disclosure provides a risk model that reliably predicts those tumors that are likely to metastasize, while minimizing the false positive rate and increasing the specificity of treatment decisions.

[0018] The risk model has been developed through the identification of copy number alterations (CNAs) around genes that were over-represented in metastases and primary tumors that later progressed to metastases. These CNAs are predictive of whether a primary tumor will metastasize. Cross-validation analysis has revealed a predictive accuracy of 80.5% and log rank analysis of the metastatic potential score has been shown to be significantly related to the endpoint of metastasis-free survival (p=0.014). In contrast to other reported risk models, the risk model disclosed herein based on the study of CNAs predicts distant metastasis progression as the clinical endpoint without the use of intermediate endpoints (such as biochemical markers of progression). The hierarchy of the genes and genomic regions that contribute to the prediction of metastatic potential has also been determined.

[0019] Accordingly, disclosed herein is a method for determining the risk of metastasis of prostate cancer in a human subject who has or had prostate cancer. This method is based on determining in a prostate sample from the subject, copy number alterations (CNAs) of genes

and genomic regions of a metastatic gene signature set, and correlating the CNAs with a risk of prostate cancer metastasis.

[0020] Metastatic Gene Signature

[0021] Metastatic gene signatures have been developed by the present inventors from studies of the genomic landscape of copy number alterations in 294 primary prostate tumors and 49 prostate metastases from 5 independent cohorts, as described in more detail in the examples hereinbelow. 368 copy number alterations have been identified around genes that are over-represented in metastases and are predictive of whether a primary tumor will metastasize. Cross-validation analysis has revealed a prediction accuracy of 80.5%.

[0022] Accordingly, in one embodiment, this disclosure provides a metastatic gene signature set which includes the 368 genes identified herein, set forth in Table 6.

[0023] As displayed in Table 6, the 368 genes include a number of "clumps", each clump identified by a "Clump Index Number". A "clump", as used herein, refers to a group of genes that are adjacent to one another on the chromosome, and copy number alterations are detected for the genomic region which includes this group of genes in connection with prostate cancer metastasis. A multi-member clump may include both drivers (genes that cause or more directly associate with metastasis) and passengers (genes that indirectly associate with metastasis because of its close proximity of a metastasis driver gene).

[0024] The term "genomic region" is used herein interchangeably with the term "clump", and is typically used herein in conjunction with the name of a member gene within the genomic region or clump. For example, the PP3CC gene listed in the first row of Table 6 belongs to Clump Index 26, which also includes the genes KIAA1967, BIN3, SORBS3, PDLIM2, RHOBTB2, SLC39A14, EGR3, and C8orf58. Therefore, Clump Index 26 is also referred to herein as "the PP3CC genomic region".

[0025] While many of the 368 genes belong to clumps, some of the genes do not belong to any clump and copy number alterations have been identified specifically around each of

these genes in connection with metastasis of prostate cancer. For example, as shown in Table 6 (with "NA" in the Clump Index column), CDH13, CDH8, CDH2 CTD8, COL19A1, YWHAG, and ENOX1, among many others, are genes which do not belong to any clump.

[0026] In other embodiments, this disclosure provides smaller metastatic gene signature sets which include at least 80, at least 40, at least 20, or at least 12, non-overlapping genes and/or genomic regions listed in Table 6.

[0027] By "non-overlapping" it is meant that the genes selected to constitute a smaller signature set do not belong to the same genomic region or clump.

[0028] As described in more detail in the examples hereinbelow, the metastatic potential score derived from the complete set of 368 genes resulted in a predictive accuracy of AUC = 81%. The hierarchy of the genes that contribute to this prediction has been determined, as shown in Table 6, based on a procedure that sought to identify genes that maximize the prediction accuracy (AUC = 81%) and also maximize the regression coefficient between the metastatic potential scores from the 368 genes versus any iteration of the randomly sampled subset of genes.

[0029] Accordingly, in one embodiment, a metastatic gene signature set includes at least the top 80 genes and genomic regions shown in Table 6.

[0030] In another embodiment, a metastatic gene signature set includes at least the top 40 genes and genomic regions shown in Table 6.

[0031] In still another embodiment, a metastatic gene signature set includes at least the top 20 genes and genomic regions shown in Table 6.

[0032] In yet another embodiment, a metastatic gene signature set includes at least the top 12 genes and genomic regions shown in Table 6.

[0033] Determination of Copy Number Alterations (CNAs)

[0034] A copy number alteration is a variation in the number of copies of a gene or genomic region present in the genome of a cell. A normal diploid cell typically has two copies of each chromosome and the genes contained therein. Copy number alterations may increase the number of copies, or decrease the number of copies.

[0035] The direction of copy number alteration for each of the 368 metastatic signature genes associated with metastasis is identified in Table 6 as -1 or 1, representing deletions and amplifications, respectively. For example, for the PP3CC genomic region (Clump Index 26), identified as "-1" in Table 6, deletions of this genomic region are overrepresented in metastatic prostate cancer or primary prostate cancers that later progressed to metastases, and are therefore indicative of a higher risk of metastasis of prostate cancer. Other genes and genomic regions whose deletions are predictive of a higher risk of metastasis of prostate cancer include, for example, the SLC7A5 genomic region, the SLC7A2 genomic region, the CRISPLD2 genomic region, the CDH13 gene, the CDH8 gene, the CDH2 gene, the ASAH1 genomic region, the CTD8 gene, the MEST genomic region, the COL19A1 gene, the MAP3K7 genomic region, the NOL4 genomic region, and the ENOX1 gene. On the other hand, for the SLCO5A1 genomic region (Clump Index 33), identified as "1" in Table 6, amplifications of this genomic region are overrepresented in metastatic prostate cancer or primary prostate cancers that later progressed to metastases, and are therefore indicative of a higher risk of metastasis of prostate cancer. Other genes and genomic regions whose amplifications are indicative of a higher risk of metastasis of prostate cancer include, for example, the KCNB2 genomic region, the KCNH4 genomic region, the JPH1 genomic region, the NCALD genomic region, and the YWHAG gene.

[0036] To determine whether there is any copy number alteration for a given gene or genomic region, a prostate sample is obtained from a subject of interest. A prostate sample refers to a cell or tissue sample taken from the prostate of a subject of interest which sample contains genomic DNA to be analyzed for CNAs. Methods of procuring cell and tissue samples are well known to those skilled in the art, including, for example, tissue sections, needle biopsy, surgical biopsy, and the like. For a cancer patient, cells and tissue can be

obtained from a tumor. A cell or tissue sample can be processed to extract, purify or partially purify, or enrich or amplify the nucleic acids in the sample for further analysis.

[0037] Nucleic acid probes are designed based on the genes and genomic regions of a metastatic signature gene set which permit detection and quantification of CNAs in the genes and genomic regions.

[0038] In one embodiment, the probes are composed of a collection of nucleic acids that specifically hybridize to the full set of 368 genes of the metastatic signature gene set.

[0039] In another embodiment, the probes are composed of a collection of nucleic acids that specifically hybridize to the top 80 genes and genomic regions shown in Table 6.

[0040] In still another embodiment, the probes are composed of a collection of nucleic acids that specifically hybridize to the top 40 genes and genomic regions shown in Table 6.

[0041] In yet another embodiment, the probes are composed of a collection of nucleic acids that specifically hybridize to the top 20 genes and genomic regions shown in Table 6.

[0042] In a further embodiment, the probes are composed of a collection of nucleic acids that specifically hybridize to the top 12 genes and genomic regions shown in Table 6.

[0043] By "specifically hybridize" it is meant that a nucleic acid probe binds preferentially to a target gene or genomic region under stringent conditions, and to a lesser extent or not at all to other genes or genomic regions.

[0044] "Stringent conditions" in the context of nucleic acid hybridization are known in the art, e.g., as described in Sambrook, *Molecular Cloning: A Laboratory Manual* (2^{nd} ed.) vol. 1-3, Cold Spring Harbor Laboratory, Cold Spring Harbor Press, New York (1989). Generally, highly stringent hybridization and wash conditions are selected to be about 5ºC lower than the thermal melting point for a specific sequence at a defined ionic strength and pH. An example of highly stringent hybridization conditions is 42ºC in standard hybridization solutions. An example of highly stringent wash conditions include 0.2 x SSC at 65ºC for 15 minutes. An

example of medium stringent wash conditions is 1X SSC at 45ºC for 15 minutes. An example of a low stringency wash is 4X-6X SSC at room temperature to 40ºC for 15 minutes.

[0045] Nucleic acid probes for purposes of this invention should be at least 15 nucleotides in length to permit specific hybridization to a target gene or genomic region, and can be 50, 100, 200, 400, 600, 800, 1000, or more nucleotides in length, or of a length ranging between any of the two above-listed values. A nucleic acid probe designed to specifically hybridize to a target gene can include the full length sequence or a fragment of the gene. A nucleic acid probe designed to specifically hybridize to a specific target genomic region can include at least a fragment of the genomic region, e.g., at least the full length sequence or a fragment of a gene (any gene) within the genomic region. Alternatively, a nucleic acid probe shares at least 80%, 85%, 90%, 95%, 98%, 99% or greater sequence identity with the target gene to permit specific hybridization.

[0046] The hybridized nucleic acids can be detected by detecting one or more labels attached to the sample or probe nucleic acids. The labels can be incorporated by a variety of methods known in the art, and include detectable labels such as magnetic beads, a fluorescent compound (e.g., Texas red, rhodamine, green fluorescent protein and the like), radio isotope, enzymes, colorimetric labels (e.g., colloidal gold particles). In other embodiments, the sample or probe nucleic acids can be conjugated with one member of a binding pair, and the other member of the binding pair is conjugated with a detectable label. Binding pairs suitable for use herein include biotin and avidin, and hapten and a hapten-specific antibody.

[0047] A number of techniques for analyzing chromosomal alterations are well known in the art. For example, fluorescence in-situ hybridization (FISH) can be used to study copy numbers of individual genetic loci or regions on a chromosome. See, e.g., Pinkel et al., Proc. Natl. Acad. Sci. USA 85: 9138-9142 (1988). Comparative genomic hybridization (CGH) can also be used to detect copy number alterations of chromosomal regions. See, e.g., U.S. Patent No. 7,638,278.

[0048] In some embodiments, hybridization is performed on a solid support. For example, probes that specifically hybridize to signature genes and genomic regions can be

spotted or immobilized on a surface, e.g., in an array format, and subsequently samples containing genomic DNA are added to the array to permit specific hybridization.

[0049] Immobilization of nucleic acid probes on various solid surfaces and at desired densities (e.g., high densities with each probe concentrated in a small area) can be achieved by using methods and techniques known in the art. See, e.g., U.S. Patent 7,482,123 B2. Examples of solid surfaces include nitrocellulose, nylon, glass, quartz, silicones, polyformaldehyde, cellulose, cellulose acetate; and plastics such as polyethylene, polypropylene, polystyrene, and the like; gelatins, agarose and silicates, among others. High density immobilization of nucleic acid probes are used for high complexity comparative hybridizations which will reduce the total amount of sample nucleic acids required for binding to each immobilized probe.

[0050] In some embodiments, the arrays of nucleic acid probes can be hybridized with one population of samples, or can be used with two populations of samples (one test sample and one reference sample). For example, in a comparative genomic hybridization assay, a first collection of nucleic acids (e.g., sample from a possible tumor) is labeled with a first label, while a second collection of nucleic acids (e.g., control from a healthy cell or tissue) is labeled with a second label. The ratio of hybridization of the nucleic acids is determined by the ratio of the two labels binding to each member in the array. Where there are genomic deletions or amplifications, differences in the ratio of the signals from the two labels will be detected and provide a measure of the copy number.

[0051] Determination of Risk

[0052] Once copy number alterations for each of a metastatic signature gene set have been determined, the risk for metastasis can be correlated with the copy number alterations detected. An increase in the copy number per cell of the sample for one or more of the genes or genomic regions of a metastatic signature gene set disclosed herein, whose amplifications have been associated with metastatic prostate cancer, will indicate a higher risk of metastasis as compared to a control (e.g., a sample obtained from a healthy individual) in which no increase in the copy number occurs. On the other hand, a decrease in the sample in the copy

number for one or more of the genes or genomic regions of a metastatic signature gene set disclosed herein, whose deletions have been associated with metastatic prostate cancer, will indicate a higher risk of metastasis as compared to a control in which no decrease in the copy number is observed.

[0053] For example, for a metastatic signature gene set composed of the top 20 genes and genomic regions listed in Table 6, an increase in the copy number per cell of the sample for all of the SLCO5A1 genomic region, the KCNB2 genomic region, the KCNH4 genomic region, the JPH1 genomic region, the NCALD genomic region, and the YWHAG gene, and a decrease in the sample in the copy number per cell of the sample for all of the PPP3CC genomic region, the SLC7A5 genomic region, the SLC7A2 genomic region, the CRISPLD2 genomic region, the CDH13 gene, the CDH8 gene, the CDH2 gene, the ASAH1 genomic region, the CTD8 gene, the MEST genomic region, the COL19A1 gene, the MAP3K7 genomic region, the NOL4 genomic region, and the ENOX1 gene, correlate with an increased risk of prostate cancer metastasis. However, it is not necessary for all the genes and genomic regions within a signature set to change in the same direction as set forth in Table 6 in order to have a reasonably reliable prediction of the risk. That is, an increased risk can be predicted based on an increase in the copy number per cell of the sample for one or more, preferably a plurality of, the SLCO5A1 genomic region, the KCNB2 genomic region, the KCNH4 genomic region, the JPH1 genomic region, the NCALD genomic region, and the YWHAG gene, and/or a decrease in the sample in the copy number per cell of the sample for one or more, preferably a plurality of, the PPP3CC genomic region, the SLC7A5 genomic region, the SLC7A2 genomic region, the CRISPLD2 genomic region, the CDH13 gene, the CDH8 gene, the CDH2 gene, the ASAH1 genomic region, the CTD8 gene, the MEST genomic region, the COL19A1 gene, the MAP3K7 genomic region, the NOL4 genomic region, or the ENOX1 gene. By "plurality" it is meant at least 10, 11, 12, 13, 14, 15, 16, 17, 18, 19 or 20 of the top 20 genes and gene regions listed in Table 6.

[0054] This disclosure also provides a quantitative measure of the risk based on the copy number alterations of a signature gene set disclosed herein. More specifically, the risk of

metastasis has been found to correlate with a metastatic potential score calculated based on the formula:

$$M(SM) = \sum_{i}^{n} Zadjust_i * Dir_{sig}(i) * Dir_{samp}(i)$$

[0055] That is, for a particular gene or genomic region, if the CNA of the signature and the sample are in the same direction (amplified or deleted), the coefficient will be 1, the logistic adjusted Z-score (*Zadjust*) for this gene or genomic region will be added; if in opposing directions, the coefficient will be -1, the logistic adjusted Z-score (*Zadjust*) for the gene or genomic region will be substracted; and if Dirsamp(i) = 0, then the entire term will not count towards the score. Thus, essentially, the logistic adjusted Z-scores from genes (i…n) that match the metastasis signature are added, whereas from genes that mismatch the signature are subtracted. The logistic adjusted Z-scores (*Zadjust*) for each of the 368 genes of the full metastatic signature set are found in Table 6.

[0056] The calculated metastatic potential score is compared to a reference distribution of samples (the metastatic potential score determined from a population of men with prostate cancer with metastasis-free survival clinical outcome information). Such reference distributions can be predetermined or calculated side-by-side in the same experiment as the sample being investigated. Therefore, an increase in the metastatic potential score as compared to the reference distributions is correlated with an increased risk of metastasis of prostate cancer. According to this disclosure, a one-point increase in the metastatic potential score corresponds to an odds ratio of 6.3 for progression to metastasis ($p = 0.01$).

[0057] The disclosed method for predicting the likelihood of distant metastases represents a significant advancement in the diagnosis and treatment of prostate cancer. This predictor may be important for correctly categorizing men at the time of diagnosis and can lead to a choice of therapy that would maximize their chances of survival and minimize adverse side effects if aggressive treatment can be avoided. Thus, both treatment outcomes and quality of life could be improved. In addition, because the proposed tool, tumor genomic analysis, is

comprehensive for identifying the genetic changes that are associated with pathogenesis and metastases, there is a greater likelihood of selecting a sufficient number of markers that are both sensitive and specific predictors. Furthermore, because these genomic alterations are themselves susceptible to manipulation with drugs, radiation or other therapies, they could provide a basis for assessing intermediate endpoints, such as androgen sensitivity and response to radiation. Ultimately, copy number alterations could guide the development of individually tailored therapies, including for cancers other than prostate.

[0058] Diagnostic Kits

[0059] Further disclosed herein are diagnostic kits for performing the methods described herein. The kits can include any and all reagents such as nucleic acid probes that bind to one or more metastatic signature genes described above, and other assay reagents. The nucleic acid probes can be provided on a solid support such as a microarray slide. The kits can also include other materials such as instructions or protocols for performing the method, which can be provided in an electronic version, e.g., on a compact disk or the like.

EXAMPLES

[0060] The present description is further illustrated by the following examples, which should not be construed as limiting in any way. The contents of all cited references (including literature references, issued patents, and published patent applications as cited throughout this application) are hereby expressly incorporated by reference.

[0061] **Example 1.**

[0062] This Example describes the methods and sample sources utilized for developing a predictive metastasis model.

[0063] PREDICTIVE BIOMARKERS

[0064] The method chosen for developing the predictive metastasis model was the analysis of copy number alterations (CNAs) in prostate cancers. These cancers have been known to harbor multiple genomic imbalances that result from CNAs (Beroukhim et al.,

Nature 463(7283):899-905 (2010); Sun et al., *Prostate* 67(7):692-700 (2007)). High-resolution measurements of CNAs have informative value -- in some cases providing direct evidence for alterations in the quantity of normal, mutant or hybrid-fusion transcripts and proteins in the cancer cells. The resulting RNA transcripts and proteins may impact the fitness of the cell and provide the mechanisms necessary for travel, invasion and growth. From the multiple CNAs identified in tumors, CNA-based gene signatures were developed to predict the likelihood of a primary tumor progressing to metastasis.

[0065] SAMPLES, COHORTS AND DATA

[0066] Four publically available prostate cancer cohorts and a fifth cohort reported here (GSE27105) were studied, as summarized in **Table 1**: 1) 294 primary tumors and matched normal tissue samples from NYU School of Medicine (NYU n=29), Baylor College of Medicine (Baylor n=20) (Castro et al., *Neoplasia* 11(3):305-12 (2009)), Memorial Sloan-Kettering Cancer Center (MSK n=181) (Taylor et al., *Cancer Cell* 18(1):11-22 (2010)), and Stanford University (SU n=64 (single normal tissue used to reference each tumor)) (LaPointe et al., *Cancer Res* 67(18):8504-10 (2007)); 2) 49 metastatic tumors and matched normal samples from Johns Hopkins School of Medicine (Hopkins n=13) (Liu et al., *Nat Med* 15(5):559-65 (2009)) and MSK (n=36) (Taylor et al., *supra*). Normal prostate and tumor tissues (NYU) were obtained from the Cooperative Prostate Cancer Tissue Resource (**Table 2**). Array data from the four publically available cohorts (Castro et al., *supra*; Taylor et al., *supra*; LaPointe et al., *supra*; Liu et al., *supra*) were downloaded from Gene Expression Omnibus (Barrett et al., *Nucleic Acids Res* 39 (Database issue):D1005-10 (2011)) (GSE12702, GSE14996, GSE6469, GSE21035). A public cell lines cohort of various tumor origins was obtained from the ArrayExpress database (Parkinson et al., *Nucleic Acids Res* 39(Database issue):D1002-4) (E-MTAB-38) to determine if the gene signature and predictive model developed herein could be applicable to other cancers.

[0067] SAMPLE PROCESSING (NYU COHORT)

[0068] Genomic DNA (gDNA) was extracted using a Gentra DNA extraction kit (Qiagen). Purified gDNA was hydrated in reduced TE buffer (10 mM Tris, 0.1 mM EDTA,

pH 8.0). The gDNA concentration was measured using the NanoDrop™ 2000 spectrophotometer at optical density (OD) wavelength of 260 nm. Protein and organic contamination were measured at OD 280nm and 230nm, respectively. Samples that passed quality control thresholds were then run on a 1% agarose gel to assess the integrity of the gDNA. 500ng of gDNA samples were run on the Affymetrix Human SNP Array 6.0 at the Rockefeller University Genomics Resource Center using standard operating procedures. Signal intensity data (.cel files) were processed using the Birdseed v2.0 software (Korn et al., *Nat Genet* 40(10):1253-60 (2008)).

[0069] STUDY DESIGN

[0070] The case samples in this study were either metastatic tumors (METS) or primary tumors from men treated with radical prostatectomy that later progressed to form distant metastasis (mPTs). METS and mPTs are clearly discernable phenotypes that can be reliably classified as cases. The control samples were defined as primary tumors that had not progressed to form distant metastases following radical prostatectomy. Given that radical prostatectomy cures both indolent primary tumors (iPTs) that would not metastasize and primary tumors that would otherwise progress to form metastasis, if left untreated, the control primary tumors would actually represent a mix of iPTs and unrealized mPTs. Assuming a randomly sampled cohort, it is expected that approximately 30% of the control group of primary tumors would be unrealized mPTs. The methods developed herein required only the prior information of whether a sample was derived from a metastasis and were designed to be robust to the confounder of mixed phenotypes.

[0071] METASTASIS PREDICTION MODEL STATISTICS

[0072] A weighted Z-score algorithm was developed to calculate a metastatic potential score (MPS) as described in Example 2, with a higher score indicating a greater likelihood of metastasis. The predictive power of the instant models was evaluated through cross-validation testing. Two prediction models were trained using a combination of four cohorts. The first model was trained using 49 primary tumors of unknown clinical outcome from NYU (n=29) and Baylor (n=20) and a metastasis cohort from Hopkins (n=13). The second model

was trained using 75% of the MSK cohort of primary tumors of unknown outcome (n=126) along with a set of metastatic tumors (n=36). The gene signatures and MPS scores derived from these 2 models were combined to fit a logistic regression model and used to predict bona fide mPTs (primary tumors that later developed into distant metastasis) and a random sample of 25% control tumors from MSK cohort not used to train either model. Prediction accuracy was measured by the area under the receiver operating characteristic curve and Kaplan-Meier metastasis-free survival.

[0073] Example 2.

[0074] This Example describes the analytical pipeline for developing a metastatic potential clinical risk model.

[0075] An analytical pipeline was developed using the R-statistical software1 comprised of four main steps:

[0076] In step 1, copy number amplification and deletion events for each tumor genome were called. A tumor genome's signal intensity profile was referenced (subtracted) from its matched normal genome intensity profile resulting in a copy number profile for each tumor. Each sample's copy number profile was represented numerically as -1, 0 or 1 (deletion, no event, or amplification) for each genomic position assayed by the array. A summary metastasis profile (indexing high frequency events) was also created where -1 and 1 represent deletions and amplifications, respectively, observed in greater than 25% of the metastasis cohort.

[0077] In step 2, a bootstrap clustering method was employed to develop an initial grouping for the unknown primary tumors. The summary copy number profile for the metastasis samples was combined with the individual profiles from the unknown primary tumors and processed using hierarchical clustering (binary distance metric and complete clustering method). For each bootstrap iteration, a subset of primary tumors were sampled with replacement and scored 1 if they were in the same cluster as the metastasis profile, and 0 if they were in the other cluster. Using the results from 20,000 iterations of the clustering, a

similarity index was generated for each sample, representing the number of times it fell in a cluster with the metastasis profile. A sample with a high score was considered to be more metastatic (mPT), while lower scoring tumors were more indolent (iPT). The similarity scores distributed throughout the possible range of values (0 to 1), allowing the formation of distinct groups of tumors with significant contrast between high and low metastatic distance.

[0078] In step 3, these mPT and iPT contrast groups were used to assess quantitative copy number differences on a probe basis. For each probe on the array, an enrichment score, E(x), was calculated, which represented the relative amount of amplifications versus deletions, observed in each subgroup (metastasis, mPT and iPT).

$$E(x) = \frac{(\#Amp - \#Del)}{\#Samples}$$

[0079] Next, the relative enrichment was modeled by contrasting the metastasis and mPT copy number alterations with those observed in the iPT group.

$$SM = e^{[E(METS) + q*E(mPT) - E(iPT)]}$$

[0080] The first two enrichment terms being summed were designed to assign a higher score when the METS and mPT samples had more amplifications than deletions. Greater amplification enrichment in the METS and mPTs resulted in higher scores. The third term was higher when the iPT samples exhibit the opposite effect (enrichment for deletions over amplifications). The middle term was multiplied by a data-driven coefficient, q, representing the average contribution of mPT on a probe basis. For example, probes that were amplified in all metastases and mPTs, but deleted in all iPTs would yield the highest possible score. Likewise, probes that were deleted in all metastasis and mPT samples, but amplified in all iPT samples, would also reach this maximum possible score. The probe scores were then aggregated by gene and a Z-score was calculated to assess each gene's score compared to the rest of the genome.

[0081] In the event that there are multiple Z-scores for each gene (see Table 6), corresponding to the various cohorts used to generate the 3 signatures. Therefore, each individual will have 3 different MPS's. The final MPS (shown in Table 6) is calculated by combining the 3 MPSs for each signature using a variation of the rank method described below.

[0082] The Z-adjust transforms each gene's Z-score derived from the above three steps to fit a logistic distribution through the following standard function:

$$Z_{adj} = \left(\frac{Z_i}{1 + e^{\frac{Z_{\min} - Z_i}{2}}} - \frac{Z_i}{2}\right)$$

[0083] The purpose of this transformation is to minimize the effect of any individual gene's Z-score on the overall MPS (makes the score robust to outliers).

[0084] Finally, in step 4, to predict whether a local prostate tumor had the capability to form distant metastasis, a weighted-Z scoring risk model was developed based on a signature of the top set of CNAs overlapping genomic regions as determined by the significance of their selection model Z-scores. The significant genes ($Z \geq 1.7$) were used from step 3 as a cutoff point. The metastatic prediction risk model score was defined as the following:

$$M(SM) = \sum_{i}^{n} Zadjust_i * Dir_{sig}(i) * Dir_{samp}(i)$$

[0085] For each tumor profile, logistic adjusted Z-scores (*Zadjust*) from genes (i…n) that match the metastasis signature were added, whereas from genes that mismatch the signature were subtracted. As the direction component of the risk model score (Dir) reflects, if the CNAs of the signature and the sample are in the same direction, the coefficient will be 1; if they are in opposing directions, the coefficient will be -1; and if Dirsamp(i) = 0, then the entire term will not count towards the score. For example, if a gene i, that is typically

amplified in metastases and mPTs is also amplified in the unknown profile, that Z-score is added, whereas if gene i in the profile is deleted, as expected in iPTs, the Z-score is subtracted. Neutral genes that are neither amplified nor deleted in the unknown profile are not scored in this model.

[0086] Example 3

[0087] This Example describes the results achieved by the predictive metastasis model developed as described in Examples 1-2.

[0088] METASTATIC POTENTIAL SCORE DISTRIBUTIONS

[0089] Significant differences in the metastatic potential score were observed for the metastasis ($p = 1.03E-18$) and mPT ($p = 0.005$) groups, compared to the control primary tumors (**Figure 1** and **Table 3**). The metastatic potential score in the lymph node positive primary tumors (derived from the MSK ($n = 9$) and SU ($n = 9$) cohorts) did not differ significantly from the control tumor group ($P_{MSK} = 0.23$, $P_{SU} = 0.19$, $P_{Combined} = 0.08$), which reflected the marginal ability of this clinical parameter to predict distant metastasis (BOORJIAN et al., *Journal of Urology* 178(3 Pt 1):864-70; discussion 70-1 (2007)). Consistent with our assumption that the control cohorts contained a fraction of mPTs, their metastatic potential score overlapped the range of the cases. Furthermore, control primary tumors that did not recur biochemically (as measured by PSA) after 80 months of follow-up, (represented by Xs in **Figure 1**) were not correlated with the metastatic potential score. To determine whether other cancer types exhibited a similar metastatic landscape of CNAs to that observed in prostate cancer, the metastatic potential scores for 337 cancer cell lines were calculated. An overall distribution that overlapped with low-risk prostate primary tumors was observed (**Figure 1**). However, 22 of the 337 cell lines emerged above the 75th percentile of the prostate primary tumors and metastases, ranked by MPS. These cell lines originated from tumors of the lung (n=10), breast (n=3), colon (n=2) and melanoma (n=2). Other singletons in this group of 22 cell lines originated from thyroid, rectum, pharynx, pancreas and kidney (**Table 4**).

[0090] CROSS-VALIDATION AND SURVIVAL ANALYSIS

[0091] A cross-validation analysis predicting a subset of primary tumors (n = 52) not used to train the model (n= 13 mPTs and n= 39 control primary tumors) resulted in an accuracy of 80.5% as measured by the area under the receiver operating characteristic curve (ROC-AUC) (**Figure 2**, left graph). Considering that control primary tumors were a mixture of treated mPTs and iPTs, the quality of fit was believed to be an underestimate. Applying the instant prediction to a Kaplan-Meier analysis with the clinical endpoint of metastasis-free survival (**Figure 2**, right graph) resulted in a significant separation (p=0.014) of the low-risk half of the cohort (based on the metastatic potential score) compared to the high-risk half. A one-point increase in the metastatic potential score corresponded to an odds ratio of 6.3 for progression to metastasis (p = 0.01).

[0092] BIOMARKER FUNCTIONAL SIGNIFICANCE

[0093] Many of the top ranking metastasis genes identified through the analysis have molecular functions related to alteration of nuclear and extra-cellular matrix structure and metabolic modification that enhance processes characteristic of metastasis, such as motility, invasion, and escape from anoikis. A heat map of the CNA events of signature genes for all prostate tumors is suggestive of a path toward the different high frequency amplification versus deletion events that contrast the high-risk and low-risk tumors. The mid-risk region with its relative paucity of genomic events may represent the starting point of two alternative pathways of subsequent copy number alteration, one leading to metastasis and the other to an indolent state. The locking in of these 'anti-metastasis' events in indolent tumors may explain why they fail to metastasize despite extended periods of watchful waiting.

[0094] Many of the genes within these amplified or deleted regions from which the predictive signature was derived have been shown previously to play a role in prostate cancer metastasis. One of the top predictor genes, the solute carrier family SLC7A5 gene deleted on chromosome 16q24.2, encodes a neutral amino acid transporter protein (LAT1) that has been implicated in multiple cancers (prostate (Sakata et al., *Pathol Int* 59(1):7-18 (2009)), breast (Kaira et al., *Cancer Science* 99(12):2380-6 (2008)), ovarian (Kaji et al., *International*

Journal of Gynecol Cancer 20(3):329-36 (2010)), lung (Imai et al., *Histopathology* 54(7):804-13 (2009)) and brain (Kobayashi et al., *Neurosurgery* 62(2):493-503; discussion -4 (2008))) and has been shown to have utility as a diagnostic (Bartlett et al., *Breast Cancer Research* 12(4):R47 (2010); Ring et al., *Mod Pathol* 22(8):1032-43 (2009); Ring et al., *Journal of Clinical Oncology* 24(19):3039-47 (2006)) and drug target in cell line (Fan et al., *Biochem Pharmacol* 80(6):811-8 (2010); Yamauchi et al., *Cancer Letter* 276(1):95-101 (2009); Kim et al., *Biol Pharm Bull* 31(6):1096-100 (2008)) and pre-clinical animal models (Oda et al., *Cancer Science* 101(1):173-9 (2010)). The normal function of LAT1 is to regulate cellular amino acid concentrations -- L-glutamine (efflux) and L-leucine (influx). Reduced activity of LAT1 results in increased concentrations of L-glutamine which has been shown to constitutively fuel mTOR activity (Nicklin et al., *Cell* 136(3):521-34 (2009)) and targeting of glutamine utilization through the use of a glutamine analog, dramatically reduced tumor growth and metastasis in cellular and *in vivo* mouse models (Shelton et al., *International Journal of Cancer* 127(10):2478-85). Seven other solute carrier superfamily members (SLCO5A1, SLC7A2, SLC10A5, SLC26A7, SLC25A37, SLC38A8 and SLC39A14) were predictive of metastatic potential in the models disclosed herein. A ninth SLC gene, SLC44A1, encoding a choline transporter (Michel et al., *Faseb J* 23(8):2749-58 (2009)), was identified as part a of a 17-gene expression signature, comparing prostate primary tumors of men treated with radical prostatectomy that metastasized versus men that recurred biochemically, but did not metastasize (Nakagawa et al., *supra*).

[0095] A second set of signature genes includes 6 Cadherin family members encoding calcium dependent cell adhesion glycoproteins (CDH2, CDH8, CDH13, CDH15, CDH17 and PCDH9). Many of the Cadherin family proteins have putative functions associated with metastasis progression (Yilmaz et al., *Mol Cancer Res* 8(5):629-42, 2010) and have been included in diagnostic panels (Celebiler et al., *Cancer Sci* 100(12):2341-5 (2009); Lu et al., *PLoS Med* 3(12):e467 (2006)). A recent study of monoclonal antibody treatment targeting CDH2 inhibited prostate cancer growth and metastasis in androgen independent prostate cancer xenograft models (Tanaka et al., *Nat Med* (2010) 16:1414-20).

[0096] A third set of 6 genes predicted to contribute to metastatic potential were potassium channels KCNB2, KCNQ3, KCNAB1, KCTD8, KCTD9 and KCNH4. Three other potassium channels reside in the highly amplified region between 8q13 and 8q24 (KCNS2, KCNV1 and KCNK9) that did not rank high in our analysis, but may have weak or modifier effects. High levels of cytoplasmic potassium ion concentration are maintained by BCL-2, a putative oncogene, through the inhibition of potassium channel transcription. These high levels were shown to inhibit a necessary precursor to the hallmark mitochondrial apoptotic cascade of membrane disruption and ensuing release of cytochrome C, caspase, and nuclease degradation of cellular components (Ekhterae et al., *American Journal of Physiol Cell Physiol* 2001;281(1):C157-65 (2001)). Furthermore, another study has shown that the hyper-methylation status of potassium channel KCNMA1 (10q22.3) has predictive value for prostate cancer recurrence (Vanaja et al., *Cancer Invest* 27(5):549-60 (2009)). The activity of voltage-gated potassium channels in prostate cancer cell lines LNCaP (low metastatic potential) and PC3 (high metastatic potential), were observed to be markedly different (Laniado et al., *Prostate* 46(4):262-74 (2001)). Mounting evidence has also been observed in the involvement of potassium channels and the migration of breast cancer cells (Zhang et al., *Sheng Li Xue Bao* 61(1):15-20 (2009)).

[0097] The complete set of metastasis signature genes used in the prediction model (n = 368, **Table 6**) represent various subsets of functions, revealing a unique profile necessary for each tumor to progress to metastasis.

[0098] **Example 4**

[0099] RANKING METASTASIS GENES ON THE BASIS OF PREDICTABILITY

[00100] The metastatic potential score as derived from the complete set of 368 metastasis genes resulted in a predictive accuracy of AUC = 81% in the cohort described in Examples 1-3. To determine the hierarchy of the genes that contribute to this prediction, several simulations (K) were performed by randomly sampling subsets genes (n) from the 368 genes, where n=20, 40, 50, 80, 100. This procedure sought to identify those genes that maximize the prediction accuracy (AUC = 81%) while also maximizing the regression coefficient

between the MPS scores from the 368 genes versus any random iteration of the randomly sampled subset of genes. For example a random subset of 20 genes that achieves a prediction accuracy = 81% and an $r^2 = 1.0$ compared to the MPS derived from the 368 gene signature would achieve the theoretical best performance (**Figure 3**).

[00101] Once gene rankings for the 5 simulations were determined, ranks *G* positions across *K* analyses were evaluated using a non-parametric ranking method (Breitling et al., *FEBS Lett* 573: 83-92, (2004)):

$$R(G) = \sum_{i=1}^{k} \log\left(\frac{1}{G_k}\right)$$

[00102] This method was selected as an improvement to a simple average of the ranks of each G across the *k* analyses because it gives more emphasis to having a high rank in any one of the analyses, regardless of rank in the others. This model of rank integration gives more weight, for example, to a gene ranked #1 and #100 in two different analyses than to a gene ranked #100 in each.

[00103] To evaluate the performance of this method, the composite ranked hierarchy of genes was assessed using an extending window. Starting with a minimum of 12 genes, and adding one gene every iteration, an AUC and r2 were calculated. The results in **Figure 4** show that the AUC plateaus at ~80 genes, achieving the optimal AUC ~0.81 and $r2 > 0.95$. Specifically, **Table 5** shows the results for the top 12, 20, 40, 80 and 100 genes.

[00104] The ranking of the 368 genes is shown in **Table 6**.

[00105] **Example 5.**

[00106] REPORTING PREDICTION TO PATIENTS

[00107] The prostate cancer metastatic potential score, assessed through a Cox proportional hazards ratio model provides the basis for determining metastasis-free probability. In **Figure**

5 (left panel, ROC curve), a conservative threshold that maximizes our sensitivity (at 100% or 1.0 on the Y-axis of the ROC curve) was chosen to identify all true positives (i.e. men that will progress to metastasis). Within this high-risk group there is a false positive rate of 59% (men who would not otherwise have developed metastasis), which will result in some men with low-risk prostate cancer to be treated aggressively. However, currently 100% of the men are treated aggressively, so the conservative threshold herein would enable 31% of them to be spared aggressive treatment.

[00108] Applying this conservative threshold to a Kaplan-Meier analysis of a Cox proportional hazards model (**Figure 5**, right panel) results in low risk and high risk probabilities of metastasis free survival at various time intervals. Therefore, for this model, a man with a low risk designation will have a very low (< 5%) chance to develop metastasis in 10 years. While the high risk designation results in a 40% chance of progressing to metastasis in 60 months and a > 90% chance of progressing to metastasis in 10 years.

[00109] As a comparison, the FDA approved breast cancer gene expression signature diagnostic "MammaPrint" uses similar Cox proportional hazards analysis to develop their risk reporting strategy (Bogarts et al., *Nat Clin Pract Oncol* 3:540-51, 2006). Currently, the FDA low risk assignment has a 10% chance of progressing to metastatic disease in 10 years, while the high risk assignment has a 29% chance of progressing in 10 years.

WHAT IS CLAIMED IS:

1. A method of determining the risk of metastasis of prostate cancer in a human subject who has or had prostate cancer, the method comprising

(a) determining in a prostate sample from the subject the number of copies per cell of at least 12 genes and/or genomic regions of a metastatic gene signature set, wherein the metastatic gene signature set consists of the PPP3CC genomic region, the SLCO5A1 genomic region, the SLC7A5 genomic region, the SLC7A2 genomic region, the CRISPLD2 genomic region, the CDH13 gene, the CDH8 gene, the CDH2 gene, the ASAH1 genomic region, the KCNB2 genomic region, the KCNH4 genomic region, the CTD8 gene, the JPH1 genomic region, the MEST genomic region, the NCALD genomic region, the COL19A1 gene, the MAP3K7 genomic region, the YWHAG gene, the NOL4 genomic region, and the ENOX1 gene,

(b) determining alternations in the number of copies per cell for each of the at least 12 genes and/or genomic regions as compared to the number of copies per cell in non-cancer cells, and

(c) determining the risk of prostate cancer metastasis based on the copy number alternations (CNAs) determined in step (b).

2. The method of claim 1, wherein the at least 12 genes and/or genomic regions include the PPP3CC genomic region, the SLCO5A1 genomic region, the SLC7A5 genomic region, the SLC7A2 genomic region, the CRISPLD2 genomic region, the CDH13 gene, the CDH8 gene, the CDH2 gene, the ASAH1 genomic region, the KCNB2 genomic region, the KCNH4 genomic region, and the CTD8 gene.

3. The method of claim 1, wherein the at least 12 genes and/or genomic regions include all of the genes and genomic regions in said metastatic gene signature set.

4. The method of claim 1 or 3, wherein an increase in the copy number per cell for any of the SLCO5A1 genomic region, the KCNB2 genomic region, the KCNH4 genomic region, the JPH1 genomic region, the NCALD genomic region, or the YWHAG gene, correlates with an increased risk of prostate cancer metastasis; and a decrease in the copy number per cell for

any of the PPP3CC genomic region, the SLC7A5 genomic region, the SLC7A2 genomic region, the CRISPLD2 genomic region, the CDH13 gene, the CDH8 gene, the CDH2 gene, the ASAH1 genomic region, the CTD8 gene, the MEST genomic region, the COL19A1 gene, the MAP3K7 genomic region, the NOL4 genomic region, or the ENOX1 gene, correlates with an increased risk of prostate cancer metastasis.

5. The method of claim 1, wherein the PPP3CC genomic region comprises the genes PPP3CC, KIAA1967, BIN3, SORBS3, PDLIM2, RHOBTB2, SLC39A14, EGR3, and C8orf58.

6. The method of claim 1, wherein the SLCO5A1 genomic region comprises the genes SLCO5A1, SULF1, NCOA2, CPA6, C8orf34, PRDM14, and PREX2.

7. The method of claim 1, wherein the SLC7A5 genomic region comprises the genes SLC7A5, CA5A, BANP, KLHDC4, CYBA, JPH3, ZFPM1, SNAI3, ZC3H18, MVD, IL17C, C16orf85, and RNF166.

8. The method of claim 1, wherein the SLC7A2 genomic region comprises the genes SLC7A2, MTMR7 and MUTS1.

9. The method of claim 1, wherein the CRISPLD2 genomic region comprises the genes CRISPLD2, ZDHHC7, KIAA0513, KLHL36, and USP10.

10. The method of claim 1, wherein the ASAH1 genomic region comprises the genes ASAH1 and PCM1.

11. The method of claim 1, wherein the KCNB2 genomic region comprises the genes KCNB2, EYA1, XKR9, and TRPA1.

12. The method of claim 1, wherein the KCNH4 genomic region comprises the genes KCNH4, RAB5C, DHX58, KAT2A, and HSPB9.

13. The method of claim 1, wherein the JPH1 genomic region comprises the genes JPH1, HNF4G, CRISPLD1, PI15, and GDAP1.

14. The method of claim 1, wherein the MEST genomic region comprises the genes MEST, COPG2, CPA5, CPA2, CPA1, CPA4, and TSGA14.

15. The method of claim 1, wherein the NCALD genomic region comprises the genes NCALD, ZNF706, GRHL2, and YWHAZ.

16. The method of claim 1, wherein the MAP3K7 genomic region comprises the genes MAP3K7 and EPHA7.

17. The method of claim 1, wherein the NOL4 genomic region comprises the genes NOL4 and DTNA.

18. The method of claim 3, further comprising determining the number of copies per cell of at least one additional gene or genomic region listed in Table 6.

19. The method of claim 18, wherein said at least one additional gene or genomic region comprises 20 genes and/or genomic regions listed in Table 6.

20. The method of claim 19, said 20 genes and/or genomic regions are the genes and genomic regions ranked 21-40 in Table 6.

21. The method of claim 1, wherein the copy number of a gene or genomic region is determined using a nucleic acid probe that hybridizes to the gene or genomic region in the genomic DNA present in the sample.

22. The method of claim 21, wherein hybridization is performed in an array format.

23. The method of claim 4, wherein the risk is determined based on calculating a metastatic potential score:

$$M(SM) = \sum_{i}^{n} Zadjust_i * Dir_{sig}(i) * Dir_{samp}(i)$$

wherein the logistic adjusted Z-scores (*Zadjust*) for each of the genes of the metastatic signature set are set forth in Table 6 and wherein if the CNAs of the signature and the sample are in the same direction, the coefficient (Dir) will be 1; if they are in opposite directions, the coefficient will be -1; and if no alternation in copy number is detected for a gene, the coefficient for that gene = 0; and comparing the metastatic potential score to a control value, wherein an increase in the score correlates with an increased risk of metastasis.

24. A kit for determining the risk of metastasis of prostate cancer in a human subject who has or had prostate cancer, comprising a plurality of nucleic acid probes which specifically hybridize to at least 12 genes and/or genomic regions of a metastatic gene signature set, wherein the metastatic gene signature set consists of the PPP3CC genomic region, the SLCO5A1 genomic region, the SLC7A5 genomic region, the SLC7A2 genomic region, the CRISPLD2 genomic region, the CDH13 gene, the CDH8 gene, the CDH2 gene, the ASAH1 genomic region, the KCNB2 genomic region, the KCNH4 genomic region, the CTD8 gene, the JPH1 genomic region, the MEST genomic region, the NCALD genomic region, the COL19A1 gene, the MAP3K7 genomic region, the YWHAG gene, the NOL4 genomic region, and the ENOX1 gene.

25. The kit of claim 24, comprising a plurality of nucleic acid probes which specifically hybridize to all of the 20 genes and/or genomic regions of said metastatic gene signature set.

ABSTRACT

A method of determining the risk of metastasis of prostate cancer in a human subject who has or had prostate cancer is disclosed herein. The method is based on detecting in a prostate sample from the subject the number of copies per cell of genes and/or genomic regions of a metastatic gene signature set disclosed herein, and determining alternations in the number of copies per cell of the genes and/or genomic regions in the signature set, as compared to the number of copies per cell in non-cancer cells, thereby determining the risk of prostate cancer metastasis.

Table 1 | Prostate cancer cohorts

Cohort	Cases (n)	Controls (n)	Pathological Stage	GEO-Accession	Array CGH Platform
NYU Langone Medical Center	0	29	T2C-T4	GSE27105*	Affy V6
Johns Hopkins School of Medicine	METS (13)	0	METS	GSE14996	Affy V6
Baylor College of Medicine	0	20	T2C-T4	GSE12702	Affy 500K
Memorial Sloan-Kettering Cancer Center	mPTs(13)/METS (36)/LN-METS (9)	159	T2C-T4/METS	GSE21035	Agilent 244A
Stanford University	LN-METS (9)	55	T2C-T4/METS	GSE6469	custom cDNA
	80	263			
	Total tumors	343			

Table 2| NYU cohort sample information

compositeID	Race	tumor_type	Stage	Gleason (primary)	Gleason (secondary)	Age at prostatectomy (years)
CA_1	CA	primary	T2c	3	3	70
CA_2	CA	primary	T4	3	3	59
AA_3	AA	primary	T2c	3	4	76
CA_4	CA	primary	T2c	3	3	58
CA_5	CA	primary	T4	3	3	73
CA_6	CA	primary	T3a	3	4	67
CA_7	CA	primary	T4	4	3	68
CA_8	CA	primary	T2c	3	3	64
CA_9	CA	primary	T3a	4	4	72
CA_10	CA	primary	T2b	3	3	69
CA_11	CA	primary	T2c	3	4	60
CA_12	CA	primary	T2c	3	3	63
CA_13	CA	primary	T3a	4	4	58
CA_14	CA	primary	T2c	4	4	64
CA_16	CA	primary	T2c	3	3	65
CA_17	CA	primary	T3b	3	4	67
CA_18	CA	primary	T3a	3	3	68
CA_19	CA	primary	T3a	4	3	68
CA_20	CA	primary	T2a	4	4	56
AA_21	AA	primary	T2b	3	3	62
AA_22	AA	primary	T2b	3	5	53
AA_23	AA	primary	T3a	4	5	47
AA_24	AA	primary	T3b	3	4	53
AA_25	AA	primary	T2b	3	4	58
CA_26	CA	primary	T4	3	4	64
AA_27	AA	primary	T2b	3	3	64
AA_28	AA	primary	T2b	3	3	62
AA_29	AA	primary	T2b	3	3	67
CA_30	CA	primary	T2b	3	4	45

Table 3| Prostate tumor metastatic potential score

sampleID	MPS	cohort	subgroup	sampleID	MPS	cohort	subgroup	sampleID	MPS	cohort	subgroup
M_3	1.70	Hopkins	METS	GSM525630	0.57	MSK	PT Control	GSM525747	1.63	MSK	PT Control
M_16	1.18	Hopkins	METS	GSM525631	1.27	MSK	PT Control	GSM525748	1.06	MSK	PT Control
M_17	1.14	Hopkins	METS	GSM525632	0.37	MSK	PT Control	GSM525749	0.42	MSK	PT Control
M_19	1.26	Hopkins	METS	GSM525633	1.01	MSK	PT Control	GSM525750	1.24	MSK	PT Control
M_21	1.51	Hopkins	METS	GSM525634	1.32	MSK	mPT	GSM525751	1.53	MSK	PT Control
M_22	1.54	Hopkins	METS	GSM525635	0.63	MSK	PT Control	GSM525752	0.93	MSK	PT Control
M_24	1.26	Hopkins	METS	GSM525636	0.31	MSK	PT Control	GSM525753	1.73	MSK	ln+
M_28	1.92	Hopkins	METS	GSM525637	1.39	MSK	PT Control	GSM525754	1.66	MSK	mPT
M_30	1.18	Hopkins	METS	GSM525638	1.18	MSK	PT Control	GSM525755	2.06	MSK	PT Control
M_31	1.85	Hopkins	METS	GSM525639	0.54	MSK	PT Control	GSM525756	1.77	MSK	METS
M_32	1.85	Hopkins	METS	GSM525640	1.08	MSK	PT Control	GSM525757	1.11	MSK	METS
M_33	1.29	Hopkins	METS	GSM525641	0.28	MSK	PT Control	GSM525758	1.43	MSK	METS
M_34	1.49	Hopkins	METS	GSM525642	1.35	MSK	PT Control	GSM525759	1.56	MSK	METS
CA_1	0.80	NYU	PT Control	GSM525643	1.14	MSK	PT Control	GSM525760	1.95	MSK	METS
CA_2	0.48	NYU	PT Control	GSM525644	1.08	MSK	PT Control	GSM525761	1.03	MSK	METS
AA_3	1.61	NYU	PT Control	GSM525645	0.58	MSK	PT Control	GSM525762	1.61	MSK	METS
CA_4	1.64	NYU	PT Control	GSM525646	0.95	MSK	PT Control	GSM525763	2.08	MSK	METS
CA_5	0.65	NYU	PT Control	GSM525647	1.55	MSK	mPT	GSM525764	2.05	MSK	METS
CA_6	1.38	NYU	PT Control	GSM525648	1.00	MSK	PT Control	GSM525765	2.00	MSK	METS
CA_7	1.39	NYU	PT Control	GSM525649	0.70	MSK	PT Control	GSM525766	1.29	MSK	METS
CA_8	0.72	NYU	PT Control	GSM525650	0.96	MSK	PT Control	GSM525767	2.04	MSK	METS
CA_9	1.49	NYU	PT Control	GSM525651	0.98	MSK	PT Control	GSM525768	2.01	MSK	METS
CA_10	0.77	NYU	PT Control	GSM525652	0.89	MSK	PT Control	GSM525769	2.02	MSK	METS
CA_11	0.75	NYU	PT Control	GSM525653	0.66	MSK	ln+	GSM525770	1.83	MSK	METS
CA_12	0.90	NYU	PT Control	GSM525654	1.62	MSK	PT Control	GSM525771	2.15	MSK	METS
CA_13	0.58	NYU	PT Control	GSM525655	1.03	MSK	PT Control	GSM525772	1.57	MSK	METS
CA_14	0.89	NYU	PT Control	GSM525656	0.27	MSK	PT Control	GSM525773	1.44	MSK	METS
CA_16	0.67	NYU	PT Control	GSM525657	0.80	MSK	ln+	GSM525774	1.63	MSK	METS
CA_17	0.86	NYU	PT Control	GSM525658	0.67	MSK	PT Control	GSM525775	1.16	MSK	METS
CA_18	0.76	NYU	PT Control	GSM525659	0.92	MSK	PT Control	GSM525776	1.80	MSK	METS
CA_19	1.10	NYU	PT Control	GSM525660	0.53	MSK	PT Control	GSM525777	1.22	MSK	METS
CA_20	0.19	NYU	PT Control	GSM525661	1.72	MSK	PT Control	GSM525778	1.47	MSK	METS
AA_21	0.25	NYU	PT Control	GSM525662	0.57	MSK	PT Control	GSM525779	1.59	MSK	METS
AA_22	1.53	NYU	PT Control	GSM525663	0.59	MSK	PT Control	GSM525780	1.64	MSK	METS
AA_23	0.29	NYU	PT Control	GSM525664	0.06	MSK	PT Control	GSM525781	1.23	MSK	METS
AA_24	1.30	NYU	PT Control	GSM525665	0.28	MSK	PT Control	GSM525782	1.94	MSK	METS
AA_25	0.91	NYU	PT Control	GSM525666	1.50	MSK	mPT	GSM525783	1.80	MSK	METS
CA_26	0.56	NYU	PT Control	GSM525667	0.46	MSK	PT Control	GSM525784	0.91	MSK	METS
AA_27	0.83	NYU	PT Control	GSM525668	1.38	MSK	PT Control	GSM525785	1.98	MSK	METS
AA_28	0.50	NYU	PT Control	GSM525669	0.81	MSK	PT Control	GSM525786	1.84	MSK	METS
AA_29	0.52	NYU	PT Control	GSM525670	0.55	MSK	PT Control	GSM525787	2.10	MSK	METS
CA_30	1.31	NYU	PT Control	GSM525671	0.57	MSK	PT Control	GSM525788	1.65	MSK	METS
AAN_24	0.90	Baylor	PT Control	GSM525672	0.77	MSK	ln+	GSM525789	1.06	MSK	METS
AAN_25	1.42	Baylor	PT Control	GSM525673	1.81	MSK	PT Control	GSM525790	2.16	MSK	METS
AAN_27	0.87	Baylor	PT Control	GSM525674	0.63	MSK	PT Control	GSM525791	1.85	MSK	METS
AAN_31	1.25	Baylor	PT Control	GSM525675	1.01	MSK	PT Control	GSM525792	1.12	MSK	METS
AAN_45	1.30	Baylor	PT Control	GSM525676	0.37	MSK	PT Control	PT130	1.35	SU	PT Control
AAN_52	0.47	Baylor	PT Control	GSM525677	0.90	MSK	PT Control	PL133	0.95	SU	ln+
AAN_58	1.18	Baylor	PT Control	GSM525678	1.61	MSK	PT Control	PT138	0.64	SU	PT Control
AAN_60	0.97	Baylor	PT Control	GSM525679	0.47	MSK	PT Control	PT171	1.16	SU	PT Control
AAN_75	0.60	Baylor	PT Control	GSM525680	0.89	MSK	PT Control	PT173	0.89	SU	PT Control
AAN_110	0.53	Baylor	PT Control	GSM525681	0.89	MSK	PT Control	PT174	1.16	SU	PT Control
AAN_115	0.43	Baylor	PT Control	GSM525682	0.48	MSK	PT Control	PT176	0.72	SU	PT Control
AAN_122	1.05	Baylor	PT Control	GSM525683	0.49	MSK	PT Control	PT177	0.60	SU	PT Control
AAN_128	1.36	Baylor	PT Control	GSM525684	0.32	MSK	PT Control	PT180	0.67	SU	PT Control
AAN_137	0.17	Baylor	PT Control	GSM525685	0.72	MSK	PT Control	PT181	0.93	SU	PT Control
AAN_138	0.87	Baylor	PT Control	GSM525686	1.20	MSK	PT Control	PT308	1.46	SU	PT Control
AAN_140	1.14	Baylor	PT Control	GSM525687	0.66	MSK	PT Control	PT311	0.94	SU	PT Control
AAN_154	1.13	Baylor	PT Control	GSM525688	1.72	MSK	PT Control	PT309	1.10	SU	PT Control
AAN_167	1.31	Baylor	PT Control	GSM525689	0.86	MSK	PT Control	PT312	0.61	SU	PT Control
AAN_80	1.01	Baylor	PT Control	GSM525690	1.22	MSK	PT Control	PT313	0.54	SU	PT Control
AAN_96	1.15	Baylor	PT Control	GSM525691	1.42	MSK	PT Control	PT310	0.66	SU	PT Control
GSM525575	1.67	MSK	PT Control	GSM525692	0.22	MSK	PT Control	PT100	1.07	SU	PT Control
GSM525576	1.83	MSK	PT Control	GSM525693	1.61	MSK	PT Control	PT148	0.39	SU	PT Control
GSM525577	0.87	MSK	ln+	GSM525694	0.67	MSK	PT Control	PT32	0.81	SU	PT Control
GSM525578	1.27	MSK	PT Control	GSM525695	0.42	MSK	PT Control	PT37	0.68	SU	PT Control
GSM525579	1.39	MSK	PT Control	GSM525696	0.37	MSK	PT Control	PT314	1.07	SU	PT Control
GSM525580	1.20	MSK	PT Control	GSM525697	0.90	MSK	PT Control	PT319	1.12	SU	PT Control
GSM525581	0.01	MSK	PT Control	GSM525698	0.25	MSK	PT Control	PT317	1.04	SU	PT Control
GSM525582	0.76	MSK	PT Control	GSM525699	1.20	MSK	PT Control	PT316	1.58	SU	PT Control
GSM525583	0.65	MSK	PT Control	GSM525700	0.57	MSK	PT Control	PT315	1.65	SU	PT Control

...continued

Table 3 | Prostate tumor metastatic potential score

sampleID	MPS	cohort	subgroup	sampleID	MPS	cohort	subgroup	sampleID	MPS	cohort	subgroup
GSM525584	1.76	MSK	PT Control	GSM525701	1.43	MSK	PT Control	PT250	1.12	SU	PT Control
GSM525585	0.65	MSK	PT Control	GSM525702	1.16	MSK	PT Control	PT265	0.76	SU	PT Control
GSM525586	0.52	MSK	PT Control	GSM525703	1.10	MSK	PT Control	PT83	0.54	SU	PT Control
GSM525587	0.83	MSK	PT Control	GSM525704	0.94	MSK	mPT	PT87	0.88	SU	PT Control
GSM525588	1.14	MSK	PT Control	GSM525705	1.11	MSK	PT Control	PT318	0.44	SU	PT Control
GSM525589	0.79	MSK	PT Control	GSM525706	0.84	MSK	PT Control	PT96	1.17	SU	PT Control
GSM525590	1.07	MSK	PT Control	GSM525707	1.32	MSK	PT Control	PT102	0.77	SU	PT Control
GSM525591	0.58	MSK	PT Control	GSM525708	0.71	MSK	PT Control	PL114	0.60	SU	ln+
GSM525592	1.36	MSK	PT Control	GSM525709	1.55	MSK	PT Control	PL115	1.11	SU	ln+
GSM525593	1.23	MSK	PT Control	GSM525710	1.47	MSK	PT Control	PL116	1.43	SU	ln+
GSM525594	1.30	MSK	PT Control	GSM525711	1.07	MSK	PT Control	PT215	0.38	SU	PT Control
GSM525595	1.46	MSK	PT Control	GSM525712	1.28	MSK	PT Control	PT205	0.92	SU	PT Control
GSM525596	0.78	MSK	PT Control	GSM525713	0.87	MSK	ln+	PT335	1.17	SU	PT Control
GSM525597	1.34	MSK	PT Control	GSM525714	1.92	MSK	mPT	PT92	0.72	SU	PT Control
GSM525598	0.82	MSK	PT Control	GSM525715	0.45	MSK	PT Control	PT168	1.41	SU	PT Control
GSM525599	0.76	MSK	PT Control	GSM525716	0.32	MSK	PT Control	PT111	0.87	SU	PT Control
GSM525600	1.54	MSK	PT Control	GSM525717	1.11	MSK	PT Control	PT112	0.63	SU	PT Control
GSM525601	0.76	MSK	PT Control	GSM525718	0.70	MSK	PT Control	PT224	0.99	SU	PT Control
GSM525602	1.80	MSK	mPT	GSM525719	0.66	MSK	PT Control	PT229	0.68	SU	PT Control
GSM525603	1.11	MSK	PT Control	GSM525720	0.70	MSK	PT Control	PT233	0.53	SU	PT Control
GSM525604	0.82	MSK	PT Control	GSM525721	0.59	MSK	PT Control	PT19	1.10	SU	PT Control
GSM525605	1.04	MSK	mPT	GSM525722	0.84	MSK	PT Control	PT05	0.70	SU	PT Control
GSM525606	2.09	MSK	mPT	GSM525723	1.66	MSK	PT Control	PT07	0.59	SU	PT Control
GSM525607	1.01	MSK	PT Control	GSM525724	1.46	MSK	PT Control	PT14	0.68	SU	PT Control
GSM525608	0.98	MSK	PT Control	GSM525725	0.91	MSK	PT Control	PT103	0.83	SU	PT Control
GSM525609	1.19	MSK	PT Control	GSM525726	0.59	MSK	PT Control	PT187	0.67	SU	PT Control
GSM525610	1.32	MSK	PT Control	GSM525727	1.03	MSK	ln+	PT190	0.82	SU	PT Control
GSM525611	1.36	MSK	PT Control	GSM525728	1.22	MSK	PT Control	PT191	1.29	SU	PT Control
GSM525612	1.24	MSK	PT Control	GSM525729	1.48	MSK	PT Control	PT195	0.79	SU	PT Control
GSM525613	1.07	MSK	PT Control	GSM525730	1.54	MSK	PT Control	PT126	0.22	SU	PT Control
GSM525614	1.21	MSK	PT Control	GSM525731	1.15	MSK	PT Control	PT235	0.75	SU	PT Control
GSM525615	0.33	MSK	PT Control	GSM525732	1.32	MSK	PT Control	PT28	0.85	SU	PT Control
GSM525616	1.59	MSK	mPT	GSM525733	0.66	MSK	mPT	PT21	0.50	SU	PT Control
GSM525617	1.15	MSK	PT Control	GSM525734	0.66	MSK	PT Control	PL27	1.43	SU	ln+
GSM525618	1.79	MSK	ln+	GSM525735	1.51	MSK	PT Control	PL118	0.47	SU	ln+
GSM525619	1.46	MSK	mPT	GSM525736	1.12	MSK	PT Control	PL122	1.59	SU	ln+
GSM525620	1.16	MSK	PT Control	GSM525737	1.12	MSK	PT Control	PL129	1.17	SU	ln+
GSM525621	0.77	MSK	PT Control	GSM525738	1.06	MSK	PT Control	PL194	1.59	SU	ln+
GSM525622	1.70	MSK	PT Control	GSM525739	1.19	MSK	PT Control	PT41	0.98	SU	PT Control
GSM525623	0.96	MSK	PT Control	GSM525740	0.80	MSK	PT Control				
GSM525624	0.39	MSK	PT Control	GSM525741	1.20	MSK	PT Control				
GSM525625	1.22	MSK	PT Control	GSM525742	1.35	MSK	PT Control				
GSM525626	2.08	MSK	PT Control	GSM525743	0.81	MSK	PT Control				
GSM525627	0.71	MSK	PT Control	GSM525744	1.60	MSK	PT Control				
GSM525628	0.64	MSK	mPT	GSM525745	1.33	MSK	PT Control				
GSM525629	1.54	MSK	ln+	GSM525746	1.26	MSK	PT Control				

Table 4| Cell line metastatic potential score

sampleID	MPS	Cat. No.	Origin
SS493134	1.78	CCL-121	Lung
SS493087	1.76	HTB-22	Lung
SS356931	1.69	CCL-155	Thyroid gland
SS356919	1.66	HTB-131	Rectum
SS364381	1.59	CRL-1420	Pancreas
SS493086	1.58	HTB-77	Lung
SS285144	1.58	CRL-5806	Lung
SS493106	1.55	CRL-2505	Lung
SS493131	1.54	ACC 298	Lung
SS320522	1.52	HTB-76	Colon
SS493080	1.52	CRL-2289	Lung
SS320536	1.50	CCL-225	Pharynx
SS320523	1.50	HTB-64	Colon
SS285160	1.49	CRL-1933	Lung
SS356911	1.44	HTB-79	Skin
SS285181	1.43	CCL-138	Skin
SS285143	1.42	HTB-112	Lung
SS493083	1.42	CRL-8083	Lung
SS320542	1.42	CRL-1718	Breast
SS285215	1.40	CRL-2064	Breast
SS320532	1.40	HTB-32	Kidney
SS364371	1.39	CRL-2270	Breast
SS356924	1.38	CRL-7898	Thyroid gland
SS320538	1.37	HTB-31	Breast
SS285163	1.37	CCL-119	Prostate
SS356942	1.37	CRL-2062	Breast
SS320553	1.35	HB-8064	Breast
SS320530	1.35	TIB-161	Colon
SS285179	1.35	CRL-5868	Bladder
SS493073	1.35	CRL-1619	Lung
SS493091	1.34	CRL-10741	Lung
SS493075	1.34	CRL-9446	Esophagus
SS285150	0.78	HTB-43	Lung
SS285196	0.78	CCL-218	Liver
SS356915	0.78	CRL-2320	Pancreas
SS285123	0.77	CRL-1611	Hematopoietic and Lymphatic System
SS493085	0.77	HTB-44	Lung
SS247758	0.77	CRL-2321	Lung
SS421711	0.77	CCL-113	Hematopoietic and Lymphatic System
SS285185	0.77	CRL-2331	Skin
SS356910	0.76	CRL-2336	Pancreas
SS493071	0.76	TIB-180	Lung
SS351252	0.76	CRL-1620	Colon
SS356921	0.76	CRL-2338	Central Nervous System
SS351245	0.76	HTB-48	Colon
SS364373	0.76	ACC 325	Bladder
SS247736	0.76	CL-188	Hematopoietic and Lymphatic System
SS285197	0.76	TIB-190	Hematopoietic and Lymphatic System
SS421685	0.76	CRL-2061	Hematopoietic and Lymphatic System
SS493125	0.75	CCL-227	Lung
SS285094	0.75	HTB-103	Central Nervous System
SS351239	0.75	CRL-1739	Stomach
SS285133	0.75	HTB-16	Hematopoietic and Lymphatic System
SS351251	0.74	CCL-228	Brain
SS493135	0.74	CRL-5974	Lung
SS493094	0.73	CRL-9591	Lung
SS351250	0.73	HTB-9	Stomach
SS364372	0.73	CCL-251	Bladder
SS285225	0.73	CRL-2158	Uterus
SS285131	0.73	CCL-235	Bone
SS351249	0.73	CCL-252	Muscle
SS351235	0.72	CRL-2020	Kidney
SS285088	0.72	HTB-13	Central Nervous System
SS493093	0.71	ACC 7	Lung

...continued

Table 4| Cell line metastatic potential score

sampleID	MPS	Cat. No.	Origin
SS356925	1.33	CRL-2049	Hematopoietic and Lymphatic System
SS320539	1.33	HB-8065	Breast
SS285138	1.31	HTB-1	Lung
SS285072	1.31	CRL-1976	Hematopoietic and Lymphatic System
SS421708	1.30	CRL-5819	Hematopoietic and Lymphatic System
SS493081	1.30	CRL-1594	Lung
SS285115	1.30	CRL-2273	Pancreas
SS285137	1.29	CRL-7920	Lung
SS364370	1.28	CRL-2105	Breast
SS320541	1.27	HTB-144	Breast
SS285109	1.27	CRL-2274	Liver
SS320537	1.26	HTB-173	Breast
SS285142	1.26	CRL-1595	Lung
SS320524	1.26	CCL-224	Colon
SS285161	1.26	CRL-2258	Lung
SS285098	1.25	HTB-36	Pharynx
SS493097	1.25	CRL-1977	Lung
SS285102	1.23	CRL-1598	Cervix Uteri
SS356922	1.23	CRL-2220	Pancreas
SS285082	1.22	CCL-85	Kidney
SS364375	1.22	CRL-9607	Hematopoietic and Lymphatic System
SS493102	1.21	CRL-10423	Lung
SS364369	1.21	CRL-1427	Breast
SS320544	1.21	CRL-5892	Breast
SS285172	1.20	CRL-2500	Hematopoietic and Lymphatic System
SS285151	1.20	HTB-46	Lung
SS493137	1.20	CCL-220.1	Lung
SS421690	1.19	CRL-1978	Hematopoietic and Lymphatic System
SS285085	1.18	CRL-1543	Ovary
SS285194	1.18	CCL-243	Liver
SS493088	1.18	CRL-5804	Lung
SS285186	1.18	CRL-2230	Skin
SS285199	0.71	CRL-1473	Bone
SS285226	0.71	HTB-12	Lung
SS356914	0.71	CRL-2315	Uterus
SS285177	0.71	CRL-1472	Prostate
SS364368	0.70	CCL-234	Hematopoietic and Lymphatic System
SS285119	0.70	ACC 448	Hematopoietic and Lymphatic System
SS493103	0.70	CRL-5971	Lung
SS285203	0.70	ACC 29	Bladder
SS421693	0.70	HTB-19	Hematopoietic and Lymphatic System
SS493116	0.70	HTB-148	Lung
SS364379	0.70	ACC 413	Central Nervous System
SS285206	0.69	93121056	Vulva
SS285176	0.69	HTB-80	Uterus
SS247725	0.68	CRL-2268	Connective Tissue
SS421705	0.68	CRL-1579	Hematopoietic and Lymphatic System
SS285099	0.68	CRL-1441	Lung
SS320512	0.67	HTB-82	Lung
SS351253	0.66	HTB-113	Hematopoietic and Lymphatic System
SS421702	0.66	ACC 279	Hematopoietic and Lymphatic System
SS493070	0.66	ACC 20	Lung
SS285065	0.66	HTB-111	Prostate
SS285068	0.66	ACC 135	Skin
SS320507	0.65	CRL-1682	Lung
SS421699	0.65	ACC 198	Hematopoietic and Lymphatic System
SS285148	0.64	CRL-2236	Lung
SS493100	0.64	ACC 360	Lung
SS351241	0.64	ACC 15	Stomach
SS356926	0.63	ACC 403	Hematopoietic and Lymphatic System
SS285219	0.63	ACC 365	Skin
SS421709	0.63	CRL-2265	Hematopoietic and Lymphatic System
SS285218	0.63	ACC 215	Lung
SS285146	0.62	CRL-5973	Lung

...continued

Table 4| Cell line metastatic potential score

sampleID	MPS	Cat. No.	Origin
SS493112	1.17	HTB-47	Lung
SS285080	1.17	HTB-185	Cervix Uteri
SS285202	1.17	CRL-1440	Cervix Uteri
SS356916	1.16	CRL-2119	Liver
SS493096	1.16	CRL-1545	Esophagus
SS493095	1.16	CRL-8294	Esophagus
SS493143	1.14	CRL-5915	Colon
SS285120	1.13	CRL-2231	Bladder
SS285100	1.11	HTB-55	Lung
SS421716	1.11	HTB-187	Hematopoietic and Lymphatic System
SS493079	1.11	CRL-11351	Lung
SS493089	1.11	CRL-1997	Lung
SS285141	1.10	CRL-1622	Lung
SS285154	1.10	CRL-1582	Lung
SS285192	1.10	CRL-2277	Liver
SS247746	1.10	HTB-75	Breast
SS285092	1.10	CCL-213	Colon
SS320540	1.09	CRL-2324	Breast
SS247731	1.09	CRL-2260	Breast
SS351242	1.08	CRL-5922	Bladder
SS285113	1.08	CRL-5808	Skin
SS356907	1.08	HTB-175	Bladder
SS285209	1.07	HTB-69	Colon
SS285164	1.06	CRL-1647	Lung
SS285170	1.06	CRL-7763	Ovary
SS285214	1.06	HTB-172	Breast
SS351246	1.05	CRL-11609	Colon
SS285118	1.05	CRL-2137	Cervix Uteri
SS356933	1.05	HTB-94	Bladder
SS356928	1.04	TIB-202	Thyroid gland
SS285162	1.04	CRL-5985	Rectum
SS285101	1.04	CRL-11732	Lung
SS285175	0.62	ACC 131	Hematopoietic and Lymphatic System
SS421687	0.61	ACC 87	Hematopoietic and Lymphatic System
SS320509	0.61	ACC 277	Hematopoietic and Lymphatic System
SS356940	0.61	ACC 231	Hematopoietic and Lymphatic System
SS285211	0.61	ACC 143	Hematopoietic and Lymphatic System
SS285217	0.61	ACC 427	Eye
SS356941	0.61	CRL-2340	Hematopoietic and Lymphatic System
SS285208	0.60	ACC 361	Synovial Membrane
SS285159	0.60	ACC 317	Lung
SS421724	0.60	ACC 48	Colon
SS421712	0.59	ACC 414	Hematopoietic and Lymphatic System
SS421719	0.59	ACC 382	Hematopoietic and Lymphatic System
SS356912	0.59	CRL-1552	Uterus
SS356932	0.59	CRL-2625	Hematopoietic and Lymphatic System
SS364376	0.58	ACC 548	Kidney
SS421695	0.58	ACC 128	Hematopoietic and Lymphatic System
SS285105	0.57	ACC 18	Kidney
SS421703	0.57	ACC 47	Hematopoietic and Lymphatic System
SS356929	0.56	ACC 399	Central Nervous System
SS493114	0.56	ACC 378	Lung
SS285174	0.55	ACC 346	Bone
SS421713	0.55	CRL-1484	Hematopoietic and Lymphatic System
SS285155	0.54	CCL-87	Lung
SS364366	0.54	CRL-2392	Hematopoietic and Lymphatic System
SS285183	0.54	CRL-2631	Cervix Uteri
SS320525	0.54	ACC 526	Colon
SS285074	0.54	CCL-248	Hematopoietic and Lymphatic System
SS421691	0.54	CCL-246	Hematopoietic and Lymphatic System
SS285126	0.53	CRL-7779	Uterus
SS421706	0.53	ACC 354	Hematopoietic and Lymphatic System
SS421707	0.52	ACC 572	Hematopoietic and Lymphatic System
SS285130	0.51	ACC 576	Uterus

...continued

Table 4| Cell line metastatic potential score

sampleID	MPS	Cat. No.	Origin
SS285190	1.04	CRL-2149	Hematopoietic and Lymphatic System
SS285087	1.03	CRL-2172	Pancreas
SS493104	1.03	CRL-1803	Lung
SS493099	1.03	CRL-5928	Lung
SS285205	1.02	HTB-182	Lung
SS285090	1.01	HTB-161	Skin
SS285066	1.00	HTB-3	Kidney
SS493136	1.00	CRL-2142	Lung
SS285067	1.00	HTB-91	Skin
SS320511	1.00	TIB-196	Skin
SS493119	1.00	CRL-5929	Lung
SS351247	0.99	CRL-5810	Central Nervous System
SS493092	0.99	HTB-62	Lung
SS421718	0.98	CRL-8033-1	Hematopoietic and Lymphatic System
SS285153	0.98	CRL-10302	Brain
SS493074	0.98	CRL-5931	Lung
SS493072	0.98	CRL-5811	Lung
SS285227	0.98	CRL-7724	Uterus
SS356906	0.97	HTB-114	Bladder
SS285193	0.97	CRL-2169	Liver
SS285158	0.97	CRL-1897	Lung
SS493113	0.96	CRL-5826	Lung
SS364374	0.94	HTB-178	Breast
SS421700	0.94	CCL-86	Hematopoietic and Lymphatic System
SS285216	0.94	CRL-2195	Bladder
SS285079	0.93	CRL-2235	Cervix Uteri
SS493108	0.93	HTB-92	Lung
SS493123	0.93	CRL-1902	Lung
SS285149	0.93	CRL-5800	Lung
SS285212	0.92	CRL-5833	Thyroid gland
SS364367	0.92	CCL-136	Stomach
SS493082	0.92	HTB-35	Lung
SS285167	0.51	ACC 546	Lung
SS285112	0.51	HTB-60	Hematopoietic and Lymphatic System
SS351237	0.51	ACC 497	Hematopoietic and Lymphatic System
SS285171	0.50	CRL-2630	Hematopoietic and Lymphatic System
SS285091	0.50	CRL-1432	Brain
SS421694	0.49	CRL-2740	Hematopoietic and Lymphatic System
SS285191	0.49	ACC 197	Uterus
SS285124	0.49	ACC 571	Hematopoietic and Lymphatic System
SS285073	0.49	ACC 577	Hematopoietic and Lymphatic System
SS493090	0.48	HTB-61	Lung
SS421704	0.47	ACC 139	Hematopoietic and Lymphatic System
SS493121	0.46	CRL-8119	Lung
SS285089	0.45	CRL-2632	Hematopoietic and Lymphatic System
SS285198	0.45	CRL-2021	Hematopoietic and Lymphatic System
SS421710	0.44	CRL-1648	Hematopoietic and Lymphatic System
SS285070	0.44	CRL-8119	Muscle
SS285077	0.44	CRL-1649	Cervix Uteri
SS285189	0.44	ACC 584	Central Nervous System
SS285103	0.43	CCL-214	Hematopoietic and Lymphatic System
SS320508	0.43	CRL-5818	Kidney
SS493139	0.43	CRL-5920	Bone
SS364378	0.43	HTB-58	Hematopoietic and Lymphatic System
SS285165	0.43	CRL-5906	Lung
SS356908	0.42	92031919	Stomach
SS351238	0.42	CRL-5883	Colon
SS285093	0.42	96071721	Colon
SS285097	0.42	CRL-5896	Hematopoietic and Lymphatic System
SS421714	0.42	CRL-5983	Hematopoietic and Lymphatic System
SS285210	0.42	CRL-5881	Connective and Soft Tissue
SS356934	0.42	CRL-2578	Brain
SS320548	0.41	HTB-56	Hematopoietic and Lymphatic System
SS320520	0.40	96070808	Hematopoietic and Lymphatic System

...continued

Table 4| Cell line metastatic potential score

sampleID	MPS	Cat. No.	Origin
SS285145	0.91	CRL-2237	Lung
SS356909	0.91	HTB-59	Breast
SS285204	0.91	CRL-1749	Connective Tissue
SS364377	0.91	CRL-5813	Hematopoietic and Lymphatic System
SS285106	0.91	HTB-166	Breast
SS421720	0.90	CRL-2233	Hematopoietic and Lymphatic System
SS285083	0.90	HTB-117	Kidney
SS421696	0.90	HTB-169	Hematopoietic and Lymphatic System
SS285139	0.90	CRL-2128	Lung
SS285086	0.89	HTB-183	Ovary
SS356927	0.89	HTB-88	Ovary
SS285116	0.89	CRL-2238	Pancreas
SS364365	0.88	HTB-118	Breast
SS285127	0.88	CCL-75	Skin
SS356918	0.87	HTB-119	Central Nervous System
SS285075	0.87	CRL-2261	Prostate
SS493078	0.87	HTB-67	Lung
SS493107	0.86	CRL-2234	Lung
SS285104	0.85	HTB-93	Ovary
SS285200	0.85	CRL-1675	Pancreas
SS285071	0.84	CRL-5807	Skin
SS285207	0.84	CRL-1671	Vulva
SS285129	0.84	CRL-2262	Central Nervous System
SS356917	0.84	CCL-237	Central Nervous System
SS320514	0.84	HTB-18	Hematopoietic and Lymphatic System
SS285173	0.83	CCL-233	Muscle
SS493098	0.83	TIB-153	Lung
SS493109	0.83	CRL-2343	Lung
SS285187	0.82	CRL-1974	Central Nervous System
SS493084	0.81	CRL-2314	Esophagus
SS285111	0.81	CRL-1621	Hematopoietic and Lymphatic System
SS421722	0.81	CCL-230	Hematopoietic and Lymphatic System
SS421715	0.40	ACC 351	Hematopoietic and Lymphatic System
SS285132	0.40	CRL-5879	Hematopoietic and Lymphatic System
SS285114	0.40	CCL-256	Sarcoma
SS421701	0.40	CRL-5889	Hematopoietic and Lymphatic System
SS285095	0.40	CRL-5899	Brain
SS285184	0.40	CRL-5893	Vulva
SS285117	0.38	CRL-5841	Hematopoietic and Lymphatic System
SS351244	0.38	HTB-171	Colon
SS285147	0.37	CRL-5942	Lung
SS285096	0.36	CRL-5844	Hematopoietic and Lymphatic System
SS247756	0.36	CRL-5855	Ovary
SS320533	0.36	CRL-5885	Placenta
SS285122	0.36	96062201	Placenta
SS421697	0.35	HTB-174	Hematopoietic and Lymphatic System
SS320531	0.35	CRL-5835	Brain
SS285220	0.34	CRL-5888	Eye
SS421686	0.33	CRL-5831	Hematopoietic and Lymphatic System
SS421723	0.33	CRL-5878	Hematopoietic and Lymphatic System
SS356935	0.32	CRL-5877	Muscle
SS320545	0.31	95062830	Hematopoietic and Lymphatic System
SS285084	0.31	CRL-5816	Lung
SS320513	0.31	CRL-5853	Colon
SS285078	0.31	CRL-2170	Liver
SS493110	0.31	96020724	Lung
SS421688	0.30	CRL-5914	Hematopoietic and Lymphatic System
SS356923	0.30	92031917	Kidney
SS421721	0.30	CRL-5865	Hematopoietic and Lymphatic System
SS285188	0.29	CRL-5895	Brain
SS285182	0.27	CRL-5909	Lung
SS285107	0.26	HTB-54	Colon
SS285121	0.25	CRL-5908	Placenta
SS351243	0.24	CRL-2066	Colon

...continued

Table 4| Cell line metastatic potential score

sampleID	MPS	Cat. No.	Origin
SS285169	0.81	CCL-98	Ovary
SS421717	0.80	TIB-223	Hematopoietic and Lymphatic System
SS285195	0.79	CRL-8644	Liver
SS421689	0.79	ACC 3	Hematopoietic and Lymphatic System
SS285213	0.79	HTB-53	Hematopoietic and Lymphatic System
SS421692	0.79	CCL-244	Hematopoietic and Lymphatic System
SS364380	0.79	CCL-238	Prostate
SS493077	0.79	HTB-25	Lung
SS285108	0.79	CCL-231	Uterus
SS320550	0.23	CRL-5838	Hematopoietic and Lymphatic System
SS351236	0.20	CRL-2098	Colon
SS247755	0.19	CRL-5884	Pancreas
SS285081	0.17	CRL-5872	Prostate
SS285128	0.17	CRL-5871	Hematopoietic and Lymphatic System
SS285125	0.12	92031918	Sarcoma
SS285201	0.08	CRL-5911	Connective Tissue
SS285110	0.00	CRL-5935	Liver

Table 5. Model predictions achieved with a range of genes.

Genes	r2	auc
top12	0.69	0.77
top20	0.78	0.81
top40	0.89	0.85
top80	0.94	0.82
top100	0.94	0.82

Table 6 (1a)

Final-RANK	gene	index	NYU-Z	NYU-dir	NYU-count	MSKs1-Z	MSKs1-dir	MSKs1-count	MSKs2-Z	MSKs2-dir	MSKs2-count	logrank-n52random	logrank-n271random	logrank-composite	gene-Chr	gene-Cytoband
1	PPP3CC	129	3.1	-1	958	2.6	-1	965	NA	NA	NA	48	41	45	8	p21.3
2	SLCO5A1	167	4.9	1	1000	4.2	1	982	NA	NA	NA	31	13	19	8	q13.3
3	SLC7A5	312	1.7	-1	508	3	-1	980	NA	NA	NA	43	37	40	16	q24.2
4	SLC7A2	110	4.1	-1	1000	NA	NA	NA	NA	NA	NA	44	43	44	8	p22
5	CRISPLD2	299	2.5	-1	735	2.9	-1	939	NA	NA	NA	54	67	61	16	q24.1
6	CDH13	288	8	-1	984	2.9	-1	767	NA	NA	NA	46	86	63	16	q23.3
7	CDH8	265	NA	NA	NA	NA	NA	NA	3.7344	-1	989	15	10	11	16	q21
8	CDH2	349	NA	NA	NA	NA	NA	NA	3.4466	-1	987	16	15	17	18	q12.1
9	ASAH1	114	7.1	-1	1000	NA	NA	NA	NA	NA	NA	105	64	80	8	p22
10	KCNB2	175	6.8	1	1000	NA	NA	NA	NA	NA	NA	59	74	66	8	q13.3
11	KCNH4	343	NA	NA	NA	NA	NA	NA	3.7501	1	983	1	1	1	17	q21.2
12	KCTD8	21	NA	NA	NA	NA	NA	NA	2.8192	-1	921	30	24	29	4	p13
13	JPH1	179	6	1	1000	NA	NA	NA	NA	NA	NA	29	35	31	8	q21.11
14	MEST	88	NA	NA	NA	NA	NA	NA	3.2232	1	940	32	32	32	7	q32.2
15	NCALD	207	5.5	1	1000	2.9	1	953	NA	NA	NA	13	12	13	8	q22.3
16	COL19A1	39	NA	NA	NA	NA	NA	NA	3.4333	-1	936	27	20	21.5	6	q13
17	MAP3K7	43	NA	NA	NA	NA	NA	NA	3.1873	-1	929	47	54	49	6	q15
18	YWHAG	67	NA	NA	NA	NA	NA	NA	2.7386	1	951	40	62	47	7	q11.23
19	NOL4	350	NA	NA	NA	NA	NA	NA	3.9113	-1	993	4	2	2	18	q12.1
20	ENOX1	247	NA	NA	NA	NA	NA	NA	5.6235	-1	1000	2	8	4	13	q14.11
21	CSMD1	94	NA	NA	NA	NA	NA	NA	4.6280	-1	971	7	6	6	8	p23.2
22	SGCZ	107	4.7	-1	926	NA	NA	NA	3.5107	-1	861	9	5	7	8	p22
23	PDE10A	54	NA	NA	NA	NA	NA	NA	4.6945	-1	999	8	7	8	6	q27
24	PCDH9	252	NA	NA	NA	NA	NA	NA	4.5416	-1	962	5	19	9	13	q21.32
25	HTR2A	250	NA	NA	NA	NA	NA	NA	3.2974	-1	966	10	11	10	13	q14.2
26	HIP1	63	NA	NA	NA	NA	NA	NA	4.4416	1	1000	11	14	12	7	q11.23
27	CD226	354	NA	NA	NA	NA	NA	NA	3.3032	-1	1000	18	9	14	18	q22.2
28	DCC	352	NA	NA	NA	NA	NA	NA	6.6211	-1	1000	12	17	15	18	q21.2
29	CC2D1A	357	NA	NA	NA	NA	NA	NA	3.9705	1	996	17	18	18	19	p13.12
30	PTK2B	152	7	-1	1000	NA	NA	NA	NA	NA	NA	20	27	21.5	8	p21.2
31	BCMO1	284	2.9	-1	943	3.6	-1	957	NA	NA	NA	26	21	23	16	q23.2
32	MACROD1	238	NA	NA	NA	1.9	1	533	2.8909	1	973	25	22	24	11	q13.1
33	GRID2	24	NA	NA	NA	NA	NA	NA	5.1103	-1	983	22	26	25	4	q22.1
34	DIAPH3	251	NA	NA	NA	NA	NA	NA	3.2653	-1	982	24	29	27	13	q21.2
35	PILRB	69	NA	NA	NA	NA	NA	NA	2.9352	1	996	28	25	28	7	q22.1
36	MEIS2	259	NA	NA	NA	NA	NA	NA	3.9428	-1	999	19	39	30	15	q14
37	MSRA	98	5.1	-1	999	NA	NA	NA	NA	NA	NA	34	31	33	8	p23.1
38	DPYD	4	NA	NA	NA	NA	NA	NA	2.8861	-1	847	33	34	34	1	p21.3

Table 6 (1b)

Final-RANK	gene	gene-start	gene-end	genesBtwn	contig	clump-index	dist-prev	dist-next	min-dist-to-RGL	Index0-Proxy1	NYU-Zadjust	MSKs1-Zadjust	MSKs2-Zadjust
1	PPP3CC	22354541	22454580	0	1	26	10616	-7079	-7079	1	0.52	0.29	NA
2	SLCO5A1	70747129	70909762	0	1	33	216812	-11428	-11428	1	1.63	1.16	NA
3	SLC7A5	86421131	86460615	0	1	58	18511	-64075	18511	1	0.00	0.47	NA
4	SLC7A2	17398975	17472357	0	1	21	6086	-83768	6086	1	1.10	NA	NA
5	CRISPLD2	83411113	83500614	0	1	56	64959	-40087	-40087	1	0.25	0.42	NA
6	CDH13	81439761	82387705	1	0	NA	102526	-750123	102526	1	3.67	0.42	NA
7	CDH8	60244866	60628240	82	0	NA	7528258	-3524069	-3524069	1	NA	NA	0.87
8	CDH2	23784934	24011189	19	0	NA	5673873	NA	5673873	1	NA	NA	0.70
9	ASAH1	17958214	17986787	1	1	22	306248	-22652	-22652	1	3.10	NA	NA
10	KCNB2	73642524	74012880	1	1	34	352193	-492151	352193	1	2.91	NA	NA
11	KCNH4	37562439	37586822	1	1	64	7810	-1891	-1891	1	NA	NA	0.88
12	KCTD8	43870683	44145581	3	0	NA	1800760	-30632257	1800760	1	NA	NA	0.38
13	JPH1	75309493	75396117	0	1	35	29056	-262534	29056	1	2.37	NA	NA
14	MEST	129913282	129933363	0	1	13	41	-45149	41	1	NA	NA	0.58
15	NCALD	102767947	103206311	1	1	40	128437	-16952	-16952	1	2.03	0.42	NA
16	COL19A1	70633169	70978878	20	0	NA	4871884	NA	4871884	1	NA	NA	0.70
17	MAP3K7	91282074	91353628	0	1	5	2654236	-7084576	2654236	1	NA	NA	0.56
18	YWHAG	75794053	75826252	126	0	NA	23787222	-260189	-260189	1	NA	NA	0.34
19	NOL4	29685062	30057513	0	1	67	269766	-5673873	269766	1	NA	NA	0.98
20	ENOX1	42685704	43259044	18	0	NA	2766260	-4175452	2766260	1	NA	NA	2.12
21	CSMD1	2780282	3258996	46	1	14	5420413	-699503	-699503	1	NA	NA	1.44
22	SGCZ	13991744	15140219	0	1	20	301882	-574978	301882	1	1.49	NA	0.74
23	PDE10A	165660766	165995578	NA	1	8	NA	-17665	-17665	1	NA	NA	1.49
24	PCDH9	65774970	66702578	0	1	49	2470149	-6138850	2470149	1	NA	NA	1.38
25	HTR2A	46305514	46368176	44	1	48	12769542	-36146	-36146	1	NA	NA	0.62
26	HIP1	75001345	75206215	5	0	NA	248023	-1543149	248023	1	NA	NA	1.32
27	CD226	65681175	65775140	NA	0	NA	NA	-12833135	-12833135	1	NA	NA	0.63
28	DCC	48121156	49311780	10	0	NA	3157834	-17395350	3157834	1	NA	NA	2.79
29	CC2D1A	13878014	13902691	1	1	68	30662	-105	-105	1	NA	NA	1.02
30	PTK2B	27224916	27372820	0	1	30	376	-165	-165	1	3.04	NA	NA
31	BCMO1	79829797	79882248	0	1	53	23828	-18320	-18320	1	0.42	0.80	NA
32	MACROD1	63522607	63690109	1	0	NA	19764	-81715	19764	1	NA	0.05	0.41
33	GRID2	93444831	94914730	186	0	NA	60460408	-30824069	-30824069	1	NA	NA	1.77
34	DIAPH3	59137718	59636120	2	0	NA	6138850	-12769542	6138850	1	NA	NA	0.60
35	PILRB	99771673	99803388	0	1	11	5616	-111895	5616	1	NA	NA	0.44
36	MEIS2	34970519	35189740	193	0	NA	24742144	NA	24742144	1	NA	NA	1.00
37	MSRA	9949189	10323803	4	1	16	697587	-271923	-271923	1	1.76	NA	NA
38	DPYD	97315890	98159203	19	0	NA	4955408	-79289745	4955408	1	NA	NA	0.41

Table 6 (2a)

39	ANKRD11	329	3	-1	948	3.7	-1	988	NA	NA	NA	37	33	35	16	q24.3
40	NRXN1	6	NA	NA	NA	NA	NA	NA	3.2327	-1	840	39	38	38	2	p16.3
41	ADCY8	225	3.1	1	980	5.4	1	1000	NA	NA	NA	52	30	39	8	q24.22
42	TRDN	49	NA	NA	NA	NA	NA	NA	3.0342	-1	898	38	44	41	6	q22.31
43	STAU2	177	4.6	1	1000	NA	NA	NA	NA	NA	NA	45	42	43	8	q21.11
44	SF1	240	NA	NA	NA	NA	NA	NA	2.4710	1	886	55	46	48	11	q13.1
45	CLIP2	62	NA	NA	NA	NA	NA	NA	3.0945	1	998	57	47	50	7	q11.23
46	CLDN3	58	NA	NA	NA	NA	NA	NA	2.6179	1	984	51	53	51	7	q11.23
47	ZSWIM4	355	NA	NA	NA	NA	NA	NA	2.8120	1	975	60	51	57	19	p13.13
48	GLRB	26	NA	NA	NA	NA	NA	NA	2.6600	-1	963	64	48	58	4	q32.1
49	DCHS2	25	NA	NA	NA	NA	NA	NA	2.7883	-1	954	68	60	64	4	q32.1
50	TRPS1	217	2.9	1	814	2.7	1	751	NA	NA	NA	63	65	65	8	q23.3
51	MDGA2	258	NA	NA	NA	NA	NA	NA	2.8345	-1	823	69	66	68	14	q21.3
52	CNBD1	193	3.8	1	999	3.8	1	940	NA	NA	NA	67	70	69	8	q21.3
53	STAG3	68	NA	NA	NA	NA	NA	NA	2.4187	1	967	78	68	71	7	q22.1
54	GATA4	102	3.2	-1	979	NA	NA	NA	NA	NA	NA	72	77	72	8	p23.1
55	VPS13B	202	3.9	1	999	NA	NA	NA	NA	NA	NA	85	69	74	8	q22.2
56	DOCK5	144	5.4	-1	1000	NA	NA	NA	NA	NA	NA	81	78	76	8	p21.2
57	ZHX2	218	NA	NA	NA	2.6	1	771	NA	NA	NA	82	80	78	8	q24.13
58	ARHGEF5	90	NA	NA	NA	NA	NA	NA	2.7472	1	760	66	102	81	7	q35
59	SDC2	198	3.4	1	991	NA	NA	NA	NA	NA	NA	75	90	82	8	q22.1
60	MYLK	10	NA	NA	NA	2.8	1	842	NA	NA	NA	93	75	83	3	q21.1
61	LPHN3	23	NA	NA	NA	NA	NA	NA	2.4806	-1	794	80	92	85	4	q13.1
62	MOSPD3	78	NA	NA	NA	NA	NA	NA	2.3144	1	904	90	82	86	7	q22.1
63	GYS2	244	NA	NA	NA	NA	NA	NA	2.7616	-1	884	99	83	92	12	p12.1
64	GAS8	336	NA	NA	NA	2.9	-1	999	NA	NA	NA	84	103	95	16	q24.3
65	RAB9A	362	NA	NA	NA	3.7	1	870	NA	NA	NA	98	97	97	23	p22.2
66	POLR3D	127	NA	NA	NA	2.7	-1	955	NA	NA	NA	91	109	98	8	p21.3
67	PSD3	116	7.3	-1	1000	NA	NA	NA	NA	NA	NA	97	104	100	8	p22
68	ZFPM2	213	4.2	1	991	6.3	1	996	NA	NA	NA	149	71	101	8	q23.1
69	ATP6V1C1	209	NA	NA	NA	2.4	1	858	NA	NA	NA	114	93	102	8	q22.3
70	MEF2C	36	NA	NA	NA	NA	NA	NA	2.2584	-1	839	109	98	103	5	q14.3
71	PKIA	185	3.3	1	999	NA	NA	NA	NA	NA	NA	115	99	104	8	q21.12
72	ADAMTS18	276	3.5	-1	902	NA	NA	NA	NA	NA	NA	100	114	105	16	q23.1
73	STYXL1	65	NA	NA	NA	NA	NA	NA	2.3049	1	863	104	110	106	7	q11.23
74	EPM2A	51	NA	NA	NA	NA	NA	NA	2.3972	-1	920	113	105	108	6	q24.3
75	LEPREL1	19	NA	NA	NA	2.6	1	755	NA	NA	NA	106	119	110	3	q28
76	GABRA2	22	NA	NA	NA	NA	NA	NA	2.2755	-1	876	119	107	111	4	p12
77	RCOR2	237	NA	NA	NA	NA	NA	NA	1.7131	1	514	108	120	114	11	q13.1
78	MFHAS1	95	3.3	-1	956	NA	NA	NA	NA	NA	NA	121	108	115	8	p23.1

Table 6 (2b)

39	ANKRD11	87861536	88084470	11	1	61	246990	-72136	-72136	1	0.47	0.85	NA
40	NRXN1	49999148	51113178	155	0	NA	28619013	NA	28619013	1	NA	NA	0.59
41	ADCY8	131861736	132123854	0	1	45	861663	-378337	-378337	1	0.52	1.97	NA
42	TRDN	123579182	123999937	96	0	NA	20654629	-5440605	-5440605	1	NA	NA	0.48
43	STAU2	74495160	74821629	1	0	NA	199555	-119303	-119303	1	1.43	NA	NA
44	SF1	64288654	64302817	1	0	NA	24747	-560058	24747	1	NA	NA	0.23
45	CLIP2	73341739	73458196	15	1	9	1543149	-35065	-35065	1	NA	NA	0.52
46	CLDN3	72821263	72822536	5	0	NA	404089	-49338	-49338	1	NA	NA	0.29
47	ZSWIM4	13767274	13804044	1	0	NA	50124	NA	50124	1	NA	NA	0.38
48	GLRB	158216788	158312299	0	1	3	48887	-2584470	48887	1	NA	NA	0.31
49	DCHS2	155375138	155632318	14	0	NA	2584470	-60460408	2584470	1	NA	NA	0.37
50	TRPS1	116489900	116750429	20	1	43	7112653	-1971482	-1971482	1	0.42	0.33	NA
51	MDGA2	46379045	47213703	NA	NA	NA	NA	NA	NA	1	NA	NA	0.39
52	CNBD1	87947840	88435220	1	1	38	683360	-122823	-122823	1	0.91	0.91	NA
53	STAG3	99613474	99659778	2	0	NA	111895	-23787222	111895	1	NA	NA	0.21
54	GATA4	11599162	11654918	0	1	18	9709	-139646	9709	1	0.57	NA	NA
55	VPS13B	100094670	100958983	1	0	NA	83469	-187596	83469	1	0.98	NA	NA
56	DOCK5	25098204	25326536	2	0	NA	14747	-1478148	14747	1	1.97	NA	NA
57	ZHX2	123863082	124055936	9	0	NA	706280	-7112653	706280	1	NA	0.29	NA
58	ARHGEF5	143683366	143708657	NA	0	NA	NA	-13747479	-13747479	1	NA	NA	0.35
59	SDC2	97575058	97693213	1	1	39	1032370	-159108	-159108	1	0.68	NA	NA
60	MYLK	124811586	125085868	2	0	NA	210407	-8462769	210407	1	NA	0.38	NA
61	LPHN3	62045434	62620762	157	0	NA	30824069	NA	30824069	1	NA	NA	0.24
62	MOSPD3	100047661	100050932	0	1	12	5043	-3929	-3929	1	NA	NA	0.17
63	GYS2	21580390	21649048	NA	NA	NA	NA	NA	NA	1	NA	NA	0.36
64	GAS8	88616509	88638880	NA	0	NA	NA	-21813	-21813	1	NA	0.42	NA
65	RAB9A	13617262	13637681	191	0	NA	35134932	NA	35134932	1	NA	0.85	NA
66	POLR3D	22158564	22164624	1	1	25	116113	-12768	-12768	1	NA	0.33	NA
67	PSD3	18429093	18915476	0	1	23	300007	-126090	-126090	1	3.23	NA	NA
68	ZFPM2	106400323	106885939	2	1	41	1444960	-729979	-729979	1	1.16	2.58	NA
69	ATP6V1C1	104102424	104154461	5	0	NA	427830	-608753	427830	1	NA	0.21	NA
70	MEF2C	88051922	88214780	63	0	NA	26727467	-19278276	-19278276	1	NA	NA	0.15
71	PKIA	79590891	79678040	2	0	NA	1007876	-1648815	1007876	1	0.63	NA	NA
72	ADAMTS18	75873527	76026512	0	1	52	287400	-722891	287400	1	0.74	NA	NA
73	STYXL1	75463592	75515257	0	1	10	72	-1679	72	1	NA	NA	0.17
74	EPM2A	145988141	146098684	2	1	7	291927	-772282	291927	1	NA	NA	0.20
75	LEPREL1	191157213	191321407	NA	1	2	NA	-49278	-49278	1	NA	0.29	NA
76	GABRA2	45946341	46086561	NA	0	NA	NA	-1800760	-1800760	1	NA	NA	0.16
77	RCOR2	63435303	63440892	3	0	NA	81715	NA	81715	1	NA	NA	0.00
78	MFHAS1	8679409	8788541	0	1	15	109315	-5420413	109315	1	0.63	NA	NA

Table 6 (3a)

79	SCARA5	156	3.3	-1	925	NA	NA	NA	NA	NA	NA	130	101	116	8	p21.1
80	CCDC25	155	4.4	-1	995	NA	NA	NA	NA	NA	NA	132	100	117	8	p21.1
81	FAM38A	323	NA	NA	NA	2.7	-1	885	NA	NA	NA	110	130	119	16	q24.3
82	CTSB	104	2.8	-1	941	NA	NA	NA	NA	NA	NA	111	136	122	8	p23.1
83	PTK2	235	NA	NA	NA	2.3	1	654	NA	NA	NA	107	144	123	8	q24.3
84	SPIRE2	331	NA	NA	NA	1.7	-1	508	NA	NA	NA	124	128	124	16	q24.3
85	C13orf23	246	NA	NA	NA	NA	NA	NA	2.2139	-1	748	141	113	125	13	q13.3
86	BOD1L	20	NA	NA	NA	NA	NA	NA	2.3508	-1	884	129	127	126	4	p15.33
87	FAM160B2	120	2.5	-1	899	1.8	-1	567	NA	NA	NA	127	133	129	8	p21.3
88	NUS1	48	NA	NA	NA	NA	NA	NA	2.2269	-1	859	123	139	130	6	q22.2
89	MTHFSD	309	NA	NA	NA	2.4	-1	824	NA	NA	NA	112	153	131	16	q24.1
90	UBR5	208	NA	NA	NA	2.2	1	733	NA	NA	NA	122	155	135.5	8	q22.3
91	GALNS	325	NA	NA	NA	2.3	-1	856	NA	NA	NA	131	147	137	16	q24.3
92	FSTL5	28	NA	NA	NA	NA	NA	NA	2.2407	-1	641	138	143	140	4	q32.2
93	SIM1	46	NA	NA	NA	NA	NA	NA	2.1943	-1	833	120	165	141	6	q16.3
94	TG	231	3.8	1	997	NA	NA	NA	NA	NA	NA	136	149	144	8	q24.22
95	BFSP2	12	NA	NA	NA	2.4	1	678	NA	NA	NA	139	154	148	3	q22.1
96	MMP16	194	NA	NA	NA	3.5	1	931	NA	NA	NA	158	138	149	8	q21.3
97	RIMS2	210	2	1	692	4	1	939	NA	NA	NA	161	141	150	8	q22.3
98	PDS5B	245	NA	NA	NA	NA	NA	NA	2.0408	-1	661	145	159	151	13	q13.1
99	CDK7	31	NA	NA	NA	2.7	-1	988	NA	NA	NA	156	148	153	5	q13.2
100	CNTNAP4	275	3.2	-1	825	NA	NA	NA	NA	NA	NA	196	126	156	16	q23.1
101	CFDP1	274	3	-1	925	NA	NA	NA	NA	NA	NA	137	187	157	16	q23.1
102	FBXL4	45	NA	NA	NA	NA	NA	NA	1.7473	-1	537	154	167	158	6	q16.2
103	RFX1	358	NA	NA	NA	NA	NA	NA	2.1724	1	861	134	201	163	19	p13.12
104	NALCN	256	NA	NA	NA	NA	NA	NA	2.1846	-1	731	182	152	165	13	q33.1
105	STX1A	57	NA	NA	NA	NA	NA	NA	2.1787	1	835	177	161	167	7	q11.23
106	CYP7B1	162	NA	NA	NA	1.7	1	508	NA	NA	NA	147	204	168	8	q12.3
107	ARHGEF10	92	NA	NA	NA	2.9	-1	923	NA	NA	NA	215	145	171	8	p23.3
108	ENTPD4	141	2.7	-1	875	NA	NA	NA	NA	NA	NA	230	137	173	8	p21.3
109	ZNF704	188	NA	NA	NA	2.5	1	815	NA	NA	NA	211	151	174	8	q21.13
110	C8orf79	105	2.9	-1	937	NA	NA	NA	NA	NA	NA	163	197	176	8	p22
111	SLC9A9	13	NA	NA	NA	2.7	1	746	NA	NA	NA	170	189	177	3	q24
112	CHMP7	139	NA	NA	NA	2.4	-1	925	NA	NA	NA	185	176	178	8	p21.3
113	GPC5	255	NA	NA	NA	NA	NA	NA	2.1374	-1	610	171	193	180	13	q31.3
114	MYC	222	4.2	1	972	NA	NA	NA	NA	NA	NA	218	157	184	8	q24.21
115	STIP1	239	NA	NA	NA	NA	NA	NA	1.7766	1	613	164	209	185	11	q13.1
116	ZBTB20	9	NA	NA	NA	1.8	1	513	NA	NA	NA	187	184	186	3	q13.31
117	MEN1	241	NA	NA	NA	NA	NA	NA	2.0513	1	737	176	203	188	11	q13.1
118	SLC26A7	195	NA	NA	NA	2.2	1	747	NA	NA	NA	213	168	189	8	q21.3

Table 6 (3b)

79	SCARA5	27783672	27906117	0	1	31	29490	-97583	29490	1	0.63	NA	NA
80	CCDC25	27646756	27686089	2	0	NA	97583	-188353	97583	1	1.29	NA	NA
81	FAM38A	87302916	87330317	0	1	59	67370	-2604	-2604	1	NA	0.33	NA
82	CTSB	11737442	11763055	7	0	NA	1084499	-55179	-55179	1	0.38	NA	NA
83	PTK2	141737683	142080514	NA	0	NA	NA	-5943220	-5943220	1	NA	0.17	NA
84	SPIRE2	88422408	88465228	0	1	62	2292	-11842	2292	1	NA	0.00	NA
85	C13orf23	38482003	38510252	21	0	NA	4175452	-6231846	4175452	1	NA	NA	0.14
86	BOD1L	13179464	13238426	76	0	NA	30632257	NA	30632257	1	NA	NA	0.19
87	FAM160B2	22002660	22017835	0	1	24	2493	-82619	2493	1	0.25	0.02	NA
88	NUS1	118103310	118138577	15	0	NA	5440605	-16667349	5440605	1	NA	NA	0.14
89	MTHFSD	85121284	85157509	5	1	57	1036491	-15714	-15714	1	NA	0.21	NA
90	UBR5	103334748	103493671	3	0	NA	608753	-128437	-128437	1	NA	0.14	NA
91	GALNS	87407644	87450885	0	1	60	122	-4478	122	1	NA	0.17	NA
92	FSTL5	162524501	163304636	NA	0	NA	NA	-4017824	-4017824	1	NA	NA	0.15
93	SIM1	100939606	101019494	0	1	6	43297	-1437036	43297	1	NA	NA	0.13
94	TG	133948387	134216325	0	1	46	-98170	-18153	-18153	1	0.91	NA	NA
95	BFSP2	134601480	134676746	58	0	NA	9790009	-8678754	-8678754	1	NA	0.21	NA
96	MMP16	89118580	89408833	9	0	NA	2921859	-683360	-683360	1	NA	0.74	NA
97	RIMS2	104582291	105333263	1	0	NA	127566	-427830	127566	1	0.07	1.04	NA
98	PDS5B	32058564	32250157	21	0	NA	6231846	NA	6231846	1	NA	NA	0.08
99	CDK7	68566471	68609004	0	1	4	3274	11239	3274	1	NA	0.33	NA
100	CNTNAP4	74868677	75150636	1	0	NA	722891	-843789	722891	1	0.57	NA	NA
101	CFDP1	73885109	74024888	7	1	51	843789	-25657	-25657	1	0.47	NA	NA
102	FBXL4	99428055	99502570	7	0	NA	1437036	-5242062	1437036	1	NA	NA	0.01
103	RFX1	13933353	13978097	NA	0	NA	NA	-30662	-30662	1	NA	NA	0.13
104	NALCN	100504131	100866814	42	0	NA	12420243	-8187438	-8187438	1	NA	NA	0.13
105	STX1A	72751472	72771925	1	0	NA	49338	NA	49338	1	NA	NA	0.13
106	CYP7B1	65671246	65873902	21	0	NA	2623061	-5476925	2623061	1	NA	0.00	NA
107	ARHGEF10	1759549	1894206	1	0	NA	86359	-115501	86359	1	NA	0.42	NA
108	ENTPD4	23299386	23371081	0	1	28	71227	18281	18281	1	0.33	NA	NA
109	ZNF704	81713324	81949571	0	1	37	93034	-870671	93034	1	NA	0.25	NA
110	C8orf79	12847554	12931653	0	1	19	53590	-1084499	53590	1	0.42	NA	NA
111	SLC9A9	144466755	145049979	50	0	NA	12271116	-9790009	-9790009	1	NA	0.33	NA
112	CHMP7	23157095	23175450	1	1	27	34647	-18511	-18511	1	NA	0.21	NA
113	GPC5	90848919	92316693	29	0	NA	8187438	-19509588	8187438	1	NA	NA	0.11
114	MYC	128816862	128822853	0	1	44	206193	-318241	206193	1	1.16	NA	NA
115	STIP1	63709873	63728596	20	0	NA	560058	-19764	-19764	1	NA	NA	0.01
116	ZBTB20	115540230	116348817	51	0	NA	8462769	-8761797	8462769	1	NA	0.02	NA
117	MEN1	64327564	64335342	0	1	47	12898	-24747	12898	1	NA	NA	0.09
118	SLC26A7	92330692	92479554	5	0	NA	2729012	-2921859	2729012	1	NA	0.14	NA

Table 6 (4a)

119	ALCAM	8	NA	NA	NA	NA	NA	NA	2.4602	1	586	194	186	191	3	q13.11
120	KIF13B	160	2.7	-1	854	NA	NA	NA	NA	NA	NA	188	194	192	8	p21.1
121	MBTPS1	291	2.7	-1	906	NA	NA	NA	NA	NA	NA	193	192	193	16	q24.1
122	PPP2R5B	243	NA	NA	NA	NA	NA	NA	1.8055	1	580	189	202	196	11	q13.1
123	VPS13C	260	NA	NA	NA	NA	NA	NA	1.7860	-1	550	201	190	197	15	q22.2
124	ASPSCR1	346	NA	NA	NA	NA	NA	NA	1.7635	1	549	219	178	198	17	q25.3
125	EPO	82	NA	NA	NA	NA	NA	NA	1.9843	1	735	169	235	201	7	q22.1
126	HEY1	187	3	1	988	NA	NA	NA	NA	NA	NA	206	195	203	8	q21.13
127	KALRN	11	NA	NA	NA	2.4	1	674	NA	NA	NA	197	205	204	3	q21.1
128	RGS22	203	2.7	1	956	NA	NA	NA	NA	NA	NA	191	215	205	8	q22.2
129	WDR7	353	NA	NA	NA	NA	NA	NA	1.9953	-1	653	200	217	210	18	q21.31
130	COL11A1	5	NA	NA	NA	NA	NA	NA	1.8924	-1	591	233	206	213	1	p21.1
131	GHDC	344	NA	NA	NA	NA	NA	NA	1.7523	1	523	221	218	215	17	q21.2
132	ATP2C2	295	3.6	-1	943	NA	NA	NA	NA	NA	NA	216	226	216	16	q24.1
133	CDH17	196	2.8	1	976	NA	NA	NA	NA	NA	NA	227	216	217	8	q22.1
134	DGKG	17	NA	NA	NA	1.9	1	568	NA	NA	NA	192	258	219	3	q27.3
135	GRK5	236	NA	NA	NA	2.4	-1	831	NA	NA	NA	210	237	220	10	q26.11
136	GRM1	52	NA	NA	NA	NA	NA	NA	1.8988	-1	587	179	283	223	6	q24.3
137	IMPA1	190	NA	NA	NA	1.9	1	647	NA	NA	NA	243	210	224	8	q21.13
138	RPL7	176	2.3	1	813	NA	NA	NA	NA	NA	NA	261	211	229	8	q21.11
139	COL21A1	38	NA	NA	NA	NA	NA	NA	1.8391	-1	596	235	246	232	6	p12.1
140	COL12A1	40	NA	NA	NA	NA	NA	NA	1.8241	-1	597	241	240	233	6	q14.1
141	MLYCD	289	2.4	-1	819	NA	NA	NA	NA	NA	NA	234	248	234	16	q23.3
142	AR	366	2.3	1	690	2.6	1	806	NA	NA	NA	266	221	235	23	q12
143	PLCB1	359	NA	NA	NA	NA	NA	NA	1.9352	-1	579	181	330	240	20	p12.3
144	ACTL8	3	NA	NA	NA	1.9	-1	582	NA	NA	NA	264	229	242	1	p36.13
145	TFDP1	257	NA	NA	NA	2.3	-1	729	NA	NA	NA	205	304	248	13	q34
146	IQCE	55	NA	NA	NA	NA	NA	NA	1.8487	1	580	250	260	255	7	p22.2
147	SMARCB1	360	NA	NA	NA	1.8	-1	523	NA	NA	NA	239	276	256	22	q11.23
148	MTDH	199	NA	NA	NA	1.9	1	584	NA	NA	NA	225	301	259	8	q22.1
149	NECAB2	290	NA	NA	NA	2	-1	688	NA	NA	NA	255	271	262	16	q23.3
150	DEF8	334	NA	NA	NA	1.9	-1	678	NA	NA	NA	214	335	266	16	q24.3
151	RNF40	262	NA	NA	NA	NA	NA	NA	2.0578	1	774	320	227	270	16	p11.2
152	TICAM2	37	NA	NA	NA	NA	NA	NA	1.8257	-1	589	303	241	271	5	q22.3
153	GLG1	271	2.1	-1	647	NA	NA	NA	NA	NA	NA	327	225	273	16	q22.3
154	MECOM	16	NA	NA	NA	2	1	587	NA	NA	NA	279	268	277	3	q26.2
155	TCEB1	178	1.8	1	590	NA	NA	NA	NA	NA	NA	275	277	279	8	q21.11
156	CTNNA2	7	NA	NA	NA	NA	NA	NA	1.8228	-1	538	331	231	280	2	p12
157	NIPAL2	200	1.9	1	654	NA	NA	NA	NA	NA	NA	289	265	282	8	q22.2
158	CDCA2	146	2	-1	686	NA	NA	NA	NA	NA	NA	301	255	283	8	p21.2

Table 6 (4b)

119	ALCAM	106568403	106778433	49	0	NA	8761797	NA	8761797	1	NA	NA	0.23
120	KIF13B	28980715	29176529	NA	1	32	NA	-14009	-14009	1	0.33	NA	NA
121	MBTPS1	82644872	82708018	0	1	54	5371	-50994	5371	1	0.33	NA	NA
122	PPP2R5B	64448756	64458523	NA	0	NA	NA	-80139	-80139	1	NA	NA	0.02
123	VPS13C	59931884	60139939	NA	0	NA	NA	-24742144	-24742144	1	NA	NA	0.02
124	ASPSCR1	77528715	77568569	6	1	65	40474	-16362	-16362	1	NA	NA	0.01
125	EPO	100156359	100159257	146	0	NA	29534682	-31553	-31553	1	NA	NA	0.07
126	HEY1	80838801	80842653	3	1	36	870671	-97933	-97933	1	0.47	NA	NA
127	KALRN	125296275	125922726	76	0	NA	8678754	-210407	-210407	1	NA	0.21	NA
128	RGS22	101042452	101187520	7	0	NA	812460	-83469	-83469	1	0.33	NA	NA
129	WDR7	52469614	52848040	45	0	NA	12833135	-3157834	-3157834	1	NA	NA	0.07
130	COL11A1	103114611	103346640	NA	0	NA	NA	-4955408	-4955408	1	NA	NA	0.04
131	GHDC	37594632	37599722	482	0	NA	39903967	-7810	-7810	1	NA	NA	0.01
132	ATP2C2	82959634	83055293	0	1	55	13315	-38746	13315	1	0.80	NA	NA
133	CDH17	95208566	95289986	14	0	NA	2053354	-2729012	2053354	1	0.38	NA	NA
134	DGKG	187347686	187562717	23	0	NA	3269193	-17000632	3269193	1	NA	0.05	NA
135	GRK5	120957091	121205118	NA	NA	NA	NA	NA	NA	1	NA	0.21	NA
136	GRM1	146390611	146800427	83	0	NA	18812721	-291927	-291927	1	NA	NA	0.04
137	IMPA1	82732751	82761115	4	0	NA	2842997	-545893	-545893	1	NA	0.05	NA
138	RPL7	74365073	74375857	1	0	NA	119303	-352193	119303	1	0.17	NA	NA
139	COL21A1	56029347	56366851	NA	NA	NA	NA	NA	NA	1	NA	NA	0.03
140	COL12A1	75850762	75972343	18	0	NA	7686493	-4871884	-4871884	1	NA	NA	0.03
141	MLYCD	82490231	82507286	1	0	NA	52452	-102526	52452	1	0.21	NA	NA
142	AR	66680599	66860844	0	1	69	318596	-904991	318596	1	0.17	0.29	NA
143	PLCB1	8061296	8813547	NA	NA	NA	NA	NA	NA	1	NA	NA	0.05
144	ACTL8	17954395	18026145	662	1	1	79289745	-57439	-57439	1	NA	0.05	NA
145	TFDP1	113287057	113343500	NA	0	NA	NA	-12420243	-12420243	1	NA	0.17	NA
146	IQCE	2565158	2620893	13	0	NA	2861062	NA	2861062	1	NA	NA	0.03
147	SMARCB1	22459150	22506703	290	0	NA	23030490	NA	23030490	1	NA	0.02	NA
148	MTDH	98725583	98807711	7	0	NA	465852	-1032370	465852	1	NA	0.05	NA
149	NECAB2	82559738	82593878	1	0	NA	50994	-52452	50994	1	NA	0.07	NA
150	DEF8	88542684	88561968	0	1	63	4521	-12678	4521	1	NA	0.05	NA
151	RNF40	30681100	30695129	NA	0	NA	NA	-392513	-392513	1	NA	NA	0.09
152	TICAM2	114942247	114989610	NA	0	NA	NA	-26727467	-26727467	1	NA	NA	0.03
153	GLG1	73043357	73198518	3	0	NA	266457	-1403582	266457	1	0.10	NA	NA
154	MECOM	170283981	170347054	89	0	NA	17000632	-8012470	-8012470	1	NA	0.07	NA
155	TCEB1	75021184	75046959	2	0	NA	262534	-199555	-199555	1	0.02	NA	NA
156	CTNNA2	79732191	80729415	NA	0	NA	NA	-28619013	-28619013	1	NA	NA	0.03
157	NIPAL2	99273563	99375797	1	0	NA	160240	-465852	160240	1	0.05	NA	NA
158	CDCA2	25372428	25421353	0	1	29	336689	-591	-591	1	0.07	NA	NA

Table 6 (5a)

159	WWP2	267	1.8	-1	527	NA	NA	NA	NA	NA	NA	251	315	284	16	q22.1
160	DDX19A	268	2.3	-1	756	NA	NA	NA	NA	NA	NA	220	363	285	16	q22.1
161	STK3	201	1.8	1	614	NA	NA	NA	NA	NA	NA	265	309	287	8	q22.2
162	DNAH2	337	1.8	-1	541	NA	NA	NA	NA	NA	NA	247	332	288	17	p13.1
163	NFAT5	266	2.3	-1	760	NA	NA	NA	NA	NA	NA	326	254	291	16	q22.1
164	CNGB1	263	1.8	-1	524	NA	NA	NA	NA	NA	NA	297	280	292	16	q13
165	UBE2CBP	41	2.8	-1	891	NA	NA	NA	NA	NA	NA	256	326	293	6	q14.1
166	C8orf16	99	2.2	-1	725	NA	NA	NA	NA	NA	NA	285	293	294	8	p23.1
167	KIAA0196	220	2.6	1	819	NA	NA	NA	NA	NA	NA	253	334	296	8	q24.13
168	CLCNKB	1	NA	NA	NA	NA	NA	NA	2.0014	1	746	276	307	297	1	p36.13
169	C16orf80	264	2.2	-1	677	NA	NA	NA	NA	NA	NA	281	302	298	16	q21
170	ZFHX3	270	2.2	-1	656	NA	NA	NA	NA	NA	NA	313	273	299	16	q22.3
171	PPM1L	15	NA	NA	NA	2	1	628	NA	NA	NA	270	329	303	3	q26.1
172	NKIRAS2	338	NA	NA	NA	NA	NA	NA	1.9634	1	679	298	299	304	17	q21.2
173	RSPO2	215	1.8	1	550	NA	NA	NA	NA	NA	NA	306	292	305	8	q23.1
174	XPO7	119	2.3	-1	735	NA	NA	NA	NA	NA	NA	329	272	306	8	p21.3
175	ME1	42	2.5	-1	728	NA	NA	NA	NA	NA	NA	282	321	307	6	q14.2
176	NLGN4Y	368	NA	NA	NA	NA	NA	NA	2.4188	-1	734	339	275	312	24	q11.221
177	LZTS1	118	2	-1	645	NA	NA	NA	NA	NA	NA	300	316	316	8	p21.3
178	FBXL18	56	NA	NA	NA	NA	NA	NA	1.8646	1	652	323	294	317	7	p22.1
179	TBC1D10B	261	NA	NA	NA	NA	NA	NA	1.8243	1	573	278	347	321	16	p11.2
180	WDR59	272	2.1	-1	653	NA	NA	NA	NA	NA	NA	304	320	322	16	q23.1
181	BLK	101	2.1	-1	671	NA	NA	NA	NA	NA	NA	315	314	325	8	p23.1
182	MEPCE	71	NA	NA	NA	NA	NA	NA	2.1134	1	782	350	285	327	7	q22.1
183	DLGAP2	91	NA	NA	NA	2.2	-1	682	NA	NA	NA	356	286	330	8	p23.3
184	ZFAT	234	2.5	1	796	NA	NA	NA	NA	NA	NA	325	317	331	8	q24.22
185	FASN	348	NA	NA	NA	NA	NA	NA	3.0027	1	963	296	350	332	17	q25.3
186	GIGYF1	81	NA	NA	NA	NA	NA	NA	2.7127	1	957	335	311	335	7	q22.1
187	ANXA13	219	2.1	1	682	NA	NA	NA	NA	NA	NA	310	345	336	8	q24.13
188	CDYL2	280	2.5	-1	699	NA	NA	NA	NA	NA	NA	316	351	339	16	q23.2
189	TOX	161	4.3	1	993	NA	NA	NA	NA	NA	NA	338	342	349	8	q12.1
190	NKX2-6	143	2.4	-1	870	NA	NA	NA	NA	NA	NA	340	366	357	8	p21.2
191	RALYL	191	2.8	1	985	NA	NA	NA	NA	NA	NA	345	362	359	8	q21.2
192	TBC1D22A	361	NA	NA	NA	4.6	-1	999	NA	NA	NA	367	346	363	22	q13.31
193	TFE3	363	NA	NA	NA	2.1	1	591	NA	NA	NA	362	353	364	23	p11.23
194	KCNAB1	14	NA	NA	NA	5.8	1	996	NA	NA	NA	363	367	367	3	q25.31
195	SULF1	166	5.2	1	1000	3.4	1	994	NA	NA	NA	3	4	3	8	q13.2
196	RAB5C	342	NA	NA	NA	NA	NA	NA	3.5399	1	998	6	3	5	17	q21.2
197	DHX58	339	NA	NA	NA	NA	NA	NA	8.9116	1	952	14	16	16	17	q21.2
198	ASAP1	224	NA	NA	NA	3.6	1	974	NA	NA	NA	21	23	20	8	q24.21

Table 6 (5b)

159	WWP2	68353710	68533145	5	0	NA	405177	-57656	-57656	1	0.02	NA	NA
160	DDX19A	68938322	68964780	0	1	50	6059	-405177	6059	1	0.17	NA	NA
161	STK3	99536037	99907074	1	0	NA	187596	-160240	-160240	1	0.02	NA	NA
162	DNAH2	7562746	7677783	NA	NA	NA	NA	NA	NA	1	0.02	NA	NA
163	NFAT5	68156498	68296054	2	0	NA	57656	-7528258	57656	1	0.17	NA	NA
164	CNGB1	56475004	56562513	3	0	NA	142487	NA	142487	1	0.02	NA	NA
165	UBE2CBP	83658836	83832269	3	0	NA	144558	-7686493	144558	1	0.38	NA	NA
166	C8orf16	11021390	11025155	0	1	17	154255	-697587	154255	1	0.14	NA	NA
167	KIAA0196	126105691	126173191	3	0	NA	2323848	-1286863	-1286863	1	0.29	NA	NA
168	CLCNKB	16242834	16256390	29	0	NA	1482527	NA	1482527	1	NA	NA	0.07
169	C16orf80	56705000	56720797	10	0	NA	3524069	-142487	-142487	1	0.14	NA	NA
170	ZFHX3	71374285	71639775	2	0	NA	1403582	-2343793	1403582	1	0.14	NA	NA
171	PPM1L	161956791	162271511	13	0	NA	8012470	-4217170	-4217170	1	NA	0.07	NA
172	NKIRAS2	37422564	37431180	1	0	NA	75799	NA	75799	1	NA	NA	0.06
173	RSPO2	108980721	109165052	9	1	42	4139285	-401262	-401262	1	0.02	NA	NA
174	XPO7	21833126	21920041	3	0	NA	82619	-1627372	82619	1	0.17	NA	NA
175	ME1	83976827	84197498	41	0	NA	7084576	-144558	-144558	1	0.25	NA	NA
176	NLGN4Y	15144026	15466924	NA	NA	NA	NA	NA	NA	1	NA	NA	0.21
177	LZTS1	20147956	20205754	2	0	NA	1627372	-850362	-850362	1	0.07	NA	NA
178	FBXL18	5481955	5523646	NA	0	NA	NA	-2861062	-2861062	1	NA	NA	0.04
179	TBC1D10B	30275925	30288587	14	0	NA	392513	NA	392513	1	NA	NA	0.03
180	WDR59	73464975	73576518	5	0	NA	243911	-266457	243911	1	0.10	NA	NA
181	BLK	11388930	11459516	1	0	NA	139646	-165868	139646	1	0.10	NA	NA
182	MEPCE	99865190	99869676	2	0	NA	32404	-29540	-29540	1	NA	NA	0.11
183	DLGAP2	1436939	1644048	1	0	NA	115501	NA	115501	1	NA	0.14	NA
184	ZFAT	135559215	135794463	8	0	NA	5943220	-1248464	-1248464	1	0.25	NA	NA
185	FASN	77629504	77649395	NA	1	66	NA	-262	-262	1	NA	NA	0.47
186	GIGYF1	100115066	100124806	1	0	NA	31553	-23059	-23059	1	NA	NA	0.33
187	ANXA13	124762216	124818828	11	0	NA	1286863	-706280	-706280	1	0.10	NA	NA
188	CDYL2	79195176	79395680	3	0	NA	248923	-1391644	248923	1	0.25	NA	NA
189	TOX	59880531	60194321	10	0	NA	5476925	NA	5476925	1	1.23	NA	NA
190	NKX2-6	23615909	23620056	6	0	NA	1478148	-129901	-129901	1	0.21	NA	NA
191	RALYL	85604112	85963979	12	0	NA	1691298	-2842997	1691298	1	0.38	NA	NA
192	TBC1D22A	45537193	45948399	NA	0	NA	NA	-23030490	-23030490	1	NA	1.43	NA
193	TFE3	48772613	48787722	NA	0	NA	NA	-35134932	-35134932	1	NA	0.10	NA
194	KCNAB1	157321095	157739621	22	0	NA	4217170	-12271116	4217170	1	NA	2.24	NA
195	SULF1	70541427	70735701	0	1	33	11428	-647617	11428	0	1.83	0.68	NA
196	RAB5C	37530524	37560548	0	1	64	1891	-1627	-1627	0	NA	NA	0.76
197	DHX58	37506979	37518277	0	1	64	380	-75799	380	0	NA	NA	4.22
198	ASAP1	131133535	131483399	0	1	45	378337	-2104073	378337	0	NA	0.80	NA

Table 6 (6a)

199	CA5A	313	2.6	-1	832	3.8	-1	955	NA	NA	NA	23	28	26	16	q24.2
200	C6orf118	53	NA	NA	NA	NA	NA	NA	2.7921	-1	976	36	36	36	6	q27
201	NCOA2	169	3.2	1	997	2.4	1	806	NA	NA	NA	35	40	37	8	q13.3
202	PKD1L2	283	4.9	-1	999	2	-1	715	NA	NA	NA	41	45	42	16	q23.2
203	BANP	314	2.6	-1	901	3.3	-1	957	NA	NA	NA	42	49	46	16	q24.2
204	KIAA1967	133	2.8	-1	925	3.1	-1	989	NA	NA	NA	50	57	52	8	p21.3
205	COPG2	89	NA	NA	NA	NA	NA	NA	3.1195	1	936	56	52	53	7	q32.2
206	ZNF706	205	NA	NA	NA	2.8	1	889	NA	NA	NA	53	56	54	8	q22.3
207	GAN	285	2.7	-1	869	2.4	-1	902	NA	NA	NA	49	61	55	16	q23.2
208	PLCG2	286	2.9	-1	833	2.7	-1	913	NA	NA	NA	61	50	56	16	q23.2
209	C19orf57	356	NA	NA	NA	NA	NA	NA	2.7945	1	992	58	58	59	19	p13.12
210	PDGFRL	111	4.8	-1	998	NA	NA	NA	NA	NA	NA	62	55	60	8	p22
211	ESD	249	NA	NA	NA	NA	NA	NA	2.5793	-1	973	65	59	62	13	q14.2
212	CPA5	85	NA	NA	NA	NA	NA	NA	2.7623	1	924	70	63	67	7	q32.2
213	BIN3	134	1.7	-1	507	2.8	-1	992	NA	NA	NA	71	73	70	8	p21.3
214	ZFHX4	184	4.3	1	1000	NA	NA	NA	NA	NA	NA	74	76	73	8	q21.11
215	CPA6	163	3.8	1	1000	NA	NA	NA	NA	NA	NA	77	81	75	8	q13.2
216	EYA1	172	3.4	1	997	NA	NA	NA	NA	NA	NA	73	89	77	8	q13.3
217	CHRNA2	153	3.5	-1	999	NA	NA	NA	NA	NA	NA	76	87	79	8	p21.2
218	TNKS	97	4	-1	1000	NA	NA	NA	NA	NA	NA	87	84	84	8	p23.1
219	HNF4G	183	4.1	1	1000	NA	NA	NA	NA	NA	NA	103	72	87	8	q21.11
220	LRCH1	248	NA	NA	NA	NA	NA	NA	2.3847	-1	801	79	94	88	13	q14.13
221	ADRA1A	149	3.9	-1	991	NA	NA	NA	NA	NA	NA	96	79	89	8	p21.2
222	EPHX2	154	3.3	-1	997	NA	NA	NA	NA	NA	NA	89	88	90	8	p21.1
223	SORBS3	130	NA	NA	NA	3	-1	957	NA	NA	NA	83	95	91	8	p21.3
224	GRIA2	27	NA	NA	NA	NA	NA	NA	2.2933	-1	843	88	96	93	4	q32.1
225	PDLIM2	131	NA	NA	NA	2.9	-1	993	NA	NA	NA	94	91	94	8	p21.3
226	MTMR7	109	3.7	-1	971	NA	NA	NA	NA	NA	NA	86	106	96	8	p22
227	FBXO24	76	NA	NA	NA	NA	NA	NA	2.4831	1	817	118	85	99	7	q22.1
228	CRISPLD1	182	4.9	1	1000	NA	NA	NA	NA	NA	NA	95	124	107	8	q21.11
229	DPYS	211	3.2	1	976	NA	NA	NA	NA	NA	NA	92	129	109	8	q22.3
230	DTNA	351	NA	NA	NA	NA	NA	NA	2.2378	-1	734	102	125	112	18	q12.1
231	KLHDC4	311	NA	NA	NA	2.5	-1	987	NA	NA	NA	116	111	113	16	q24.2
232	CYBA	319	NA	NA	NA	2.9	-1	941	NA	NA	NA	117	121	118	16	q24.3
233	JPH3	310	2.4	-1	766	2.4	-1	908	NA	NA	NA	101	142	120	16	q24.2
234	TMEM120A	64	NA	NA	NA	NA	NA	NA	1.7093	1	511	128	115	121	7	q11.23
235	MTUS1	112	3.6	-1	976	NA	NA	NA	NA	NA	NA	143	116	127	8	p22
236	C8orf34	165	6	1	1000	NA	NA	NA	NA	NA	NA	126	132	128	8	q13.2
237	GRHL2	206	NA	NA	NA	2.4	1	790	NA	NA	NA	125	140	132	8	q22.3
238	CPA2	83	NA	NA	NA	NA	NA	NA	2.1399	1	717	153	117	133	7	q32.2

Table 6 (6b)

199	CA5A	86479126	86527613	0	1	58	14926	-18511	14926	0	0.29	0.91	NA
200	C6orf118	165613148	165643101	0	1	8	17665	-18812721	17665	0	NA	NA	0.37
201	NCOA2	71178380	71478574	1	1	33	233471	-32264	-32264	0	0.57	0.21	NA
202	PKD1L2	79691985	79811477	0	1	53	18320	-4504	-4504	0	1.63	0.07	NA
203	BANP	86542539	86668425	0	1	58	378801	-14926	-14926	0	0.29	0.63	NA
204	KIAA1967	22518202	22533920	0	1	26	-14	-597	-14	0	0.38	0.52	NA
205	COPG2	129933404	129935887	106	1	13	13747479	-41	-41	0	NA	NA	0.53
206	ZNF706	102278444	102287136	0	1	40	287026	-243699	-243699	0	NA	0.38	NA
207	GAN	79906076	79971441	0	1	53	398967	-23828	-23828	0	0.33	0.21	NA
208	PLCG2	80370408	80549399	0	1	53	76965	-398967	76965	0	0.42	0.33	NA
209	C19orf57	13854168	13877909	0	1	68	105	-50124	105	0	NA	NA	0.37
210	PDGFRL	17478443	17545655	0	1	21	-71	-6086	-71	0	1.56	NA	NA
211	ESD	46243393	46269368	0	1	48	36146	-20607	-20607	0	NA	NA	0.28
212	CPA5	129771892	129795807	0	1	13	11661	-20643	11661	0	NA	NA	0.36
213	BIN3	22533906	22582553	0	1	26	18566	14	14	0	0.00	0.38	NA
214	ZFHX4	77756078	77942076	1	1	35	1648815	-1114478	-1114478	0	1.23	NA	NA
215	CPA6	68496963	68821134	0	1	33	205773	-2623061	205773	0	0.91	NA	NA
216	EYA1	72272222	72437021	0	1	34	479311	-463009	-463009	0	0.68	NA	NA
217	CHRNA2	27373196	27392730	0	1	30	11832	-376	-376	0	0.74	NA	NA
218	TNKS	9450855	9677266	0	1	16	271923	-522716	271923	0	1.04	NA	NA
219	HNF4G	76482732	76641600	0	1	35	1114478	-373386	-373386	0	1.10	NA	NA
220	LRCH1	46025304	46222786	0	1	48	20607	-2766260	20607	0	NA	NA	0.20
221	ADRA1A	26661584	26778839	0	1	30	370899	-89977	-89977	0	0.98	NA	NA
222	EPHX2	27404562	27458403	2	1	30	188353	-11832	-11832	0	0.63	NA	NA
223	SORBS3	22465196	22488952	0	1	26	3247	-10616	3247	0	NA	0.47	NA
224	GRIA2	158361186	158506677	9	1	3	4017824	-48887	-48887	0	NA	NA	0.17
225	PDLIM2	22492199	22511483	0	1	26	1584	-3247	1584	0	NA	0.42	NA
226	MTMR7	17199923	17315207	0	1	21	83768	-1533557	83768	0	0.85	NA	NA
227	FBXO24	100021892	100036674	0	1	12	1144	-180	-180	0	NA	NA	0.24
228	CRISPLD1	76059531	76109346	0	1	35	373386	-129712	-129712	0	1.63	NA	NA
229	DPYS	105460829	105548453	0	1	41	22190	-127566	22190	0	0.57	NA	NA
230	DTNA	30327279	30725806	62	1	67	17395350	-269766	-269766	0	NA	NA	0.15
231	KLHDC4	86298920	86357056	0	1	58	64075	-9657	-9657	0	NA	0.25	NA
232	CYBA	87237199	87244958	0	1	58	891	-2814	891	0	NA	0.42	NA
233	JPH3	86194000	86289263	0	1	58	9657	-1036491	9657	0	0.21	0.21	NA
234	TMEM120A	75454238	75461913	0	1	10	1679	-248023	1679	0	NA	NA	0.00
235	MTUS1	17545584	17702666	1	1	21	121980	71	71	0	0.80	NA	NA
236	C8orf34	69405511	69893810	0	1	33	647617	-99060	-99060	0	2.37	NA	NA
237	GRHL2	102574162	102750995	0	1	40	16952	-287026	16952	0	NA	0.21	NA
238	CPA2	129693939	129716870	0	1	13	3360	-29534682	3360	0	NA	NA	0.11

Table 6 (7a)

239	NAT2	115	3.3	-1	993	NA	NA	NA	NA	NA	NA	140	134	134	8	p22
240	DPYSL2	148	3.3	-1	967	NA	NA	NA	NA	NA	NA	155	122	135.5	8	p21.2
241	ZDHHC7	300	NA	NA	NA	2.5	-1	839	NA	NA	NA	159	123	138	16	q24.1
242	ELP3	158	3.4	-1	939	NA	NA	NA	NA	NA	NA	166	118	139	8	p21.1
243	RHOBTB2	136	NA	NA	NA	1.7	-1	501	NA	NA	NA	133	150	142	8	p21.3
244	NEIL2	103	2.7	-1	921	NA	NA	NA	NA	NA	NA	150	135	143	8	p23.1
245	HR	122	NA	NA	NA	2.7	-1	896	NA	NA	NA	186	112	145	8	p21.3
246	EFR3A	226	3.1	1	985	NA	NA	NA	NA	NA	NA	144	146	146	8	q24.22
247	STMN4	150	3.3	-1	994	NA	NA	NA	NA	NA	NA	162	131	147	8	p21.2
248	PRDM14	168	4.7	1	996	NA	NA	NA	NA	NA	NA	135	171	152	8	q13.3
249	MARVELD2	35	NA	NA	NA	3	-1	988	NA	NA	NA	142	164	154	5	q13.2
250	SLC39A14	128	1.8	-1	560	2.2	-1	791	NA	NA	NA	152	160	155	8	p21.3
251	ACTL6B	80	NA	NA	NA	NA	NA	NA	1.7362	1	538	168	158	159	7	q22.1
252	TUSC3	108	3.1	-1	945	NA	NA	NA	NA	NA	NA	157	170	160	8	p22
253	COX4NB	305	NA	NA	NA	2.5	-1	938	NA	NA	NA	148	181	161	16	q24.1
254	XKR9	171	2.7	1	929	NA	NA	NA	NA	NA	NA	165	163	162	8	q13.3
255	C16orf46	281	NA	NA	NA	2.2	-1	768	NA	NA	NA	151	183	164	16	q23.2
256	TAF9	33	NA	NA	NA	2.6	-1	963	NA	NA	NA	175	162	166	5	q13.2
257	KCNQ3	228	6	1	1000	NA	NA	NA	NA	NA	NA	167	180	169	8	q24.22
258	UTRN	50	NA	NA	NA	NA	NA	NA	2.3296	-1	766	174	174	170	6	q24.2
259	RAD17	34	NA	NA	NA	2.6	-1	969	NA	NA	NA	172	182	172	5	q13.2
260	ZFPM1	315	NA	NA	NA	2.5	-1	924	NA	NA	NA	146	219	175	16	q24.2
261	PTDSS1	197	2.5	1	874	NA	NA	NA	NA	NA	NA	184	177	179	8	q22.1
262	IRF8	307	NA	NA	NA	2.5	-1	976	NA	NA	NA	199	169	181	16	q24.1
263	YWHAZ	204	NA	NA	NA	2.2	1	722	NA	NA	NA	204	166	182	8	q22.3
264	MRPS36	30	NA	NA	NA	2.6	-1	962	NA	NA	NA	195	175	183	5	q13.2
265	LACTB2	170	2.6	1	932	NA	NA	NA	NA	NA	NA	160	223	187	8	q13.3
266	SNAI3	321	NA	NA	NA	2.4	-1	914	NA	NA	NA	231	156	190	16	q24.3
267	TMEM71	229	2.9	1	993	NA	NA	NA	NA	NA	NA	180	207	194	8	q24.22
268	PREX2	164	7.5	1	1000	NA	NA	NA	NA	NA	NA	190	199	195	8	q13.2
269	CPA1	86	NA	NA	NA	NA	NA	NA	2.0683	1	716	228	173	199	7	q32.2
270	PHF20L1	230	2.8	1	901	NA	NA	NA	NA	NA	NA	198	200	200	8	q24.22
271	KIAA0513	301	NA	NA	NA	2.1	-1	816	NA	NA	NA	212	188	202	16	q24.1
272	PI15	181	3	1	991	NA	NA	NA	NA	NA	NA	238	179	206	8	q21.11
273	PCM1	113	1.7	-1	529	NA	NA	NA	NA	NA	NA	183	234	207	8	p22
274	SH2D4A	117	2.9	-1	908	NA	NA	NA	NA	NA	NA	249	172	208	8	p21.3
275	C16orf74	304	NA	NA	NA	2.3	-1	939	NA	NA	NA	202	214	209	16	q24.1
276	TP63	18	NA	NA	NA	3	1	822	NA	NA	NA	203	228	211	3	q28
277	DACH1	254	NA	NA	NA	NA	NA	NA	1.8675	-1	570	252	185	212	13	q21.33
278	TNFRSF10A	138	NA	NA	NA	2.2	-1	774	NA	NA	NA	245	196	214	8	p21.3

Table 6 (7b)

239	NAT2	18293035	18303003	0	1	23	126090	-306248	126090	0	0.63	NA	NA
240	DPYSL2	26491327	26571607	0	1	30	89977	-533035	89977	0	0.63	NA	NA
241	ZDHHC7	83565573	83602642	0	1	56	16269	-64959	16269	0	NA	0.25	NA
242	ELP3	27999759	28104584	6	1	31	699246	-2452	-2452	0	0.68	NA	NA
243	RHOBTB2	22913059	22933655	2	1	26	115396	-306299	115396	0	NA	0.00	NA
244	NEIL2	11664627	11682263	1	1	18	55179	-9709	-9709	0	0.33	NA	NA
245	HR	22027877	22045326	0	1	24	6152	-4474	-4474	0	NA	0.33	NA
246	EFR3A	132985517	133095071	0	1	45	10596	-861663	10596	0	0.52	NA	NA
247	STMN4	27149738	27171843	0	1	30	26478	-370899	26478	0	0.63	NA	NA
248	PRDM14	71126574	71146116	0	1	33	32264	-216812	32264	0	1.49	NA	NA
249	MARVELD2	68746699	68773646	82	1	4	19278276	-315	-315	0	NA	0.47	NA
250	SLC39A14	22280737	22347462	0	1	26	7079	-116113	7079	0	0.02	0.14	NA
251	ACTL6B	100078678	100092007	1	1	12	23059	-1569	-1569	0	NA	NA	0.01
252	TUSC3	15442101	15666366	6	1	20	1533557	-301882	-301882	0	0.52	NA	NA
253	COX4NB	84369737	84390601	0	1	57	96	-27547	96	0	NA	0.25	NA
254	XKR9	71755848	71809213	0	1	34	463009	-11902	-11902	0	0.33	NA	NA
255	C16orf46	79644603	79668373	0	1	53	5057	-248923	5057	0	NA	0.14	NA
256	TAF9	68696327	68701596	0	1	4	-716	-31935	-716	0	NA	0.29	NA
257	KCNQ3	133210438	133561961	1	1	45	217672	-43354	-43354	0	2.37	NA	NA
258	UTRN	144654566	145215859	0	1	7	772282	-20654629	772282	0	NA	NA	0.18
259	RAD17	68700880	68746384	0	1	4	315	716	315	0	NA	0.29	NA
260	ZFPM1	87047226	87128890	0	1	58	18723	-378801	18723	0	NA	0.25	NA
261	PTDSS1	97343340	97415950	0	1	39	159108	-2053354	159108	0	0.25	NA	NA
262	IRF8	84490275	84513710	0	1	57	587924	-92166	-92166	0	NA	0.25	NA
263	YWHAZ	101999980	102034745	0	1	40	243699	-812460	243699	0	NA	0.14	NA
264	MRPS36	68549329	68577710	0	1	4	-11239	-7390	-7390	0	NA	0.29	NA
265	LACTB2	71712045	71743946	0	1	34	11902	-233471	11902	0	0.29	NA	NA
266	SNAI3	87271591	87280383	0	1	58	10028	-14572	10028	0	NA	0.21	NA
267	TMEM71	133779633	133842010	0	1	46	14776	-217672	14776	0	0.42	NA	NA
268	PREX2	69026907	69306451	0	1	33	99060	-205773	99060	0	3.36	NA	NA
269	CPA1	129807468	129815165	0	1	13	8446	-11661	8446	0	NA	NA	0.09
270	PHF20L1	133856786	133930234	0	1	46	18153	-14776	-14776	0	0.38	NA	NA
271	KIAA0513	83618911	83685327	2	1	56	517197	-16269	-16269	0	NA	0.10	NA
272	PI15	75899327	75929819	0	1	35	129712	-457439	129712	0	0.47	NA	NA
273	PCM1	17824646	17935562	0	1	22	22652	-121980	22652	0	0.00	NA	NA
274	SH2D4A	19215483	19297594	5	1	23	850362	-300007	-300007	0	0.42	NA	NA
275	C16orf74	84298624	84342190	0	1	57	27547	-18535	-18535	0	NA	0.17	NA
276	TP63	190831910	191107935	0	1	2	49278	-3269193	49278	0	NA	0.47	NA
277	DACH1	70910099	71339331	28	1	49	19509588	-1329507	-1329507	0	NA	NA	0.04
278	TNFRSF10A	23104916	23138584	0	1	27	18511	-27431	18511	0	NA	0.14	NA

Table 6 (8a)

279	MDH2	66	NA	NA	NA	NA	NA	NA	1.9653	1	728	236	208	218	7	q11.23
280	PAG1	189	NA	NA	NA	2	1	776	NA	NA	NA	173	290	221	8	q21.13
281	SLC25A37	142	2.6	-1	845	NA	NA	NA	NA	NA	NA	226	222	222	8	p21.2
282	BCAR1	273	2.5	-1	846	NA	NA	NA	NA	NA	NA	240	213	225	16	q23.1
283	COX4I1	306	NA	NA	NA	2.6	-1	911	NA	NA	NA	178	289	226	16	q24.1
284	EIF4H	59	NA	NA	NA	NA	NA	NA	2.0065	1	775	224	236	227	7	q11.23
285	ZC3H18	317	NA	NA	NA	2.1	-1	878	NA	NA	NA	217	244	228	16	q24.2
286	STMN2	186	2.8	1	962	NA	NA	NA	NA	NA	NA	284	198	230	8	q21.13
287	AFG3L1	335	NA	NA	NA	2.3	-1	947	NA	NA	NA	254	224	231	16	q24.3
288	HSD17B2	287	2.6	-1	791	NA	NA	NA	NA	NA	NA	229	259	236	16	q23.3
289	MVD	320	NA	NA	NA	2.3	-1	901	NA	NA	NA	223	266	237	16	q24.3
290	DLC1	106	6.5	-1	1000	NA	NA	NA	NA	NA	NA	207	288	238	8	p22
291	EPHA7	44	NA	NA	NA	NA	NA	NA	1.7755	-1	529	237	252	239	6	q16.1
292	TRIM35	151	2.6	-1	926	NA	NA	NA	NA	NA	NA	209	287	241	8	p21.2
293	LRRC50	293	2.4	-1	830	NA	NA	NA	NA	NA	NA	232	262	243	16	q24.1
294	CNGB3	192	1.8	1	534	NA	NA	NA	NA	NA	NA	319	191	244	8	q21.3
295	ASCC3	47	NA	NA	NA	NA	NA	NA	1.7954	-1	535	246	249	245	6	q16.3
296	RFC2	61	NA	NA	NA	NA	NA	NA	1.8399	1	625	208	295	246	7	q11.23
297	CLEC3A	278	2.3	-1	781	NA	NA	NA	NA	NA	NA	267	232	247	16	q23.1
298	IL17C	318	NA	NA	NA	1.8	-1	639	NA	NA	NA	244	256	249	16	q24.3
299	BMP1	125	NA	NA	NA	2.2	-1	819	NA	NA	NA	259	242	250	8	p21.3
300	CPA4	84	NA	NA	NA	NA	NA	NA	1.9432	1	632	242	261	251	7	q32.2
301	OC90	227	1.9	1	640	NA	NA	NA	NA	NA	NA	262	243	252	8	q24.22
302	HEPH	364	1.8	1	537	NA	NA	NA	NA	NA	NA	292	220	253	23	q12
303	LRP12	212	NA	NA	NA	2	1	635	NA	NA	NA	277	233	254	8	q22.3
304	AGFG2	74	NA	NA	NA	NA	NA	NA	2.2839	1	749	317	212	257	7	q22.1
305	TRPA1	174	2.3	1	803	NA	NA	NA	NA	NA	NA	257	263	258	8	q13.3
306	GINS2	303	NA	NA	NA	2.1	-1	861	NA	NA	NA	268	253	260	16	q24.1
307	CENPH	29	NA	NA	NA	1.9	-1	693	NA	NA	NA	286	238	261	5	q13.2
308	KLHL36	297	NA	NA	NA	1.8	-1	606	NA	NA	NA	222	312	263	16	q24.1
309	ARHGEF10L	2	NA	NA	NA	2.1	-1	730	NA	NA	NA	258	269	264	1	p36.13
310	TRAPPC2L	326	NA	NA	NA	1.9	-1	670	NA	NA	NA	302	230	265	16	q24.3
311	TCF25	332	NA	NA	NA	2.1	-1	821	NA	NA	NA	272	264	267	16	q24.3
312	TNFRSF10D	137	1.9	-1	603	NA	NA	NA	NA	NA	NA	288	250	268	8	p21.3
313	MYOM2	93	2.1	-1	705	NA	NA	NA	NA	NA	NA	295	245	269	8	p23.3
314	GCSH	282	NA	NA	NA	1.9	-1	673	NA	NA	NA	248	296	272	16	q23.2
315	KIAA1609	296	NA	NA	NA	1.9	-1	641	NA	NA	NA	260	284	274	16	q24.1
316	FANCA	330	NA	NA	NA	1.9	-1	612	NA	NA	NA	299	247	275	16	q24.3
317	ERI1	96	1.9	-1	607	NA	NA	NA	NA	NA	NA	312	239	276	8	p23.1
318	HSDL1	292	NA	NA	NA	2	-1	685	NA	NA	NA	273	278	278	16	q24.1

Table 6 (8b)

279	MDH2	75515329	75533864	2	1	10	260189	-72	-72	0	NA	NA	0.06
280	PAG1	82042605	82186858	8	1	37	545893	-93034	-93034	0	NA	0.07	NA
281	SLC25A37	23442308	23486008	1	1	28	129901	-71227	-71227	0	0.29	NA	NA
282	BCAR1	73820429	73859452	0	1	51	25657	-243911	25657	0	0.25	NA	NA
283	COX4I1	84390697	84398109	0	1	57	92166	-96	-96	0	NA	0.29	NA
284	EIF4H	73226625	73249358	0	1	9	12304	-404089	12304	0	NA	NA	0.07
285	ZC3H18	87164343	87225756	0	1	58	6746	-294	-294	0	NA	0.10	NA
286	STMN2	80685916	80740868	0	1	36	97933	-1007876	97933	0	0.38	NA	NA
287	AFG3L1	88566489	88594696	1	1	63	21813	-4521	-4521	0	NA	0.17	NA
288	HSD17B2	80626364	80689638	1	1	53	750123	-76965	-76965	0	0.29	NA	NA
289	MVD	87245849	87257019	0	1	58	14572	-891	-891	0	NA	0.17	NA
290	DLC1	12985243	13416766	1	1	19	574978	-53590	-53590	0	2.71	NA	NA
291	EPHA7	94007864	94185993	9	1	5	5242062	-2654236	-2654236	0	NA	NA	0.01
292	TRIM35	27198321	27224751	0	1	30	165	-26478	165	0	0.29	NA	NA
293	LRRC50	82736366	82769024	3	1	54	116798	-101	-101	0	0.21	NA	NA
294	CNGB3	87655277	87825017	0	1	38	122823	-1691298	122823	0	0.02	NA	NA
295	ASCC3	101062791	101435961	79	1	6	16667349	-43297	-43297	0	NA	NA	0.02
296	RFC2	73283770	73306674	0	1	9	35065	-1671	-1671	0	NA	NA	0.03
297	CLEC3A	76613944	76623495	0	1	52	67557	-280292	67557	0	0.17	NA	NA
298	IL17C	87232502	87234385	0	1	58	2814	-6746	2814	0	NA	0.02	NA
299	BMP1	22078645	22125782	0	1	25	7380	-8355	7380	0	NA	0.14	NA
300	CPA4	129720230	129751249	0	1	13	20643	-3360	-3360	0	NA	NA	0.06
301	OC90	133105667	133167084	0	1	45	43354	-10596	-10596	0	0.05	NA	NA
302	HEPH	65299388	65403956	0	1	69	328248	NA	328248	0	0.02	NA	NA
303	LRP12	105570643	105670344	0	1	41	729979	-22190	-22190	0	NA	0.07	NA
304	AGFG2	99974770	100003778	0	1	12	5792	-44412	5792	0	NA	NA	0.16
305	TRPA1	73096040	73150373	0	1	34	492151	-176755	-176755	0	0.17	NA	NA
306	GINS2	84268782	84280089	0	1	57	18535	-1471	-1471	0	NA	0.10	NA
307	CENPH	68521131	68541939	0	1	4	7390	NA	7390	0	NA	0.05	NA
308	KLHL36	83239632	83253416	0	1	56	37634	-143838	37634	0	NA	0.02	NA
309	ARHGEF10L	17738917	17896956	0	1	1	57439	-1482527	57439	0	NA	0.10	NA
310	TRAPPC2L	87451007	87455020	0	1	60	13748	-122	-122	0	NA	0.05	NA
311	TCF25	88467520	88505287	0	1	62	7881	-2292	-2292	0	NA	0.10	NA
312	TNFRSF10D	23049051	23077485	0	1	27	27431	-115396	27431	0	0.05	NA	NA
313	MYOM2	1980565	2080779	0	1	14	699503	-86359	-86359	0	0.10	NA	NA
314	GCSH	79673430	79687481	0	1	53	4504	-5057	4504	0	NA	0.05	NA
315	KIAA1609	83068608	83095794	1	1	55	143838	-13315	-13315	0	NA	0.05	NA
316	FANCA	88331460	88410566	0	1	62	11842	-246990	11842	0	NA	0.05	NA
317	ERI1	8897856	8928139	1	1	15	522716	-109315	-109315	0	0.05	NA	NA
318	HSDL1	82713389	82736265	0	1	54	101	-5371	101	0	NA	0.07	NA

Table 6 (9a)

319	KIAA0182	302	NA	NA	NA	2	-1	781	NA	NA	NA	305	251	281	16	q24.1
320	CBFA2T3	327	NA	NA	NA	1.9	-1	698	NA	NA	NA	274	297	286	16	q24.3
321	EGR3	135	NA	NA	NA	2	-1	751	NA	NA	NA	308	267	289	8	p21.3
322	PCOLCE	77	NA	NA	NA	NA	NA	NA	1.8050	1	608	294	281	290	7	q22.1
323	C16orf85	316	NA	NA	NA	2.1	-1	801	NA	NA	NA	290	291	295	16	q24.2
324	HMBOX1	159	1.8	-1	553	NA	NA	NA	NA	NA	NA	287	306	300	8	p21.1
325	MTMR9	100	1.9	-1	674	NA	NA	NA	NA	NA	NA	343	257	301	8	p23.1
326	MSC	173	2	1	675	NA	NA	NA	NA	NA	NA	291	305	302	8	q13.3
327	ST3GAL2	269	2.4	-1	774	NA	NA	NA	NA	NA	NA	269	340	308	16	q22.1
328	FOXF1	308	NA	NA	NA	2.2	-1	894	NA	NA	NA	344	270	309	16	q24.1
329	C8orf58	132	NA	NA	NA	3	-1	999	NA	NA	NA	334	279	310	8	p21.3
330	KCTD9	145	2	-1	663	NA	NA	NA	NA	NA	NA	271	344	311	8	p21.2
331	ANGPT1	214	2.4	1	816	NA	NA	NA	NA	NA	NA	333	282	313	8	q23.1
332	GDAP1	180	2	1	663	NA	NA	NA	NA	NA	NA	283	333	314	8	q21.11
333	RNF166	322	NA	NA	NA	2.2	-1	877	NA	NA	NA	263	360	315	16	q24.3
334	KLHL1	253	NA	NA	NA	NA	NA	NA	1.8637	-1	566	293	325	318	13	q21.33
335	LOXL2	140	NA	NA	NA	1.9	-1	675	NA	NA	NA	322	298	319	8	p21.3
336	WISP1	233	2.2	1	777	NA	NA	NA	NA	NA	NA	280	343	320	8	q24.22
337	C8orf80	157	3.6	-1	957	NA	NA	NA	NA	NA	NA	357	274	323	8	p21.1
338	LAT2	60	NA	NA	NA	NA	NA	NA	1.9646	1	697	328	300	324	7	q11.23
339	USP10	298	2.3	-1	691	NA	NA	NA	NA	NA	NA	321	310	326	16	q24.1
340	CDH15	328	NA	NA	NA	1.9	-1	673	NA	NA	NA	330	303	328	16	q24.3
341	WFDC1	294	2.3	-1	713	NA	NA	NA	NA	NA	NA	311	327	329	16	q24.1
342	C7orf51	73	NA	NA	NA	NA	NA	NA	2.1914	1	773	307	339	333	7	q22.1
343	EBF2	147	5.1	-1	999	NA	NA	NA	NA	NA	NA	309	337	334	8	p21.2
344	CCDC125	32	NA	NA	NA	2	-1	721	NA	NA	NA	336	319	337	5	q13.2
345	LGI3	124	NA	NA	NA	2	-1	678	NA	NA	NA	332	323	338	8	p21.3
346	NUDT18	121	NA	NA	NA	2.3	-1	786	NA	NA	NA	314	354	340	8	p21.3
347	PHYHIP	126	NA	NA	NA	2.2	-1	860	NA	NA	NA	361	308	341	8	p21.3
348	PILRA	70	NA	NA	NA	NA	NA	NA	1.8998	1	701	353	318	342	7	q22.1
349	KAT2A	340	NA	NA	NA	NA	NA	NA	3.1978	1	993	318	357	343	17	q21.2
350	CSMD3	216	4.9	1	998	4.2	1	809	NA	NA	NA	351	324	344	8	q23.3
351	REEP4	123	NA	NA	NA	2.5	-1	847	NA	NA	NA	324	352	345	8	p21.3
352	TUBB3	333	NA	NA	NA	2.6	-1	843	NA	NA	NA	348	328	346	16	q24.3
353	CDT1	324	NA	NA	NA	2	-1	745	NA	NA	NA	365	313	347	16	q24.3
354	EDA2R	365	2	1	629	NA	NA	NA	NA	NA	NA	349	331	348	23	q12
355	DUS1L	347	NA	NA	NA	NA	NA	NA	2.2705	1	904	364	322	350	17	q25.3
356	LRCH4	75	NA	NA	NA	NA	NA	NA	2.2304	1	831	342	349	351	7	q22.1
357	TMEM75	223	3.5	1	992	NA	NA	NA	NA	NA	NA	337	356	352	8	q24.21
358	NUDT7	277	2.2	-1	730	NA	NA	NA	NA	NA	NA	355	338	353	16	q23.1

Table 6 (9b)

319	KIAA0182	84202524	84267311	0	1	57	1471	-517197	1471	0	NA	0.07	NA
320	CBFA2T3	87468768	87570902	2	1	60	194762	-13748	-13748	0	NA	0.05	NA
321	EGR3	22601119	22606760	0	1	26	306299	-18566	-18566	0	NA	0.07	NA
322	PCOLCE	100037818	100043732	0	1	12	3929	-1144	-1144	0	NA	NA	0.02
323	C16orf85	87147613	87164049	0	1	58	294	-18723	294	0	NA	0.10	NA
324	HMBOX1	28803830	28966706	0	1	32	14009	-699246	14009	0	0.02	NA	NA
325	MTMR9	11179410	11223062	6	1	17	165868	-154255	-154255	0	0.05	NA	NA
326	MSC	72916332	72919285	0	1	34	176755	-479311	176755	0	0.07	NA	NA
327	ST3GAL2	68970839	69030492	28	1	50	2343793	-6059	-6059	0	0.21	NA	NA
328	FOXF1	85101634	85105570	0	1	57	15714	-587924	15714	0	NA	0.14	NA
329	C8orf58	22513067	22517605	0	1	26	597	-1584	597	0	NA	0.47	NA
330	KCTD9	25341283	25371837	0	1	29	591	-14747	591	0	0.07	NA	NA
331	ANGPT1	108330899	108579459	0	1	42	401262	-1444960	401262	0	0.21	NA	NA
332	GDAP1	75425173	75441888	0	1	35	457439	-29056	-29056	0	0.07	NA	NA
333	RNF166	87290411	87300312	1	1	58	2604	-10028	2604	0	NA	0.14	NA
334	KLHL1	69172727	69580592	0	1	49	1329507	-2470149	1329507	0	NA	NA	0.04
335	LOXL2	23210097	23317667	0	1	28	-18281	-34647	-18281	0	NA	0.05	NA
336	WISP1	134272494	134310751	2	1	46	1248464	-88015	-88015	0	0.14	NA	NA
337	C8orf80	27935607	27997307	0	1	31	2452	-29490	2452	0	0.80	NA	NA
338	LAT2	73261662	73282099	0	1	9	1671	-12304	1671	0	NA	NA	0.06
339	USP10	83291050	83371026	0	1	56	40087	-37634	-37634	0	0.17	NA	NA
340	CDH15	87765664	87789400	0	1	61	72136	-194762	72136	0	NA	0.05	NA
341	WFDC1	82885822	82920888	0	1	55	38746	-116798	38746	0	0.17	NA	NA
342	C7orf51	99919486	99930358	0	1	12	44412	-4648	-4648	0	NA	NA	0.13
343	EBF2	25758042	25958292	2	1	29	533035	-336689	-336689	0	1.76	NA	NA
344	CCDC125	68612278	68664392	0	1	4	31935	-3274	-3274	0	NA	0.07	NA
345	LGI3	22060290	22070290	1	1	24	8355	-4897	-4897	0	NA	0.07	NA
346	NUDT18	22020328	22023403	0	1	24	4474	-2493	-2493	0	NA	0.17	NA
347	PHYHIP	22133162	22145796	0	1	25	12768	-7380	-7380	0	NA	0.14	NA
348	PILRA	99809004	99835650	1	1	11	29540	-5616	-5616	0	NA	NA	0.05
349	KAT2A	37518657	37526872	0	1	64	1489	-380	-380	0	NA	NA	0.57
350	CSMD3	113304337	114518418	0	1	43	1971482	-4139285	1971482	0	1.63	1.16	NA
351	REEP4	22051478	22055393	0	1	24	4897	-6152	4897	0	NA	0.25	NA
352	TUBB3	88513168	88530006	1	1	62	12678	-7881	-7881	0	NA	0.29	NA
353	CDT1	87397687	87403166	1	1	59	4478	-67370	4478	0	NA	0.07	NA
354	EDA2R	65732204	65775608	0	1	69	904991	-328248	-328248	0	0.07	NA	NA
355	DUS1L	77609043	77629242	0	1	66	262	-40474	262	0	NA	NA	0.16
356	LRCH4	100009570	100021712	0	1	12	180	-5792	180	0	NA	NA	0.14
357	TMEM75	129029046	129029462	2	1	44	2104073	-206193	-206193	0	0.74	NA	NA
358	NUDT7	76313912	76333652	0	1	52	280292	-287400	280292	0	0.14	NA	NA

Table 6 (10a)

359	TSGA14	87	NA	NA	NA	NA	NA	NA	9.3754	1	966	354	341	354	7	q32.2
360	CDC42BPG	242	NA	NA	NA	NA	NA	NA	2.3279	1	813	360	336	355	11	q13.1
361	TSC22D4	72	NA	NA	NA	NA	NA	NA	2.1304	1	867	341	359	356	7	q22.1
362	NOTUM	345	NA	NA	NA	NA	NA	NA	2.6756	1	963	358	348	358	17	q25.3
363	HSPB9	341	NA	NA	NA	NA	NA	NA	2.9366	1	987	346	361	360	17	q21.2
364	TFR2	79	NA	NA	NA	NA	NA	NA	2.6230	1	950	352	355	361	7	q22.1
365	SLA	232	2.2	1	786	NA	NA	NA	NA	NA	NA	347	365	362	8	q24.22
366	WWOX	279	9.3	-1	1000	NA	NA	NA	NA	NA	NA	359	364	365	16	q23.1
367	POU5F1B	221	2.9	1	989	NA	NA	NA	NA	NA	NA	366	358	366	8	q24.21
368	OPHN1	367	5.8	1	999	NA	NA	NA	NA	NA	NA	368	368	368	23	q12

Table 6 (10b)

359	TSGA14	129823611	129868133	0	1	13	45149	-8446	-8446	0	NA	NA	4.49
360	CDC42BPG	64348240	64368617	2	1	47	80139	-12898	-12898	0	NA	NA	0.18
361	TSC22D4	99902080	99914838	0	1	12	4648	-32404	4648	0	NA	NA	0.11
362	NOTUM	77503689	77512353	0	1	65	16362	-39903967	16362	0	NA	NA	0.32
363	HSPB9	37528361	37528897	0	1	64	1627	-1489	-1489	0	NA	NA	0.44
364	TFR2	100055975	100077109	0	1	12	1569	-5043	1569	0	NA	NA	0.29
365	SLA	134118155	134184479	0	1	46	88015	98170	88015	0	0.14	NA	NA
366	WWOX	76691052	77803532	2	1	52	1391644	-67557	-67557	0	4.45	NA	NA
367	POU5F1B	128497039	128498621	0	1	44	318241	-2323848	318241	0	0.42	NA	NA
368	OPHN1	67179440	67570372	NA	1	69	NA	-318596	-318596	0	2.24	NA	NA